UNIVERSITY
OF TRENTO - Italy
DEPARTMENT OF INDUSTRIAL ENGINEERING

XXX cycle

Doctoral School in Materials, Mechatronics and Systems Engineering

THERAPEUTIC SILK FIBROIN-BASED SYSTEMS FOR TISSUE ENGINEERING APPLICATIONS

Rosasilvia Raggio

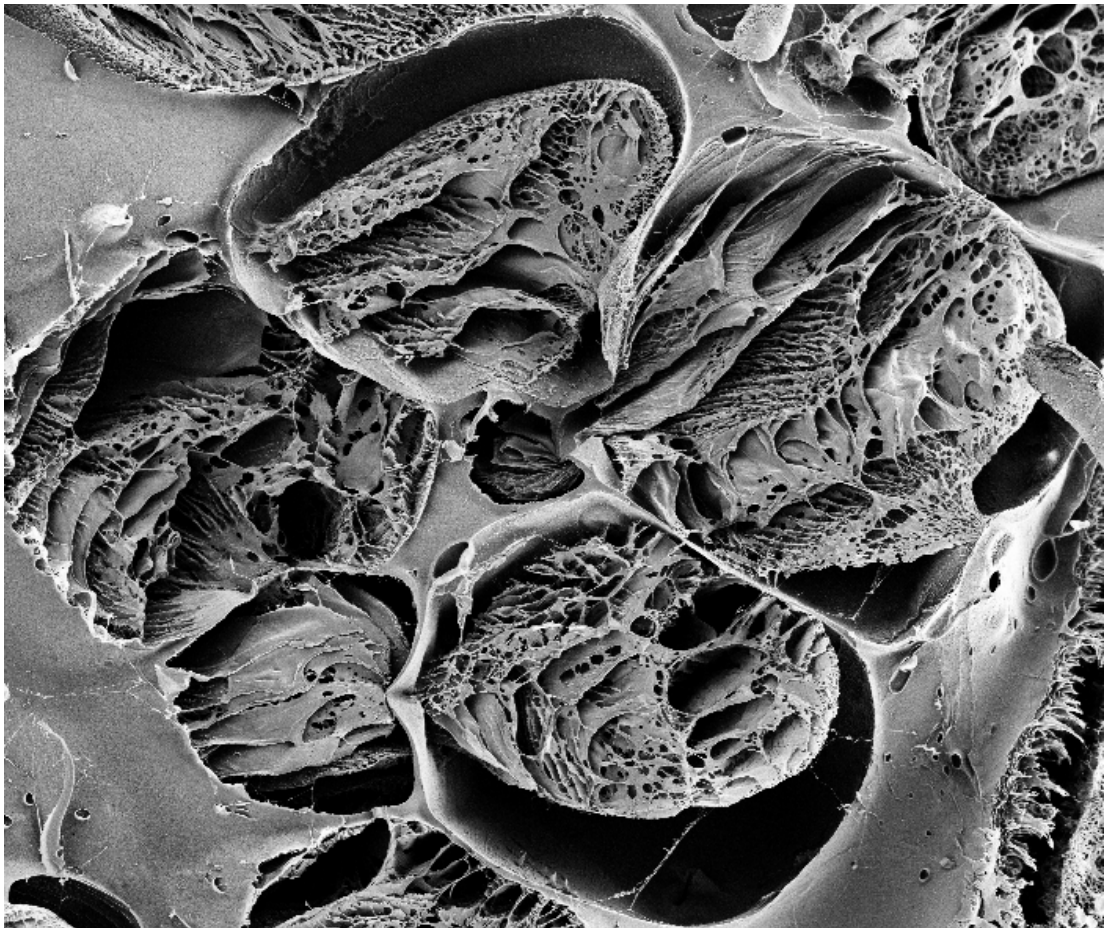

October 2019

THERAPEUTIC SILK FIBROIN-BASED SYSTEMS FOR TISSUE ENGINEERING APPLICATIONS

Rosasilvia Raggio

E-mail: raggio.rosasilvia@gmail.com; rosasilvia.raggio@unitn.it

Approved by:

Prof. Antonella Motta,
Department of Industrial Engineering
University of Trento, Italy.

Ph.D. Commission:

Prof. Devid Maniglio,
Department of Industrial Engineering
University of Trento, Italy.

Prof. Biman B. Mandal,
Department of Bioscience and Bioengineering
Indian Institute of Technology Guwahati, India.

Prof. Martin Humenik,
Department of Biomaterials
University of Bayreuth, Germany.

University of Trento,

Department of Industrial Engineering

October 2019

University of Trento - Department of Industrial Engineering

Doctoral Thesis

Rosasilvia Raggio - 2019
Published in Trento (Italy) – by University of Trento

ISBN: - - - - - - - - -

To my family

Abstract

Tissue engineering (TE) is an interdisciplinary field, in continuous evolution, that possesses as main goal the creation of efficient systems for tissues and organs healing and regeneration. For bone, TE strategies are typically based on the combined use of scaffolds, cells, and bioactive molecules.

Different materials were successfully studied and proposed for the fabrication of scaffolds. Among them, silk fibroin (SF) was evaluated as particularly promising for different TE applications, especially for bone tissue regeneration. Silk fibroin, a natural protein forming the structural core of silk filaments, holds biocompatibility, mechanical properties and biodegradation rate suitable for applications in bone regeneration. However, in the past, SF has shown some limitations, especially in terms of bioactivity and effective differentiating ability of hMSCs in regenerating bone tissue.

In this work, we wanted to demonstrate that SF, properly processed, chemically modified, and conjugated with selected bioactive species, can be used to prepare different systems: a functionalised scaffold; a bioresorbable material with mineralization ability; an implantable immunomodulatory material. The experimental activities performed and the deep investigation of the properties of the SF-based systems prepared, led to promising results, indicating that SF could be a flexible and powerful platform for the realization of different therapeutic tools. For some of the SF-based systems described in this dissertation, further studies are needed to assess the biological activity of the materials prepared.

Table of contents

Preface

This manuscript contains the report of the research activities conducted during my PhD program, at the BIOtech Research Center and Industrial Engineering Department of the University of Trento, under the supervision of Professor Antonella Motta. Parts of the researches were performed at the Department of Biomedical Engineering of Tufts University (Medford, USA), under the supervision of Professor David Kaplan, and at the Department of Chemical Engineering of Chulalongkorn University (Bangkok, Thailand), under the supervision of Professor Sorada Kanokpanont.

We had the opportunity to design and conduct part of the experiments in collaboration with other university laboratories and research institutes, in particular: the "Klaus Müller" NMR Lab, at the Department of Industrial Engineering of the University of Trento (Professor Sandra Dirè and Doctor Emanuela Callone); the RAMSES Laboratory at Istituto Ortopedico Rizzoli in Bologna, Italy (Doctor Francesco Grassi); the Regenerative Medicine Laboratory at the Ospedale Policlinico San Martino in Genoa, Italy (Doctor Roberta Tasso). The existence of collaborations is stated in the text.

The general goal of this work was to develop original strategies for the realization of silk fibroin (SF)-based devices with therapeutic properties for bone tissue engineering and regenerative medicine (TERM) applications. By presenting the experimental activities conducted and the results obtained from the deep investigation of the properties and *in vitro* performances of the SF-based systems prepared, we aimed to demonstrate that SF could be a flexible and powerful platform for the realization of different therapeutic tools. The one and only source of silk used in the research activities performed was silkworm cocoon; the material details are given in Chapter III.

The materials and methods adopted, the experiments performed, and the results obtained are described and discussed in this manuscript, structured in the following chapters:

- Chapter I: *Introduction*. In the first part, an overview of silk proteins composition, structure and properties is reported, with a specific focus on silk fibroin. The concepts of bioactivity, biodegradation and biocompatibility are explained. Fibroin is described for its applications as a biomaterial and the state-of-the art of the research about fibroin for biomedical applications is discussed. In the second part, since the most promising applications for the fibroin-based systems investigated in this work are in the field of bone tissue engineering, a general introduction on bone biology, specifically bone tissue characteristics, common diseases and healing processes, is given.
- Chapter II: *Rationale, aims and design of the research activity*. In this chapter, the goals and the outline of the research work are presented together, in order to expose the logic of the dissertation.
- Chapter III: *Silk fibroin scaffolds loaded with a sulphur (H_2S) donor agent as a novel therapeutic approach for bone regeneration applications.* This chapter describes the preparation of a novel type of SF scaffold loaded with the H_2S donor GYY4137, intended to operate as H_2S releasing system to be used in bone regeneration studies. The results obtained, reported and discussed concern the chemico-physical characterization of the scaffolds. This study was supported by the grant “Ricerca Finalizzata” awarded by the Italian Ministry of Health to the coordinator Doctor

Francesco Grassi (number and title of the project: RF PE-2011-02348395; “Novel approach for bone regeneration and repair using sulphur donor-based therapy”).

- Chapter IV: *Biological evaluation of silk fibroin scaffolds loaded with GYY4137*. The results of the biological evaluation performed on the scaffolds, in order to explore their ability to induce bone formation *in vitro*, are presented and discussed.
- Chapter V: *Fibroin/alginate beads containing β-TCP for the treatment of bone defects.* This chapter describes an alternative SF-based strategy to treat some classes of bone diseases. Spheres consisting of a source of calcium phosphate encapsulated in fibroin and alginate gel were produced to work as bioresorbable bone void filler. The results obtained from the structural and chemico-physical characterization of the spheres are reported and discussed in this chapter. This work was funded by “REMIX” Project, G.A. 778078 H2020-MSCA-RISE-2017.
- Chapter VI: *Fibroin films combined with the neuropeptide substance P as models of immunomodulatory systems.* The immunity system is always activated when a biomaterial is implanted, and its response is determinant for the success of the treatment. Fibroin films combined with the neuropeptide substance P (SP) were chosen as prototypes to study the potential immunomodulatory effects of a functionalized fibroin biomaterial. The results obtained by investigating the chemico-physical properties and the bioactivity of the films are reported and discussed.
- Chapter VII: *Conclusions and future perspectives*. The conclusions deduced from the results discussed in the

previous chapters are reported and considered as a starting point to suggest possible future developments of the research activities addressed in this dissertation.

Chapter I. Introduction

1.1. A brief history of silk

The etymology of *silk* in all the different European dictionaries comes from Old Chinese, the language of the geographic area where the production of silk began (Wang, 1993; Hildebrandt and Gillis, 2017). Many scholars agree that the word was transmitted together with the trade of silk fabric in antiquity, along the transcontinental "Silk Road". During this historical route, the Old Chinese **sə* or **siəg*, meaning "thread" or "string", was rearranged but maintained as common root in the different languages.

In fact, the domestication of the mulberry silkworms for silk production and silk textiles fabrication started in China, around 2500 BC, but the techniques regarding these practices were maintained secret for many years (Good, 2002; Kuzmina, 2008). The important procedure of boiling the cocoons to unroll silk fibers was developed in China as well and guarded jealously until the official initiation of silk trade outside the country, authorised by the imperial dynasty of the Han (roughly contemporaneous with the Romans), in 200 BC. Since then, silk materials diffused and sericulture, together with mulberry tree cultivation, could spread first in Korea and Japan, then towards western countries, particularly from India to central Asia, from Greece to Italy and finally to France. The silk industry in Europe prospered until the 19th century, but when it was at its peak in France, an epidemic disease of silkworms broke out and marked the end of sericulture in major part of Europe and the Middle East (International Sericultural Commission). Nowadays, the major silk producing countries are: China, India, Thailand, Uzbekistan, Brazil, Japan, Republic of Korea, and Vietnam.

Silk is a natural material of animal origin, produced by various insects and arachnids to serve for a variety of functions, in different periods of their lifecycles. The domesticated mulberry silkworm *Bombyx mori* is the species that produces most of the silk fibers used nowadays. The larvae of their moths can secrete significant amounts of silk to form the cocoons that protect them during the metamorphosis (Fig. 1).

Fig. 1 The pictures show details of a silkworm eating mulberry leaves (on the left), and a moth that just exited the cocoon at the end of its metamorphosis (on the right).

Silk farmers stop the larvae life cycle at the cocoon stage in order to obtain the silk in a continuous filament and process it for different commercial uses, mainly for the fabrication of textiles.
Beyond this application, it is of great importance the use of silk fibers as medical sutures since hundreds of years ago. The Greek surgeon, Galen of Pergamon (131-211), was probably the first to describe the use of silk to treat and suture injured tendons in gladiators (Muffly et al., 2011). Successively, silk fibers were kept in use as sutures for different tissues, and, in 1887, Johnson & Johnson became the first mass-producer of sterile silk fibers for medical applications (Mackenzie, 1973).

Fig. 2 The first sterile silk materials fabricated for suturing by J&J. Reproduced from https://ourstory.jnj.com/sterile-surgical-sutures.

More recently, from the late 90s, the pioneering studies conducted in Japan by different research groups were determinant for the diffusion of silk materials in the biomedical field. Silk was studied for its biological properties, and the use of silk-based materials to fabricate scaffolds for tissue engineering started to be reported (Minoura et al., 1990). In the following paragraphs, the concepts needed to describe silk as biopolymer and biomaterial are presented and investigated.

1.2. Composition, structure and properties of silk proteins

1.2.1. General properties of *Bombyx mori* silk

Silkworm silk is typically obtained from natural cocoons spun by domesticated *Bombyx mori* silkworms at the larvae stage. The larvae spin variously shaped cocoons, which are characteristic of particular races: some build globular cocoons, others ellipsoidal or even cocoons with a peanut-like shape. The process of cocooning is characterized by the spinning speed and periodical reverse changes

of larval body direction, and it consists of two phases: first the larvae makes a scaffold for the cocoon by spinning small amount of silk, then it begins to spin the cocoon, anchored to the scaffolding net (Kiyosawa et al., 2004). Silkworms larvae produce silk fibers by their spinning glands, which contain the silk proteins in the liquid state (Akai et al., 1987). In a normal larva, the gland is divided into three regions, two of which are designated to the spinning of the different proteins constituting silk fibers: fibroin and sericin. By applying shear and elongation stresses on the solution (present at a protein concentration up to 30% weight/volume), the silkworm spins through the gland spinneret fibroin and sericin, which become solid and crystallize together in a unique fiber outside the animal (Jin and Kaplan, 2003). In particular, it was observed that a fine structural change occurs, when the liquid columnar fibroin in the lumen of silk gland passes from the posterior to the anterior silk gland during the spinning stage. In the posterior silk gland, the columnar fibroin locates in the lumen in spherical masses of fibroin fibers (MFFs). These fibers adhere closely together and become homogeneous and compact in the anterior silk gland. It was concluded that the cocoon filament is composed of oriented elementary fibroin fibers derived from MFFs. On the other hand, liquid sericin in the middle silk gland is easily crystallized by drying, thanks to its amino acid composition, and becomes film of non-oriented crystal conformation (Mondal et al., 2007).The structure of the final natural fiber consists of two filaments of fibroin, accounting for about 75% in weight, surrounded by a sericin film (20-25% in weight) that coats fibroin and sticks together the folded fiber thus forming the silk cocoon (Fig. 3).

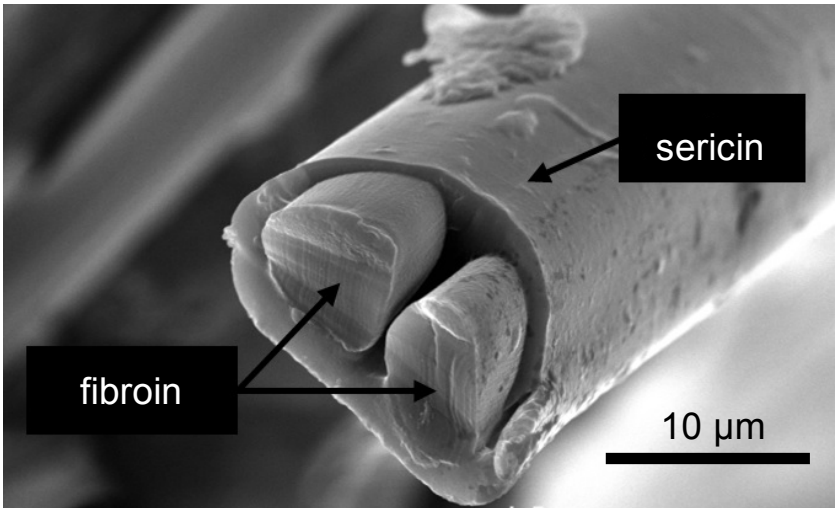

Fig. 3 SEM image of silk fiber cross-section (photo courtesy of Rungnapha Yamdech, adapted from www.chulapedia.chula.ac.th).

For any of the different uses of silk, after the harvest and larvae removal, cocoons must undergo various treatments. The first one generally involves boiling in selected conditions to unravel the cocoons, and obtain fibers of natural silk fibroin cleared from the sericin coating (Shao and Vollrath, 2002). This step is known as silk fibers degumming, and it can be executed under a range of different experimental conditions. After this step, fibers mechanical properties result only slightly modified if compared with natural sericin-coated ones, with tensile strength of about 0.5 GPa, a breaking elongation of 15%, and toughness (breaking energy) of $6x10^4$ J kg^{-1} (Wilding and Hearle, 1996). Both sericin and fibroin are processed and applied in research or in the fabrication of commercial products, but there are differences between their chemico-physical properties and amino acid composition. Moreover, raw silk and the isolated silk proteins have different bioactivity in terms of macrophages response and inflammation processes, therefore they have different ranges of medical application (Panilaitis et al., 2003; Meinel et al., 2005).

Sericin is a macromolecule and a globular protein, highly hydrophilic, insoluble in cold water and soluble in hot aqueous solutions (Aramwit, 2012). The molecular weight (MW) ranges from around 10 to 300 kDa. Sericin contains 18 different amino acids, most of which have polar side chain groups such as hydroxyl, carboxyl, and amino groups. In terms of composition, it consists of principally serine (32%), aspartic acid (18%), and glycine (16%).

Regarding its utilization, thanks to its properties and processability, sericin was reported to be useful as a coating or blending material for natural and artificial polymers, fabrics, gels, membranes, foams, fibers, and composite materials for biomedical applications. Moreover, sericin can also be used to produce cryopreservatives, anticoagulants, and biocompatible materials mainly for wound healing applications (Zhang, 2002).

Like sericin, fibroin is a macromolecular protein. Its properties and characteristics are described in detail in the following paragraphs.

1.2.2. Fibroin composition and protein structure

Fibroin, the constituent of the core of silk fibers, is a fibrous protein of approximately 2.3 MDa (Asakura and Miller, 2014). Its “elementary unit” consists of heavy (H) and light (L) chain polypeptides of around 350 and 25 kDa respectively, linked by a disulfide bond. In addition, another 30-kDa polypeptide, a glycoprotein named P25 unit, associates with the H and L polypeptides by hydrophobic interactions. This P25 fraction has a standard amino acid composition and a non-repetitive sequence, playing only a minor role in the fiber. By experiments of quantitative enzyme-linked immunosorbent assays, it was revealed that the three protein

components are present with a molar ratio of 6:6:1 (H:L:P25) in the fibroin elementary unit (Inoue et al., 2000).

The heavy chain is the most determinant component in terms of chemico-physical properties conferred to the fibroin fiber, and its protein sequence was deduced from that of the genomic DNA (Zhou et al., 2000). It consists of 5263 amino acid residues organized in 12 domains, forming the bulk (around 94%) of the polypeptide H. They constitute the crystalline fraction of the fibroin fiber, and are considered sequences of “low-complexity”, because their primary structure consists of Gly-X repeats, where Gly is glycine and X is alanine (Ala) in 65%, serine (Ser) in 23%, or tyrosine (Tyr) in 9% of the repeats. Non-repetitive and “amorphous” peptide chains, consisting of 151 N-terminal residues, 50 C-terminal residues, and linkers of around 40 residues that connect the crystalline domains, compose the remainder (Fig. 4) (Zhou et al., 2001). The following figure shows the hierarchical structure of a naturally spun silk thread, with focuses on the polymorphs (Silk I and Silk II) and secondary protein structures (mainly β-sheet) constituting fibroin fibers.

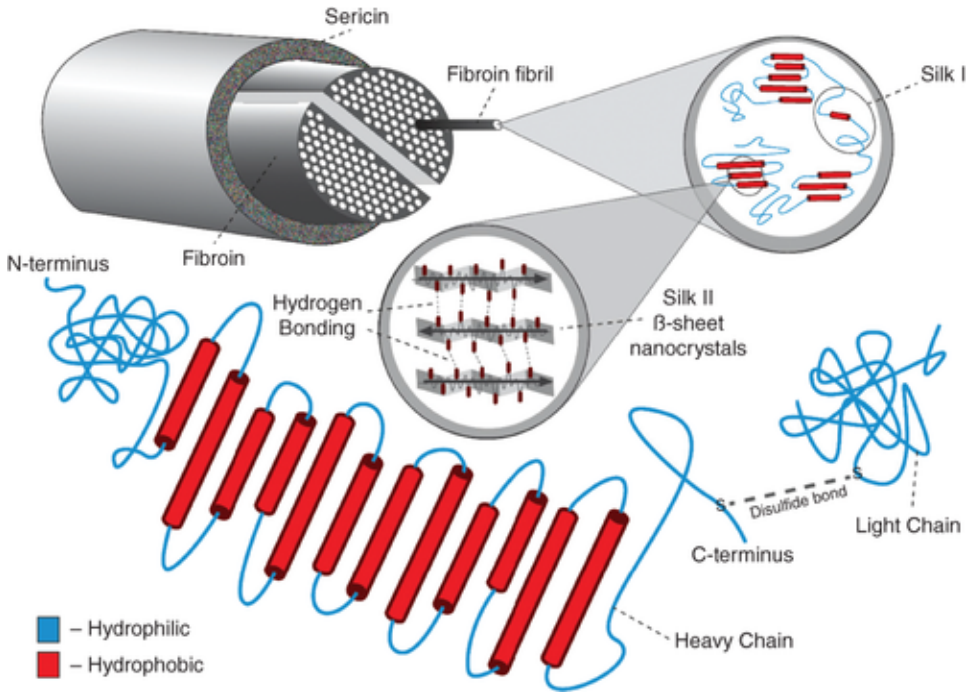

Fig. 4 Schematic representation of the SF fiber structure (DeBari and Abbott, 2019). With permission of John Wiley and Sons.

The typical composition of a sample of fibroin is reported in Table 1.

Amino acid	Mol %
Glycine	49.9
Alanine	27.7
Serine	7.9
Tyrosine	5.3
Valine	2.7
Isoleucine	1.2
Aspartic acid	1.0
Glutamic acid	0.9
Threonine	0.8
Phenylalanine	0.8
Leucine	0.6
Arginine	0.6

Table 1 From BIOtech Research Center analyses on Bombyx mori fibroin.

The peptide sequence of silk fibroin contributes to the resulting structure and function of the fiber. From the table, the prevalence of amino acids with -H (glycine) and -CH_3 (alanine) side chains is evident. The hydrophobic nature of these functional groups and the position of the correspondent amino acids along the chain are at the base of the secondary structure that fibroin adopts in the different passages before and after spinning from the silkworm gland, in its natural state (Akai et al., 1987; Kiyosawa et al., 2004). The most common secondary structure of fibroin is the anti-parallel β-sheet, which consists of amino acid chains organized in a pleated shape, with cross-linking hydrogen bonds between adjacent portions of each chain (Asakura et al., 2013). Other secondary structures that fibroin can form are: α-helix; β-sheet-derived structures, such as β-turns, distorted β-sheets, or β-sheets with parallel or alternating Ala-CH_3 residues; random coil (Asakura et al., 2015). The two most common protein secondary structures that can be found in fibroin are illustrated in Fig. 5.

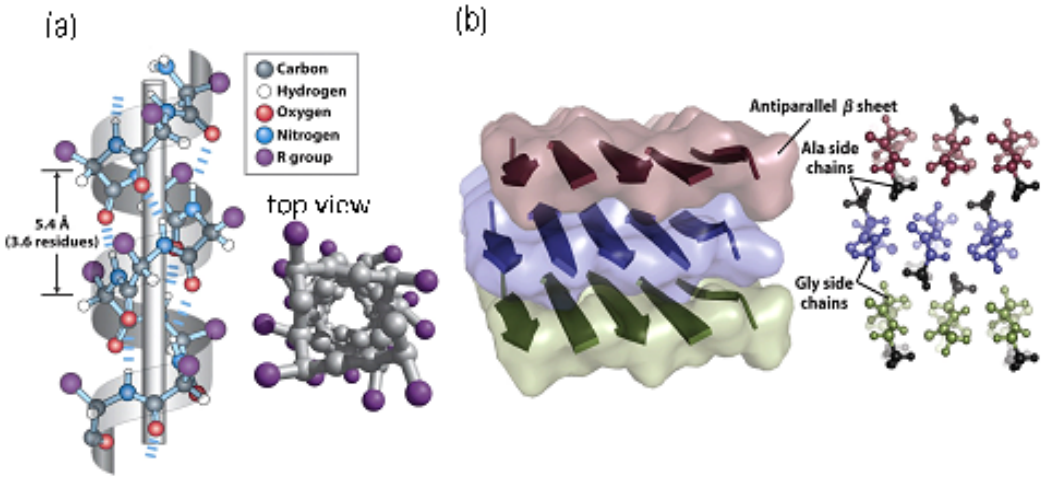

Fig. 5 (a) Ball-and-stick models of the α-helix, showing different aspects of its structure: the intrachain hydrogen bonds; the view from one end, looking down the longitudinal axis. (b) Layers of antiparallel β sheets rich in Ala and Gly residues. With permission of (Nelson et al., 2008).

Depending on the nature and amount of the different secondary structures combined to form the overall protein "architecture", different polymorphs were defined for fibroin.

For fibroin in the natural state, the most important polymorph is the Silk II (Hu et al., 2006). Silk II is the β-sheet-dominated crystal conformation, it is water insoluble and it forms after the spinning of silk fibers from the spinneret of the silkworm. In this polymorph, portions of crystalline β-sheets are found embedded in an amorphous fibroin matrix, formed by other secondary protein structures (Callone et al., 2016).

Then, Silk I is the complex structure dominated by α-helices, existing within the silkworm gland just before the spinning. Interestingly, it is a soluble polymorph of fibroin, however it is not all in the random coil structure (*i.e.* the typical disordered conformation adopted by proteins in solution): in fact, it was demonstrated by thermodynamic studies that a direct transition from random coil to β-sheet, during the spinning process of the fibers, would not be possible (Asakura et al., 2015). Silk I is still not completely clear, but it is reasonably considered as a semi-ordered structure that guides the formation of the solid fibers from the liquid state of the glands (Jin and Kaplan, 2003).

These two polymorphic phases described for native fibroin, together with other additional conformations, can be also found for regenerated fibroin materials (Lawrence et al., 2008).

1.2.3. Preparation, properties and processing of regenerated fibroin

After sericin removal through degumming, by using a combination of solvents, salts, temperature and time conditions, fibroin fibers can be

dissolved into clear and homogeneous solutions (Aznar-Cervantes et al., 2013). In these solutions, fibroin undergoes denaturation, because it completely loses its secondary protein structure and adopts a random coil conformation: in this state, fibroin is typically termed regenerated fibroin. Common examples of solutions used to dissolve fibroin fibers are: the Ajisawa's reagent ($CaCl_2$/ethanol/water, 111/92/144 in weight, used at 75 °C); lithium thiocyanate (LiSCN) solution around 9 M at room temperature; N-methylmorpholine N-oxide; lithium bromide solution 9.3 M at around 60 °C; different ionic liquids (Yamada et al., 2001; Phillips et al., 2004; Cho et al., 2012). A purification step, usually concerning a dialysis process, is then executed in order to remove from fibroin any trace of solvents, salts and ions.

Regenerated fibroin solutions are thermodynamically unstable and, in periods of time going from few days up to around two weeks, tend to spontaneously convert towards more ordered phases generally dominated by β-sheets structures. Different techniques, such as sonication, heating, application of electric fields, and vortex shearing, can be used to accelerate and guide self-assembly of fibroin chains in solution to form β-sheet crystals (Rockwood et al., 2011b). These physical stimuli can provide sufficient energy to fibroin solutions to alter the protein hydrophobic interactions. They induce, as consequences, physical entanglements and hydrogen bonding between hydrophobic domains, and the sol-gel transition of the material (Matsumoto et al., 2006). Moreover, the acquisition of a structural conformation by the protein chains is also driven by other various factors, such as: fibroin concentration in the solution; environmental factors (temperature, pressure, humidity, pH); processing treatment on fibroin solutions (*e.g.*, solution casting, foaming, mixing with porogens, chemical reactions, blending with

other polymers, etc.); post-processing treatment on solid fibroin materials (*e.g.*, incubation of fibroin material in alcohols solutions, exposition to vapour, sterilization, etc.). Polymorphic phases similar to the Silk I or Silk II, or a combination of them, can be found in regenerated fibroin materials, *i.e.* materials formed starting from regenerated fibroin solutions. Recently, another polymorphic crystalline phase was discovered, and termed Silk III: it typically forms at the air-water interface of thin fibroin cast films, and consists of an insoluble structure of distorted three-fold helices and sheet-like structures (Valluzzi et al., 1999). In

, the structural changes induced on fibroin cast films by two common treatments (*i.e.,* water-annealing by setting in a water-filled desiccator at 0,8 atm vacuum for 5 h, and steam sterilization at T = 121 °C and P = 1 atm for 25 minutes) are illustrated (Lawrence et al., 2008). In particular, the bottom left picture represents the structure of a cast film, with semi-ordered Silk I polymorph. On the top right corner, the Silk II-like polymorph, obtained by treating the cast film and with the highest % of β-sheet structure, is depicted.

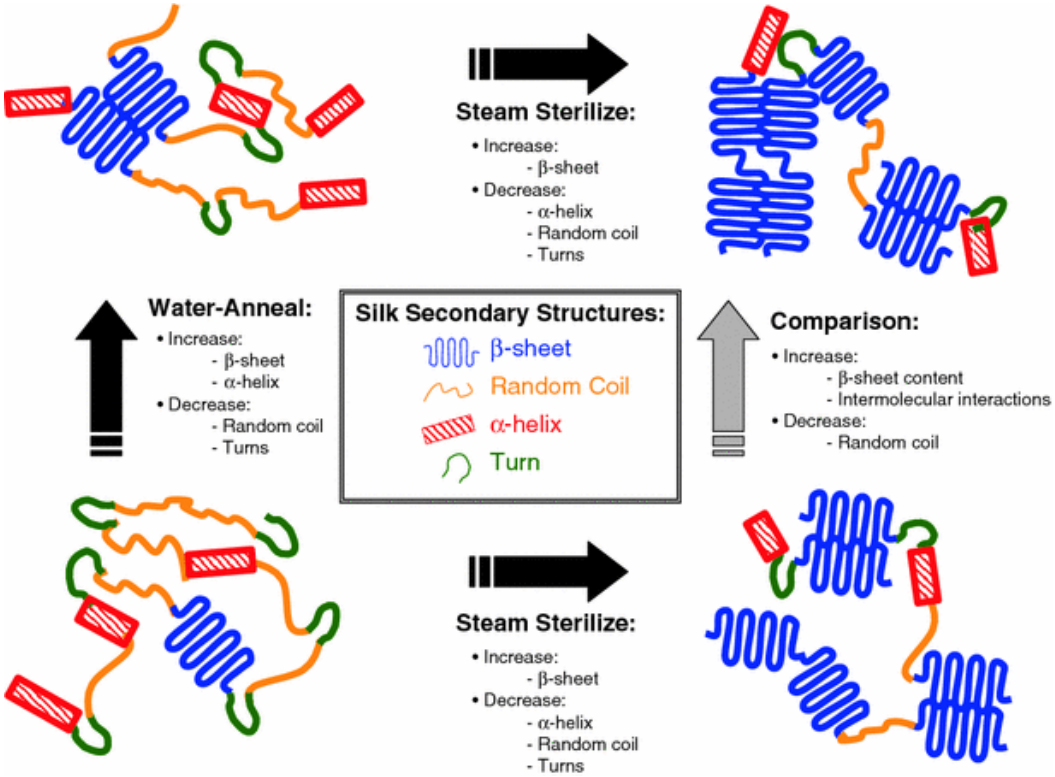

Fig. 6 Schematic diagram illustrating fibroin secondary structural changes exhibited during water-annealing and steam sterilization processing. Adapted from (Lawrence et al., 2008). With permission of Springer Nature.

It is now clear the most interesting peculiarity of fibroin: depending on the "history", regenerated materials display specific and complex molecular and supra-molecular structure, hierarchical organization, and ability to self-assemble. As a consequence of processing, changes in conformation, at any dimensional level, result in variation in water content, crystalline domain extension, mechanical properties as well as bioactivity and biological behaviour of the resulting material (Kim et al., 2005; Motta et al., 2009; Lin et al., 2013; Qi et al., 2017).

Degradability is also affected by silk fibroin inter- and supramolecular structure. Indeed, fibroin materials are stable or degradable, depending on the specific conformation. In general, the amount of beta sheet structure influences the degradation rate, which is lower

for a high percentage of crystalline structure (Liu et al., 2015). In fact, native fibroin fibers can be considered almost non-degradable, while degradation of regenerated fibers is slow but present.

For this reason, it is fundamental to investigate by different techniques the sensitivity of fibroin conformations to synthesis, processing or environment. Changes in fibroin secondary structure or interactions at the intermolecular level between protein chains particularly affect the position and shape of the Nuclear Magnetic resonances (NMR) and the infrared and Raman spectra peaks. These spectrometry techniques, which can be matched with complementary analyses performed, for example, by calorimetry or X-ray diffraction are typically exploited for two purposes: to identify the structures of fibroin materials; to quantify the contents of the different structures detected (Jin et al., 2005; Callone et al., 2016). The use of these techniques to study fibroin conformation is explained in the experimental part of this dissertation.

1.2.4. Regenerated fibroin materials

Fibroin solutions can be processed into a variety of solid constructs, for different applications, especially in the biomedical field. In this paragraph, some examples of fibroin materials and techniques for their preparation are briefly presented. SF films can be produced by casting fibroin aqueous, acid, and ionic solutions (Phillips et al., 2005; Gupta et al., 2007; Bucciarelli et al., 2017). Manual or spin-assisted deposition techniques have been used to produce films of various thickness (Lu et al., 2010). Since the stability of the as-cast films is low, techniques such as water annealing, controlled drying and alcohol immersion have been employed.

Silk hydrogels are formed through the sol-gel transition of aqueous silk fibroin solution in the presence of acids, dehydrating agents, under sonication or lyophilization (Motta et al., 2004). Silk fibroin mats were prepared by electrospinning from silk fibroin solution (Pignatelli et al., 2018). Porous silk scaffolds have been prepared by freeze-drying, porogen leaching, and solid freeform fabrication techniques like gas foaming (Rockwood et al., 2011b; Maniglio et al., 2018). Silk micro- and nanopowders have been produced from silk solution by freeze drying and grinding, spray drying, self-assembly (Zhang et al., 2007; Wenk et al., 2008). Milling silk fibers is an alternative approach to produce silk particles directly from fibers without the use of chemicals (Rajkhowa et al., 2010).

1.2.5. Chemical modifications of fibroin

The majority of fibroin is composed of the non-reactive amino acids glycine and alanine (Geddes et al., 1969). However, fibroin contains significant quantities of residues with functional groups that can be modified with known chemistries (Murphy and Kaplan, 2009). These residues are:

- serine (R = CH_2OH);
- tyrosine (R = CH_2PhOH);
- aspartic (R = CH_2COO^-) and glutamic acid (R = $CH_2CH_2COO^-$);
- threonine (R = $CHOHCH_3$).

Chemical reactions can be carried out on fibroin in solution or on formed solid fibroin materials, depending on the type of chemistry and reagents used, and on the characteristics required for the final potential application of the silk product.

In general, chemical modifications of silk fibroin involving the formation of covalent bonds can be performed with these main objectives:

- to induce fibroin chains chemical crosslinking (Kim et al., 2018);
- to make fibroin chains more reactive towards successive modifications or physical stimuli (*e.g.,* light radiation for photocrosslinkable fibroin) (Applegate et al., 2016);
- to link to fibroin chains molecules or macromolecules, such as sugars and synthetic polymers, which can enhance specific chemico-physical properties (*e.g.,* mechanical, optical and surface properties) (Wenk et al., 2010);
- to link to fibroin chains biomolecules or biomacromolecules (*e.g.,* proteins, growth factors, glycosaminoglycans, extracellular matrix proteins) that can give specific bioactivities to fibroin and guide its biological response in biomedical applications (Font Tellado et al., 2017).

Several recent interesting researches focusing on fibroin chemical modification by different strategies have been published.

In this context, one of the most appreciated, simple and adopted strategies to modify fibroin, both in solution and in the solid state, is the use of crosslinkers for protein conjugation, such as N-hydroxysuccinimide (NHS) esters and carbodiimides (*e.g.*, EDC hydrochloride). These reactions typically target the carboxyl groups of aspartic and glutamic acids. The surface of silk fibroin membranes was modified by binding chemically the GRGDSPC peptide, a well-known sequence recognized by cell integrins, using a water-soluble carbodiimide (Bray et al., 2013). Fibroin solution with covalently bound RGD sequences was also fabricated into scaffolds, to assess

the effects of enhanced cell attachment and biodegradation (Meinel et al., 2004).

Fibroin tyrosine residues were exploited in different reactions, thanks to their relative abundance and ease of modification. For example, diazonium coupling was performed on silk in different phases. These reactions involve an electrophilic aromatic substitution between the tyrosine side chains and a diazonium salt, resulting in an azobenzene derivative that can carry a variety of functional groups, depending on the nature of the starting reagents (Murphy et al., 2008). To demonstrate the relevance of this approach to medical applications, various commercial biological molecules, such as biotin and fibroblast growth factor 2 (FGF-2), were conjugated to fibroin previously modified by diazonium coupling reaction (Wenk et al., 2010; Raynal et al., 2018).

Recently, other successful chemical modifications of fibroin were obtained by using horseradish peroxidase (HRP). HRP is an enzyme with a wide substrate specificity that catalyzes the oxidation of phenolic residues into radical species in the presence of hydrogen peroxide. HRP was either used to induce gelation by intermolecularly crosslinking fibroin chains, or to conjugate molecules and polymers to fibroin tyrosine residues (Partlow et al., 2014; Simmons et al., 2016). The cases cited here are only few examples of the many studies conducted on fibroin chemical modification and had a relevant impact on the design of some of the experiments conducted during my research.

1.3. Silk fibroin as a biomaterial

Silk fibroin is a biopolymer and a biomaterial. As a protein and a nature derived material, fibroin can be defined as a biopolymer.

Thanks to the biocompatibility demonstrated in various applications, fibroin can be also classified as a biomaterial, *i.e.* a source for the preparation of materials with biomedical applications (Minoura et al., 1990; Motta et al., 2013). This fundamental peculiarity of SF is examined in the following chapter.

1.3.1. Biocompatibility of fibroin materials

Since the first reported cases of implantations of materials in the human body for therapeutic applications, the concept of biocompatibility has evolved, in parallel with the development of new biomedical devices materials and with their diffusion in the medical field. About the definition of biocompatibility given by Williams in 1987 ("it is the ability of a material to perform with an appropriate host response in a specific application"), Ratner objected that it offers no insights into its mechanisms, how to test, optimize or enhance the biocompatibility of a material (Williams, 1987). For these reasons, Ratner recently proposed the following definition: "biocompatibility is the ability of materials to locally trigger and guide normal wound healing, reconstruction and tissue integration" (Ratner, 2015). In this paragraph, the different aspects that lead to the assessment of fibroin biocompatibility are investigated.

Many cells, including bone cells progenitors, are anchorage-dependent cells, namely they require a matrix to adhere to in order to develop their specific phenotypic characteristics. Cell-matrix interactions are essential for a variety of cell events including morphological changes, spreading, proliferation and differentiation. For these reasons, it is fundamental to study the cell interactions of materials designed and fabricated for medical uses that will be implanted in human body. Typically, this is one of the first steps

accomplished while assessing the bioactivity of materials, which is the ability to integrate with biological molecules or cells and regenerate tissues. The bioactivity of fibroin materials was deeply investigated *in vitro* and *in vivo*. The pioneering studies of Minoura and collaborators firstly showed strong cell attachment on fibroin matrices (Minoura et al., 1995). Successively, another Japanese research identified in the two peptides VITTDSDGNE and NINDFDED the bioactive amino acid portions of fibroin chains (Yamada et al., 2004). Electrospun silk fibroin mats supported extensive human bone marrow stromal cells (hBMSC) proliferation and matrix coverage, over 14 days of incubation *in vitro*. (Jin et al., 2004). In general, cell adherence to silk surfaces has been reported to be strongly related to the cell phenotype, the primary structure of the protein (and consequently the secondary and tertiary structures), the processing conditions and the chemico-physical treatments (Leal-Egaña and Scheibel, 2010). For these reasons, many efforts were devoted to the research on strategies for fibroin processing and modification with the goal of enhancing or modulating cell adhesion.

In various attempts to study the biological response to silk materials, it was shown that silk fibroin, after proper extraction of sericin, was non-immunogenic. Toxicity, which can be quantified by measuring leached compounds, vascularity and cytokines in cell cultures, was generally negligible for silk fibroin materials. Exposition to different SF preparations did not induce a consistent response in macrophages cultured *in vitro*. In fact, minimum levels of pro-inflammatory factors (specifically, TNF or tumour necrosis factor) were detected (Panilaitis et al., 2003). Fini *et al.* studied the biocompatibility of SF hydrogels and observed the absence of pro-inflammatory effects due to the biomaterial extract *in vitro.* After implantation in rabbits, they could confirm that neither *in vivo* the

fibroin hydrogels could evoke inflammation or foreign body reaction, in the surrounding bone tissue (Fini et al., 2005).

Biodegradability is one of the properties required to materials designed to promote the regeneration and reconstruction of human organs (Ghalia and Dahman, 2016). According to the U.S. Pharmacopeia an absorbable or biodegradable biomaterial is a material that “loses most of its tensile strength within 60 days” post-implantation *in vivo* (U.S. Pharmacopeia). According to this definition, fibroin is correctly classified as non-degradable, since *in vivo*, in general, silk is slowly absorbed (Altman et al., 2003). However, silk fibroin is degradable, via both enzymatic (biodegradation) and non-enzymatic (hydrolysis) processes (Wang et al., 2008). Several studies have been performed to evaluate the biodegradability of films, fibers and porous sponges. To this purpose, different proteolytic enzymes have been used in *in vitro* experiments, including chymotrypsin, which is produced by macrophages during an inflammatory response. Regarding *in vivo* studies, it was shown that fibroin is degradable but over long time periods, due to proteolytic degradation (Cao and Wang, 2009; Liu et al., 2015). The rate of degradation depends on many factors, generally related to structural and morphological features (*e.g.* crystallinity, porosity and MW) induced mainly by the processing conditions, as well as characteristics of the biological environment at the implantation site, mainly in terms of mechanical and chemical stresses. The final wastes of SF are the corresponding amino acids, which are non-toxic and easily absorbed *in vivo*.

In summary, SF, thanks to its chemical composition and structure, has been shown to exhibit a good biocompatibility, at least comparable to commonly used biomaterials. SF has been proven to be a promising material for biomedical applications, and particularly

for the fabrication of scaffolds for tissue engineering, as discussed in the following paragraphs.

1.3.2. Fibroin-based systems for TERM

Tissue engineering (TE) and regenerative medicine (RM) can be considered innovative biomedical approaches to the treatment of a range of human diseases (Blitterswijk and Boer, 2015). The aim is therefore the regeneration of structures in the organism, which have been compromised by traumas and/or pathologies, by implanting in the damaged site new tissue artificially produced or biocompatible constructs able to support the tissue formation *in vivo* (Chan and Leong, 2008). In many successful TE approaches, a scaffold made of a biocompatible material has been used as support to produce and grow the new functional tissue (O'Brien, 2011). A scaffold is a three-dimensional structure able to guide tissue development, eventually combined with a cell source able to regenerate the tissue (Motta et al., 2013). From the various attempts to create an optimal substrate for cell guidance and tissue formation, a crucial evidence was the importance to mimic the natural cell environment (Zhang et al., 2012b). In all tissues, cells exist within a 3D viscoelastic and fibrillar matrix, the ECM, with multiple roles (Yi et al., 2017). ECM is synthesized by cells and provides not only the structural and mechanical properties of tissues but also the regulation of cell behaviour through chemical and physical signalling. Accordingly, extensive efforts were dedicated to the design of systems inspired by the natural cell microenvironment (Wu et al., 2014). Scaffolds and other cell substrates for TE need to offer appropriate surface morphology and chemistry, mechanical properties, and degradation time, in order to promote the development of the selected cells. Also,

the influence of scaffold structure on the transport of nutrients and cell metabolic wastes has to be considered, usually by regulating the porosity with specific size and distribution (Kuboyama et al., 2013). Many materials can be used for scaffolds production, and silk fibroin is one of the most promising ones. Silk fibroin offers versatility in matrix scaffold design with mechanical performance and biological interactions that can fit for a variety of tissue engineering needs, such as reconstruction of bone, ligaments and tendons, blood vessels, epithelium and cartilage (Vepari and Kaplan, 2007). In fact, as previously described, SF can be dissolved, and its solutions can be processed by different tunable strategies into solid constructs. Hydrogels, sponges, fibers, particles, microspheres, powders, tubes, membranes and films, and electro-spun fiber mats have been prepared from such solutions (Fig. 7) (Unger et al., 2004; Stoppato et al., 2013). For example, the surface properties of fibroin films were exploited to guide and enhance cell growth (Cai et al., 2017). The mechanical properties of silk hydrogels, obtained by sonication after incorporation of cell suspension into SF solution, have been found to be suitable for the preparation of scaffolds for cartilage regeneration (Chao et al., 2010). In another study, *in vivo*, SF hydrogel healed a critical size defect in the trabecular bone of rabbits. The result was comparable with that obtained with the synthetic polymeric control gel, but, in case of SF, the hydrogel improved bone remodelling and growth (Fini et al., 2005). Electrospun silk nanofiber mats, that have large surface areas with porous structures, are useful for cell seeding. Three-dimensional constructs of silk nanofibers have been used as blood vessel grafts and nerve guides (Zhang et al., 2009). Such regenerated fibers have important advantages over native silk fibers: their morphology and properties can be tuned according to the application, and biomolecules can be incorporated during the silk

solution regeneration step. Silk fibroin nets pre-seeded with cell co-culture were implanted in mice and the results showed that they stimulated the host capillaries to rapidly grow into the scaffold, which was vascularized in two weeks of *in vivo* experiment (Unger et al., 2010). Porous 3D sponges can closely mimic the *in vivo* physiological cell microenvironment, therefore are ideal structures for tissue engineering scaffolds. Salt leached 3D silk scaffolds have been commonly used in bone and cartilage engineering applications, because they guarantee good control over the porosity and pore size (Meinel et al., 2004; Kim et al., 2005). In addition, SF materials have been designed and fabricated for drug delivery applications. SF films and fibroin hydrogels have been studied as release vehicles for drug delivery systems (Coburn et al., 2015). Regenerated silk powders are used for drug carrier applications, and, secondly, for reinforcing scaffolds to improve mechanical properties and cellular processes (Rockwood et al., 2011). Some of these constructs can be visualized in Fig. 7.

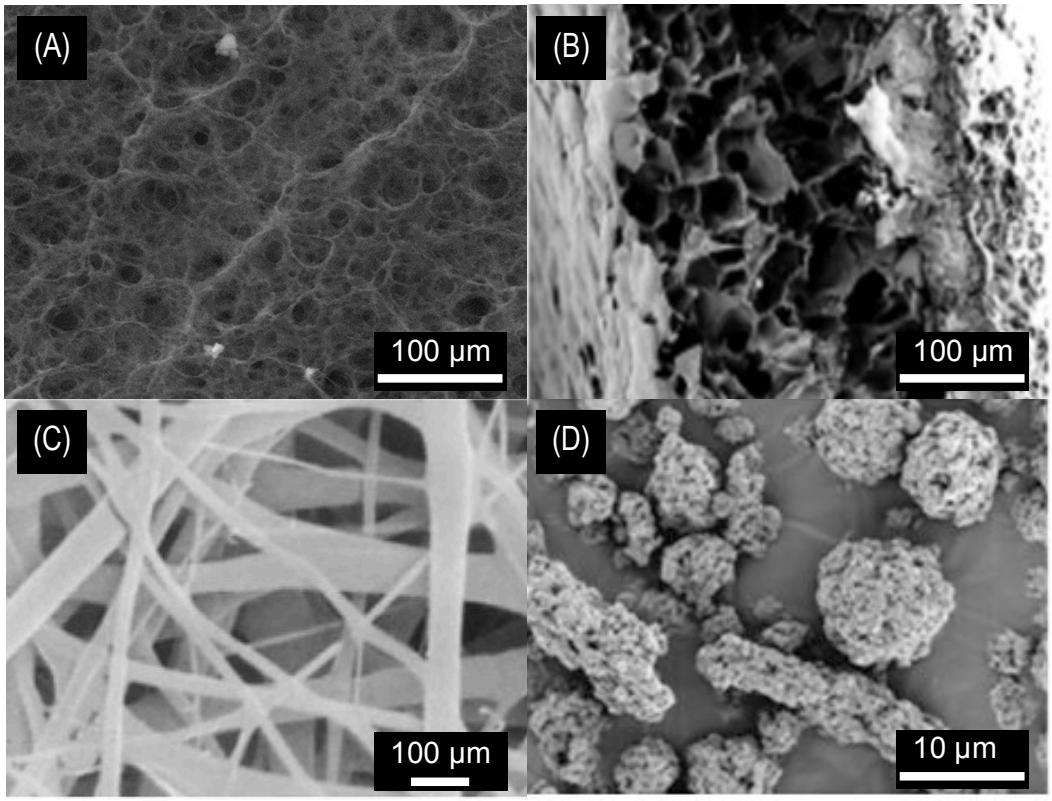

Fig. 7 Electron microscope pictures of constructs that can be obtained by processing SF solutions with different strategies: (A) SF hydrogel (Motta et al., 2004); (B) SF porous membrane (Cai et al., 2017); (C) non-woven SF fibers scaffold (Zhang et al., 2009); (D) SF particles obtained by milling process (Rajkhowa et al., 2010).

Finally, an important aspect to consider when designing a scaffold or a system with medical applications is the type of process that can be used for its sterilization before usage (implantation, administration, injection). Different sterilization methods (*e.g.*, autoclaving, ethylene oxide gas, gamma-irradiation, UV-irradiation, and ethanol treatments) can be selected for fibroin materials (Gil et al., 2014). Since these techniques can influence the secondary structure, crystal size, and supramolecular features of silk fibroin, they can also have some effects on the degradation rate and mechanical properties, and should be always evaluated (Gil et al., 2014).

1.3.3. Fibroin-based commercial products for biomedical applications

In recent years, from the translational point of view, only few silk fibroin-based medical products have obtained regulatory approval for clinical use in the world. This aspect of the biomedical silk topic is reviewed and discussed in detail in the very recent manuscript published by Holland et al., and is briefly reported here with some of the most relevant example of commercial silk-based products (Holland et al., 2019). One of them is SERI® Surgical Scaffold (Sofregen Medical Inc., Medford, MA, U.S.; approved by the U.S. FDA). SERI® is a knitted silk mesh intended for tissue support and repair in breast reconstruction. In China, HQ® Matrix Medical Wound Dressing and Sidaiyi® wound dressing (Suzhou Soho Biomaterial Science and Technology Co., Ltd, Suzhou, China) were approved by the China Food and Drug Administration (CFDA), and both of the products underwent clinical trials approved by the NIH, specifically by the U.S. Department of Health and Human Services. Tympasil (Daewoong-Bio, Seoul, Korea), a silk fibroin patch used as a tympanic membrane, was approved by the Ministry of Food and Drug Safety of South Korea.

1.4. Bone tissue engineering

All the three systems described in the experimental section of this manuscript rely on the use of silk fibroin as starting and main component for their fabrication. Considering the chemico-physical, structural and morphological features of these fibroin devices, and considering the well reported biological outcomes of the potential therapeutic agents (the H_2S donor morpholin-4-ium 4-methoxyphenyl-morpholino-phosphinodithioate, the inorganic phase

beta-tricalcium phosphate, and the neuropeptide substance P, respectively) (Ng et al., 2008; Leal et al., 2015; Grassi et al., 2016) combined with fibroin, these systems could be reasonably considered for application in bone tissue engineering and regeneration. For this reason, in this paragraph, bone biology is introduced along with the description of tissue-engineering approaches as treatments for orthopaedic defects.

1.4.1. Characteristics of bone, a highly dynamic tissue

Bone is the connective tissue that provides an internal support system in higher vertebrates (Bilezikian et al., 2008). Similarly to other organs in the body, bone tissue has a hierarchical organization that moves from the macro-scale to the nanostructured components of the ECM. Different loading conditions influence the development of distinct bones with specific shapes, mechanical properties, and location in the body. Bone tissue itself is arranged in a compact pattern (cortical bone) or a trabecular and porous pattern (cancellous or spongy bone). Cortical bone is composed of densely packed collagen fibrils forming concentric lamellae. In contrast, cancellous bone has a loosely organized, porous matrix and provides metabolic functions. The pores are filled with bone marrow or fat. The morphology is characterized by a 50-90% porosity with pore sizes in the order of 1 mm in diameter, and cortical bone surrounding it (Cooper et al., 2004; Morgan et al., 2013).

The composition of bone tissue is approximately 35% organic and 65% inorganic. The organic ECM of bone consists of a complex self-assembly of collagens (around 95% of the organic ECM), mainly of type I, which is a fibrillar collagen essential for bone strength. Other

macromolecules are osteocalcin, osteopontin, osteonectin, bone sialoprotein, hyaluronic acids and proteoglycans (Bilezikian et al., 2008). The inorganic mineral phase consists of crystalline salts deposited in the organic matrix by specific cell metabolic processes. They are primarily calcium (Ca) and phosphate in the form of hydroxyapatite (HA), and other inorganic salts (Yan et al., 2012). The mineral content confers rigidity and strength to the skeleton while still maintaining some elasticity. Moreover, it makes bone the major source of inorganic ions thus participating actively in the calcium homeostasis of the whole body. Regarding the cell population, bone is composed of four different cell types: osteoblasts; osteoclasts and bone lining cells, distributed on bone surfaces; osteocytes populating the mineralized internal matrix (Fig. 8).

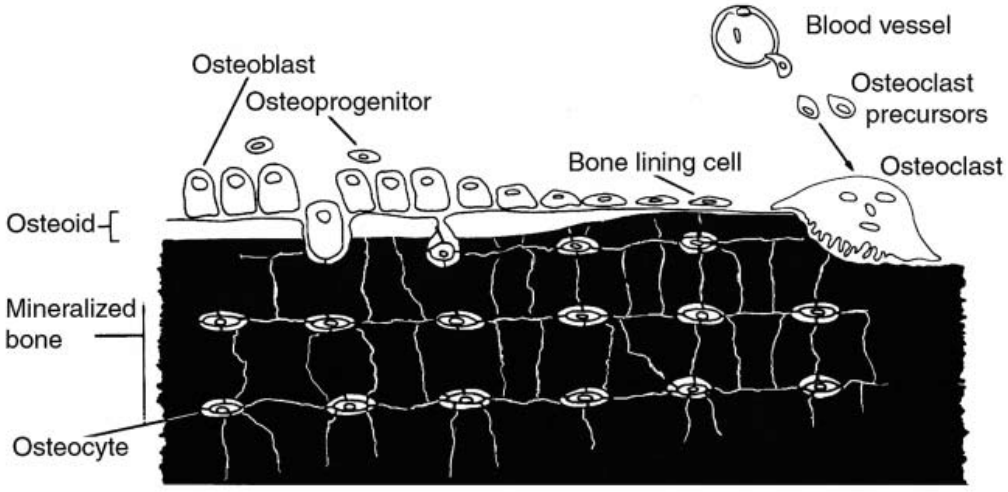

Fig. 8 Type and location of bone cells (Marks and Popoff, 1988). With permission of John Wiley and Sons.

Osteoclasts originate from the fusion of mononuclear precursors, deriving from the various hematopoietic tissues, while osteoblasts, osteocytes, and bone-lining cells originate from local osteoprogenitor cells, the mesenchymal stem cells (MSCs), located in the bone marrow (Bilezikian et al., 2008). Osteoblasts are fully differentiated

cells that produce the bone matrix, by secreting type I collagen and the other non-collagenous proteins. Osteoblasts regulate the mineralization of bone matrix, and collagen is the template for its initiation and propagation (Marks and Popoff, 1988).

Bone lining cells are flat, elongated, inactive cells that cover bone surfaces that are undergoing neither bone formation nor resorption. Even if little is known regarding the function of these cells, they could be precursors for osteoblasts (Marks and Popoff, 1988).

Osteoclasts are large cells that resorb bone. Their membranes possess two specific activities: bone resorption that takes place in the ruffled membrane area, and attachment of the osteoclast to the underlying bone matrix.

Osteocytes are the mature osteoblasts located within the bone matrix. Since deposition of mineral makes the matrix impermeable, osteocytes are responsible to ensure cell metabolic processes by establishing numerous cytoplasmic connections (filopodia) with adjacent cells, internal and external surfaces of bone, and with the blood vessels traversing the matrix. Osteocytes have also the capacity both to synthesize and to resorb matrix, even if to a limited extent (Marks and Popoff, 1988).

Thanks to cell activities, bone tissue undergoes a continuous renewal in a delicate equilibrium of processes between synthesis and degradation of the extracellular matrix. In fact, bone is considered a dynamic tissue and it possesses a high regenerative capacity. It is continually remodelled during formation and resorption processes operated by the interactive activity of osteoblasts and osteoclasts, as an adaption to different stimuli such as mechanical loads, biochemical regulatory factors, and other environmental parameters. In particular, in bone remodelling processes, mineral homeostasis is fundamental. There are various elements that are relevant for bone

formation. As anticipated, the most abundant is calcium, followed by magnesium (Mg), silicon (Si), and others (such as Al, B, etc.).

More than 99% of body calcium is stored in bone and teeth. The reservoir functions of bone are highly dynamic and modulate, on a moment-to-moment basis, the balance between new bone formation and old bone resorption (Bilezikian et al., 2008). Calcium functionality in human body is very broad; in fact, all cells have regulatory systems (based on ion channels) used to balance calcium ions (Ca^{2+}) concentration between the cell interior and the extracellular fluid surrounding the cell. These systems permit cells to use calcium as a versatile signalling substance throughout the body. Recently, it was discovered that a key player in Ca^{2+} homeostasis in bone is hydrogen sulfide (Liu et al., 2014). This is one of the central topics of this dissertation and is deeply discussed in the Chapter 3.

Mg influences the formation and activity of hormones that regulate skeletal homeostasis. Mg can also directly affect bone cell function, and influences hydroxyapatite crystal formation and growth. Mg supplement has generally led to an increase in bone mineral density and bone mass in osteoporotic patients, and Mg-based alloys were successfully used as bone scaffolds (Witte et al., 2007).

Si is considered as an essential element for healthy bone and vascular development. It holds many functions in bone tissue: it may acts as a primary nucleation centre for apatite formation; silicon-substituted calcium phosphates are very effective in bone formation; the presence of silicon improves collagen and proteoglycans synthesis, which are critical point the structural integrity and mechanical strength of the tissue (Jugdaohsingh, 2007; Bilezikian et al., 2008). In *in vitro* and *in vivo* experiments, administration of Si ions from exogenous sources have been verified to stimulate the osteogenic differentiation of human bone marrow stromal cells and

enhance the pro-angiogenesis of endothelial cells (Li et al., 2017). Bioactive glasses and other Si-based materials have shown osteoconductive and osteoinductive properties, and are used to fabricate bone implants and implant coatings (Carlomagno et al., 2018; Le et al., 2018).

1.4.2. Tissue engineering for bone repair

In case of injury, bone healing generally occurs without the need for major intervention, especially in younger people. Despite this, serious events like large bone tumour resections or non-union fractures may compromise a complete regeneration of the tissue and require surgical operations (Einhorn and Gerstenfeld, 2015). The gold standard approach is the treatment with autografts (transplantation of tissue harvested from the same patient), but their short supply and the risks connected with the harvest generated the need to adopt alternative strategies (Cypher and Grossman, 1996).

For multiple clinical reasons, a bone tissue-engineering approach can be considered an excellent alternative solution to traditional treatments for orthopaedic defects. For example, the need for better filler materials for bone reconstruction, and the need for implants with suitable mechanical properties in relation with their biological environment.

Bone TE relies on the knowledge of bone structure, composition, mechanics and tissue formation (Melke et al., 2016). Guiding stem cells along the osteogenic lineage is a critical step in bone regeneration and it is well known that the ECM plays a main role in regulating the stem cell fate. MSCs recruitment, adhesion and differentiation also play an important role in the repair of bone fractures. ECM is extremely important because it supports cells and

helps in immobilizing signalling biomolecules, such as growth factors and cytokines, which guide MSCs differentiation. As stated before, the major components of human bone ECM are collagen type I and inorganic hydroxyapatite, with small amounts of other macromolecules.

In the case of bone, tissue engineered scaffolds materials should preferably be osteoinductive (capable of promoting the differentiation of progenitor cells down an osteoblastic lineage), osteoconductive (able to support bone growth and encourage the ingrowth of surrounding bone), and thus capable of osseointegration (Stevens, 2008). In other words, bone scaffolds should be matrices with high porosity and interconnectivity, to allow cell ingrowth and distribution, facilitate the neovascularization of the construct from the surrounding tissue, and permit diffusion of nutrients and gases and removal of metabolic waste (Hutmacher, 2000). Moreover, surface properties (chemical and topographical) should promote cell functions (adhesion, proliferation and differentiation), and scaffold mechanical strength should withstand the natural hydrostatic pressures and maintain the spaces required for cell ingrowth and matrix production (Salgado et al., 2004). Degradation rate must be tuned appropriately with the growth time of the new tissue. These characteristics might make the scaffold biomimetic, *i.e.,* able to provide an environment supportive for bone formation and elicit specific cell responses.

Fibroin constructs, produced by different strategies and in different morphologies, demonstrated great biocompatibility as biomaterials (scaffolds, 2D-constructs, particles, drug delivery systems) for bone tissue engineering, thanks to all the featured properties described previously. In particular, 3D-porous systems were shown to have the ability to enhance cell attachment, proliferation and migration, good biodegradability properties, and suitable morphology, in terms of

quality and degree of porosity, to serve as scaffolds for bone regeneration (Correia et al., 2012). In different experiments, SF scaffolds were shown to be osteoconductive, by promoting *in vitro* osteogenesis in a range of bone-related cell types (Karageorgiou and Kaplan, 2005; Fuchs et al., 2009; Ghanaati et al., 2011; Li et al., 2014), and supporting the formation of new bone tissue when implanted *in vivo* (Maraldi et al., 2011; Riccio et al., 2011). In addition, thanks to the stability and the flexibility of these materials, various modifications of SF scaffolds have been generated with chemical, structural and biological innovations. SF scaffolds were also successfully combined with various bioactive agents, growth factors, and inorganic materials containing Ca, Si or Mg (Mouriño and Boccaccini, 2010; Wenk et al., 2011; Le et al., 2018), with the final goal of enhancing the osteoinductive properties and the regenerative potentials.

Considering the increasing demand of specialized therapies and the potentialities of silk fibroin-based systems, more and more medical strategies based on the use of this biomaterial to fabricate scaffolds and drug delivery systems are expected to emerge in the next years.

Chapter II. Rationale, aims and design of the research activity

The wide processability of fibroin solutions and the biocompatibility of the fibroin-based systems obtained for a range of biomedical applications have been demonstrated and are still under investigation in many studies conducted in different laboratories all around the world.

In the biomedical field, the functional material fabricated starting from fibroin protein generally consist of a scaffold, if it is designed to function as a support for cell adhesion and tissue growth, or in a drug delivery system, when the scope is the encapsulation of bioactive compounds for the controlled delivery and release in body tissues. For some advanced applications, these two approaches are combined in a unique system with multiple biomedical functions.

The goal of this PhD work is to prove that regenerated fibroin can function as a flexible platform to produce multifunctional systems for bone tissue regeneration application. Moreover, this dissertation aims to demonstrate that different chemico-physical and engineering approaches can be adopted to fabricate fibroin materials, and to provide them with additional tunable properties and functionalities.

In particular, with the increasing knowledge of the roles that different bioactive molecules and inorganic materials play in specific bone pathologies and/or injuries, researchers are now focusing on designing biomaterials to actively control the metabolism of cells of different phenotypes and promote healing outcomes. In the context of this dissertation, which focuses on bone tissue engineering, compounds with a specific bioactivity versus bone derived cells and cells of the immune system were considered.

To address the goals of this work, the experimental activity has been divided in three main research lines, schematically represented in Fig. 9.

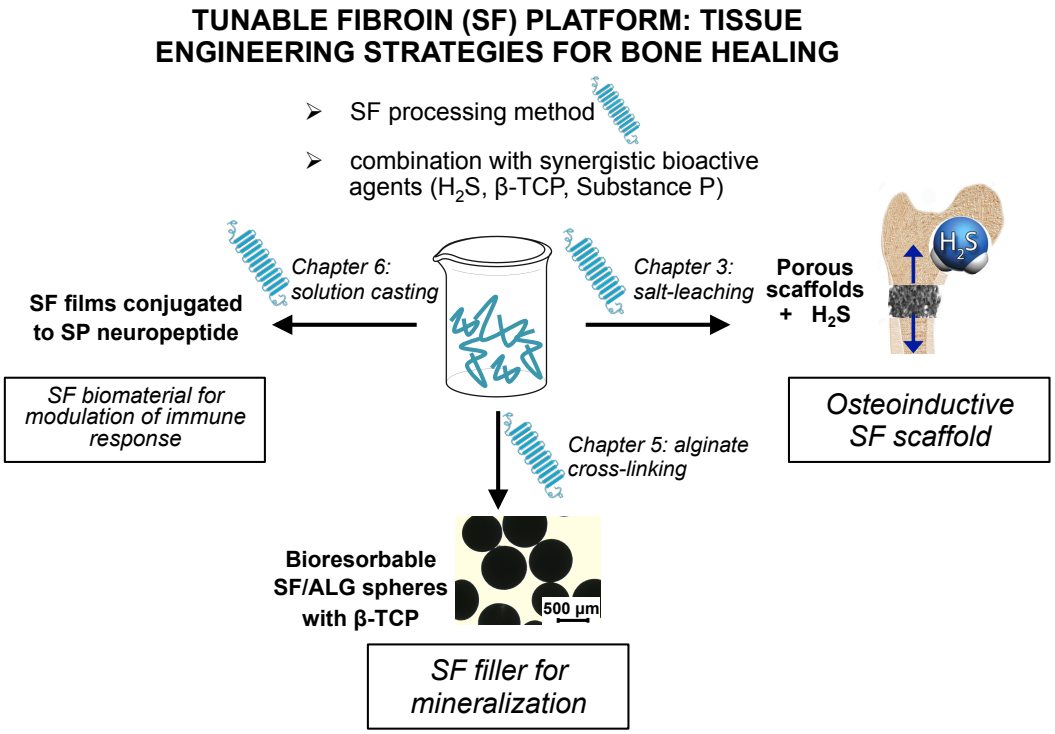

Fig. 9 Schematic representation of the organization of the research activities described in this dissertation. The chapter where each research line is described is indicated.

The research activities consisted of:

1) Preparation and characterization of fibroin porous scaffolds loaded with the hydrogen sulfide donor GYY4137. The production of salt-leached fibroin scaffolds was optimized, in order to obtain highly porous matrices. Then, a strategy to combine the scaffolds with GYY4137 was designed and applied in order to obtain a controlled loading process of the matrices and a successive sustained release of H_2S upon incubation in liquid media. The scaffolds were tested in *in*

vitro experiments with an osteogenic 3D culture in dynamic conditions, to evaluate their ability to sustain cell adhesion, proliferation and viability, and to induce cell differentiation and bone formation. This study was supported by the grant "Ricerca Finalizzata" awarded by the Italian Ministry of Health to the coordinator Doctor Francesco Grassi (number and title of the project: RF PE-2011-02348395; "Novel approach for bone regeneration and repair using sulphur donor-based therapy").

2) Design and fabrication of a new composite system based on calcium phosphate and silk fibroin that could be potentially exploited in bone tissue engineering applications. Thanks to its excellent osteoconductive and osteointegrative properties, β-tricalcium phosphate (β-TCP) is an effective inorganic filler to treat small bone defects already applied in clinics. β-TCP commercially occurs as a fine powder, which can be difficult to measure and manipulate. A good strategy to work with β-TCP and to implant it into bone defects is the dispersion of its powder into polymer solutions that can be formed into different shapes, typically micro/millimetric beads. By combining in solution SF and alginate (ALG), the ability of ALG to easily gel when contacted with Ca^{2+} ions was exploited to form SF-based beads, with an easy, low-cost, organic solvent-free. SF/ALG/β-TCP beads were prepared and characterized, in order to obtain a biocompatible and effective system for the implantation of β-TCP into bone defects. This work was funded by "REMIX" Project, G.A. 778078 H2020-MSCA-RISE-2017.

3) Preliminary studies on strategies for the treatment of inflammation induced by the implantation of a scaffold. Silk

fibroin films combined with the neuropeptide substance P (SP) were used as models to study conjugation and release mechanisms of SP with SF and investigate the possibility of fabricating a multifunctional material able to modulate inflammation processes.

Chapter III. Silk fibroin scaffolds loaded with a H_2S-donor as a novel therapeutic approach for bone regeneration

Part of this chapter has been published in:

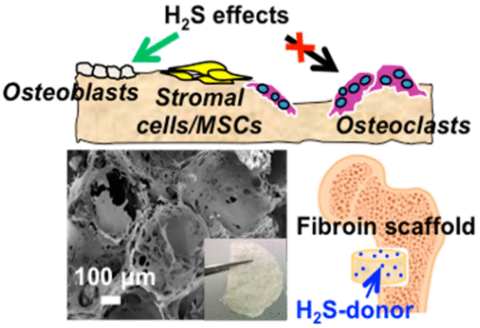

Rosasilvia Raggio, Walter Bonani, Emanuela Callone, Sandra Dirè, Laura Gambari, Francesco Grassi, and Antonella Motta

Silk Fibroin Porous Scaffolds Loaded with a Slow-Releasing Hydrogen Sulfide Agent (GYY4137) for Applications of Tissue Engineering

ACS Biomaterials Science & Engineering 4 (2018) 2956-2966

3.1. Introduction

3.1.1. Hydrogen sulfide in bone homeostasis

Hydrogen sulfide (H_2S) is a colourless gaseous compound under ambient temperature and pressure. It is a weak acid, water soluble (solubility of around 80 mM at 37°C), and exists in solution as an equilibrium between the gas and two aqueous species:

$H_2S_{(g)} \rightleftharpoons H_2S_{(aq)} \rightleftharpoons HS^- + H^+ \rightleftharpoons S^{2-} + H^+$

The pKa values for the first and second dissociation steps are 7.0 and >12.0, respectively. Therefore, at pH of 7.4, the major form of hydrogen sulfide exists as HS^-, with a minor amount of free H_2S (the

ratio of HS^-/H_2S is around 3/1). It is not clear which form is the active biological species, so the term H_2S is used to refer to the total sulfide present in the solution (*i.e.*, $H_2S + HS^- + S^{2-}$) (Zhao et al., 2014).

Hydrogen sulfide is known to be toxic for mammals even in low concentrations. The direct inhibition of the activity of cytochrome oxidase is the primary biochemical effect associated with lethal H_2S exposure (Eghbal et al., 2004). However, H_2S is also physiologically present in mammalian tissues, produced by cells in nanomolar quantities as a signal-transducing gasotransmitter molecule (Vandiver and Snyder, 2012). The lipid-soluble nature of H_2S determines its ubiquitous presence in different tissues and enables this gasotransmitter to easily reach its molecular targets, in cells and intracellular organelles.

In particular, numerous cellular effects of H_2S are considered to be due to its interactions with cell membrane ion channels.

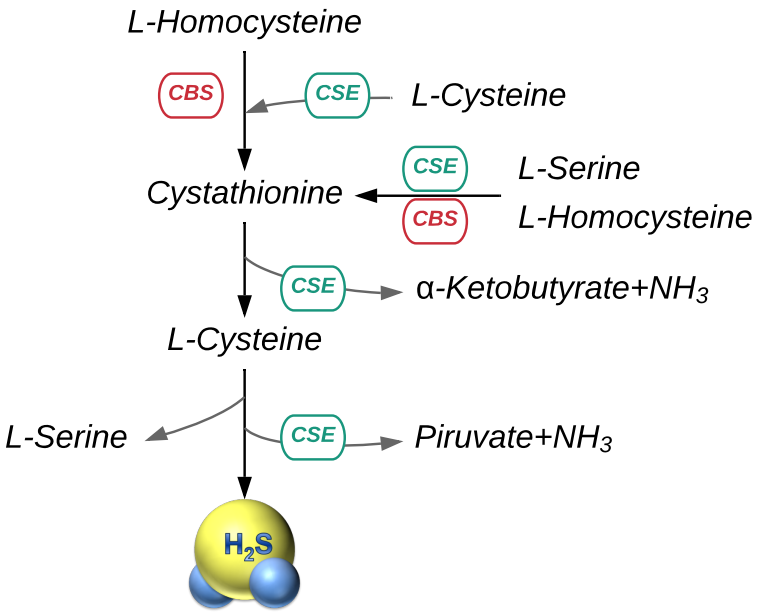

Fig. 10 Biological pathway, composed of trans-sulfuration reactions, of the enzymatic generation (by CBS and CSE enzymes) of hydrogen sulfide in mammalian cells.

In mammals, H_2S is mainly generated by L-cysteine reactions with two enzymes, termed cystathionine-β-synthase (CBS) and cystathionine-γ-lyase (CSE), which are expressed in many human cells types (Fig. 10).

Anomalous H_2S metabolism has been linked to some human diseases, including Alzheimer's disease, hypertension, heart disease, atherosclerosis, ocular pathologies, pancreatitis, type I diabetes, and bone pathologies. Interestingly, regarding bone, it was shown that CBS deficiency is the most frequent cause of two inherited disorders, hyperhomocysteinemia and homocystinuria, characterized by an increased risk of bone fracture and significantly reduced H_2S levels (Morris et al., 2017). Even if the increased incidence of osteoporotic symptoms in these patients remains unclear, there are evidences that a stable, low level of H_2S may play a role in maintaining the homeostasis of bone tissue. The studies of Liu and collaborators firstly showed that H_2S regulates the amount of Ca^{2+} influx through bone cells membranes (Liu et al., 2014). As result of the experiments, H_2S appeared to be relevant for the formation and preservation of bone mass, whereas H_2S deficiency impaired the osteogenic differentiation of SCs.

3.1.2. Administration of hydrogen sulfide as potential therapeutic agent

The advances in understanding hydrogen sulfide physiological roles in human body tissues and in relation with certain categories of pathologies have been followed very quickly by attempts to develop novel therapeutics based on the delivery of exogenous H_2S (Sestito et al., 2017). Strategies were developed considering two important factors: physiological concentrations of H_2S in human body tissues

are different and difficult to measure, going from 30-100 μM in the blood to 50-160 μM in the brain (Wallace, 2007); H_2S is a gaseous compound, therefore is difficult to manipulate.

For this reason, reagents classified as H_2S-donor are usually employed to generate H_2S in the environment required for the application. They are typically injected, after dissolution in proper media. The sodium salt NaHS is the typical example of an H_2S-donor: in solution, it rapidly decomposes generating hydrogen sulfide. It is widely used for experimental purposes, since it is easy to dissolve and cheap. However, because it is easily oxidized in air, and it rapidly generates H_2S with possible toxic effects, neither NaHS nor equivalent sulfide salts are suitable for medical applications.

Garlic is rich in organosulfur compounds (the main one is allicin, or diallyl thiosulfinate), which are unstable in aqueous solution, and rapidly decomposes mainly to diallyl sulfide, diallyl di- and tri-sulfide. It was shown that human red blood cells can slowly convert garlic-derived organic polysulfides into hydrogen sulfide (H_2S), just after consumption, indicating that these compounds are rapidly metabolized. Garlic products were proven to be natural bioavailable sources of hydrogen sulfide, with promising therapeutic applications (Benavides et al., 2007).

The most common H_2S-donors are of synthetic origin. Among them, a successful example is the phosphinodithioate derivative morpholin-4-ium 4-methoxyphenyl-morpholino-phosphinodithioate (GYY), which has been used in a large number of experimental studies (Li et al., 2008b). For example, Grassi *et al.* reported that ovariectomy (ovx) was applied on mice to induce downregulation of the key enzymes CBS and CSE. In operated mice the production of H_2S in the MSCs and total number of bone marrow cells were impaired by this procedure. Then, they reported that pharmacological restoration of

normal serum levels of H_2S with GYY injections could prevent ovx-induced bone loss by enhancing bone formation (Grassi et al., 2016).
Other H_2S-donors investigated as therapeutic agent are for example arylthioamides, such as 4-hydroxybenzothioamide (Martelli et al., 2012), and perthiols with the general chemical structure R-S-SH (Zhao et al., 2013).
Even after systemic administration of H_2S donors at doses that produce pharmacological effects, plasma H_2S concentrations rarely rise above the physiological range, or do so for only a very brief period of time (few minutes), due to the efficient systems for metabolizing H_2S. Consequently, for treatments that necessitate of a slow, prolonged and sustained release of hydrogen sulfide, strategies different from injection of donors' solutions should be explored.
In the last two years, the investigation of suitable matrices for the encapsulation or loading of hydrogen sulfide donors for different applications has been conducted, ranging from the design of systems for cardiovascular therapies to nanostructured patches with antioxidant and anti-inflammatory properties for tissue repair.
In a recently published study, a hydrogel, made of alginate crosslinked with gelatine and loaded with adipose derived stem cells (ADSC), with properties of controllable H_2S-release, has been constructed. The hydrogels were combined with an organic thiol-dependent H_2S-releasing compound (2-aminopyridine-5-thiocarbox-amide or APTC), and investigated for the ability to target the symptoms of myocardial infarction (Liang et al., 2019). They could prove that the conductivity and hydrogen sulfide-releasing properties of the hydrogels effectively improved the myocardial infarction zone.
Another almost contemporary research was focused on the production of poly(lactic) acid fibrous membranes, functionalized with an H_2S slow-releasing donors extracted from garlic. These innovative

H_2S-releasing mats were characterized and their effects on the *in vitro* human cardiac MSC growth were investigated. Thanks to their ability to stimulate the cardiac MSC proliferation and reduce the oxidative damage induced by hydrogen peroxide treatments, H_2S-releasing membranes were considered to be promising for biomedical applications in tissue repair (Cacciotti et al., 2018).
Examples of H_2S-releasing biomaterials can be found in literature. However, the study reported in this chapter, and published in a 2018 article by our research group, was the first one targeting bone tissue regeneration applications.

3.2. Materials and methods

3.2.1. Preparation of SF aqueous solution

White polyhybrid *Bombyx mori* cocoons (purchased from Chul Thai Silk Co., Phetchabun, Thailand) were used as source of silk and silk fibroin. The commercial reagents sodium carbonate (Na_2CO_3) and lithium bromide (LiBr) were purchased from Sigma-Aldrich (Saint Louis, MO, USA). Deionized water (DI water) was produced by using the Elix® Reference 5 water purification system (Merck KGaA, Darmstadt, Germany).
Silk cocoons were cut in pieces, and some of their concentric layers were separated, obtaining small silk “sheets”. Silk of cocoon pieces was degummed by immersion and boiling in aqueous sodium carbonate solutions. The process was divided in two consecutive treatments with Na_2CO_3 aqueous solutions, at a concentration of 1.1 g/l, and 0.4 g/l respectively, at 98°C for 1.5 hours each time. The fibers mass obtained was deeply rinsed with DI water, and then air-dried. At this point, dry fibroin fibers can be stored at room temperature and pressure and low humidity. To prepare fibroin

solution in water, degummed SF was dissolved at a concentration of 20% w/V in 9.3 M aqueous LiBr at 65°C for 4 h. After the set time, the mixture appeared as a yellowish, limpid and viscous solution, with no fibers left in suspension. To eliminate dissolved LiBr, the solution was transferred by syringe in a Slide-A-Lyzer™ Dialysis Cassette (Thermo Fisher Scientific, Waltham, MA, USA) with 3.5 KDa of molecular weight cut-off (MWCO), and dialyzed against DI water for 3 days, with regular water changes 3 times/day. Finally, SF aqueous solution was filtered using a glass porous septum to eliminate any solid residue in suspension. The pH of SF was measured with a Crison pHmeter (Hach Lange, Spain), to assess the typical pH of aqueous fibroin solutions at around 6.5.

The concentration was measured using a NanoDrop® microvolume spectrophotometer and a standard curve registered at 280 nm, suitable for the determination of protein solutions. For scaffold preparation, the concentration was always adjusted to 8% w/V, by a pre-concentration step consisting in a short dialysis (around 4 hours) against PEG (poly (ethylene glycol), Merck KGaA, Darmstadt, Germany) at 25% w/V in water.

3.2.2. Preparation of SF-based scaffolds

Porous SF scaffolds were produced by solvent casting and particulate leaching method, adopting a protocol adapted from Rockwood *et al.* (Rockwood et al., 2011b). Every sponge was prepared by placing 14 g of granular sodium chloride (NaCl; Sigma-Aldrich, Saint Louis, MO, USA) in a polystyrene Petri dish. Since the scaffold pore sizes typically results slightly smaller than the salt particles used, as the salt is partially dissolved while the fibroin solution gels, it is important to start with salt particles slightly larger

than the final required pore volume. In this case, the particle size selected was between 425 and 800 μm. Then, around 6.5 ml of 8% w/V fibroin aqueous solution were poured on the salt, maintaining the ratio of grams of NaCl to grams of fibroin around 25 to 1. After 48 hours at room temperature, gelation of SF solution occurred. The gelation mechanism relies on the presence of NaCl that partially dissociate in free Na^+ and Cl^- ions. Na^+ and Cl^- remove the molecules of water that coordinate to the hydrophilic domains of fibroin when the protein is dissolved, consequently promoting chain-chain interactions and organization of the hydrophobic domains, with the creation of a stable β-sheet conformation. NaCl was then dissolved and removed by washing samples in DI water for 4 days, with regular water changes. A solid, white, spongy and water insoluble fibroin matrix was obtained. Cylindrical-shaped scaffolds were produced using a 6 mm biopsy punch. Afterwards, samples were frozen and freeze-dried, in order to remove water while maintaining the structure.

3.2.3. Donors of hydrogen sulfide

Two different donors of hydrogen sulfide were used for the research activities: a sodium salt; an organic Lawesson's reagent derivative. Sodium sulfide nonahydrate (Na_2S*9H_2O) was purchased from Sigma-Aldrich (Saint Louis, MO, USA). As previously explained, sodium sulfide salts release H_2S very fast, and are not suitable for biomedical applications. However, Na_2S*9H_2O was used in this work to perform preliminary experiments of H_2S dissolution and evaporation studies and detection in solution, and for the calibration of the amperometric system adopted to perform H_2S-release studies from SF scaffolds.

H_2S donor GYY (M_w = 376.47 g/mol) was purchased from Cayman Chemical (Ann Arbor, MI, USA). GYY was supplied as the morpholinium salt of (p-methoxyphenyl) morpholino-phosphinodithioic acid, a white crystalline solid (Fig. 11)

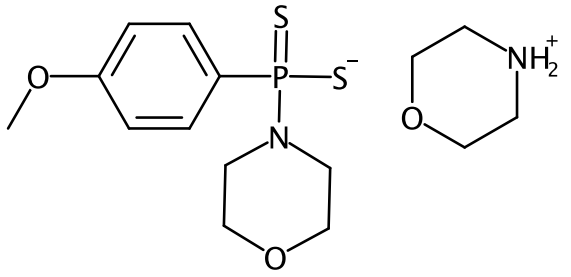

Fig. 11 Structural formula of the H_2S donor GYY4137.

Structural formulas were drawn using MarvinSketch (ChemAxon, Budapest, Hungary).

3.2.4. Preparation of SF scaffolds loaded with GYY

Anhydrous dimethyl sulfoxide (DMSO) was purchased from Sigma-Aldrich (Saint Louis, MO, USA). GYY was dissolved in DMSO to prepare three solutions at different concentration (1.5, 7.5 and 15.0 mg/ml of GYY in DMSO, respectively). Each scaffold was impregnated with 40 µl of solution of GYY in DMSO, and GYY-loaded scaffolds with 1%, 5% and 10% of GYY content in weight with respect to the SF weight were prepared. A set of samples where only pure anhydrous DMSO was poured on the scaffolds was also fabricated. The volume of loading solution was chosen based on DMSO uptake by the scaffolds, which was determined as equal to 6.9 ± 1.0 (mean ± standard error of the mean or SE) times the

weight of each scaffold (Fig. 12). The DMSO uptake was calculated according to the procedure described in paragraph 3.2.11.

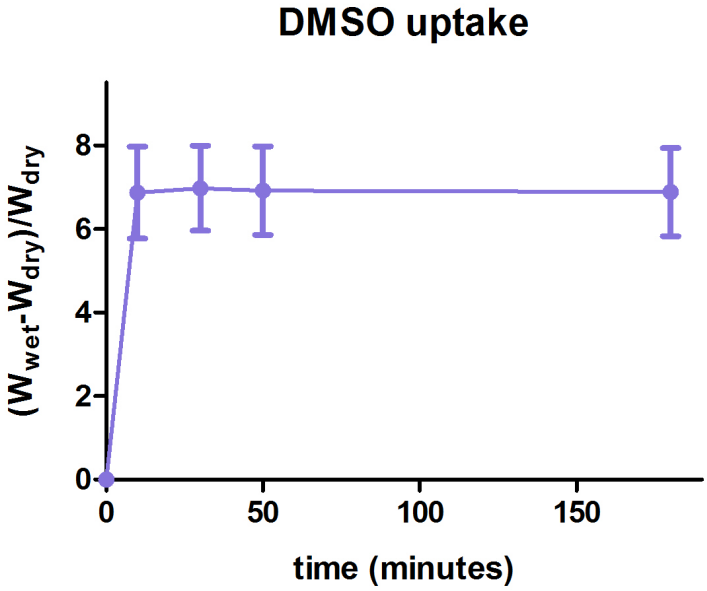

Fig. 12 DMSO uptake curve of the SF scaffolds (mean with SE, n=3), measured by calculating the ratio between the weight of DMSO absorbed and the weight of dry scaffold.

The scaffolds were then frozen at -80°C and freeze-dried for around 24 hours to remove DMSO.

3.2.5. Scaffolds sterilization

All scaffolds were sterilized by Cobalt-60 gamma (γ) irradiation in a standard cycle of 25.0 kGy (nominal dose) by Sterigenics Italy (Minerbio, Italy). Facilities and control procedures validated in conformity with the guidelines ISO 9001, ISO 13485, EN ISO 13485 and the good manufacturing practices (GMP) were used. All the characterizations were performed on the scaffolds before and after the treatment with γ-rays. Since materials modifications due to the sterilization process were not detected, in the following chapter only results obtained on γ-irradiated samples are reported.

3.2.6. Scheme of the scaffolds prepared

The different types of scaffolds obtained starting from fibroin solution, with the sample codes, and the main steps for their preparation are listed in Fig. 13.

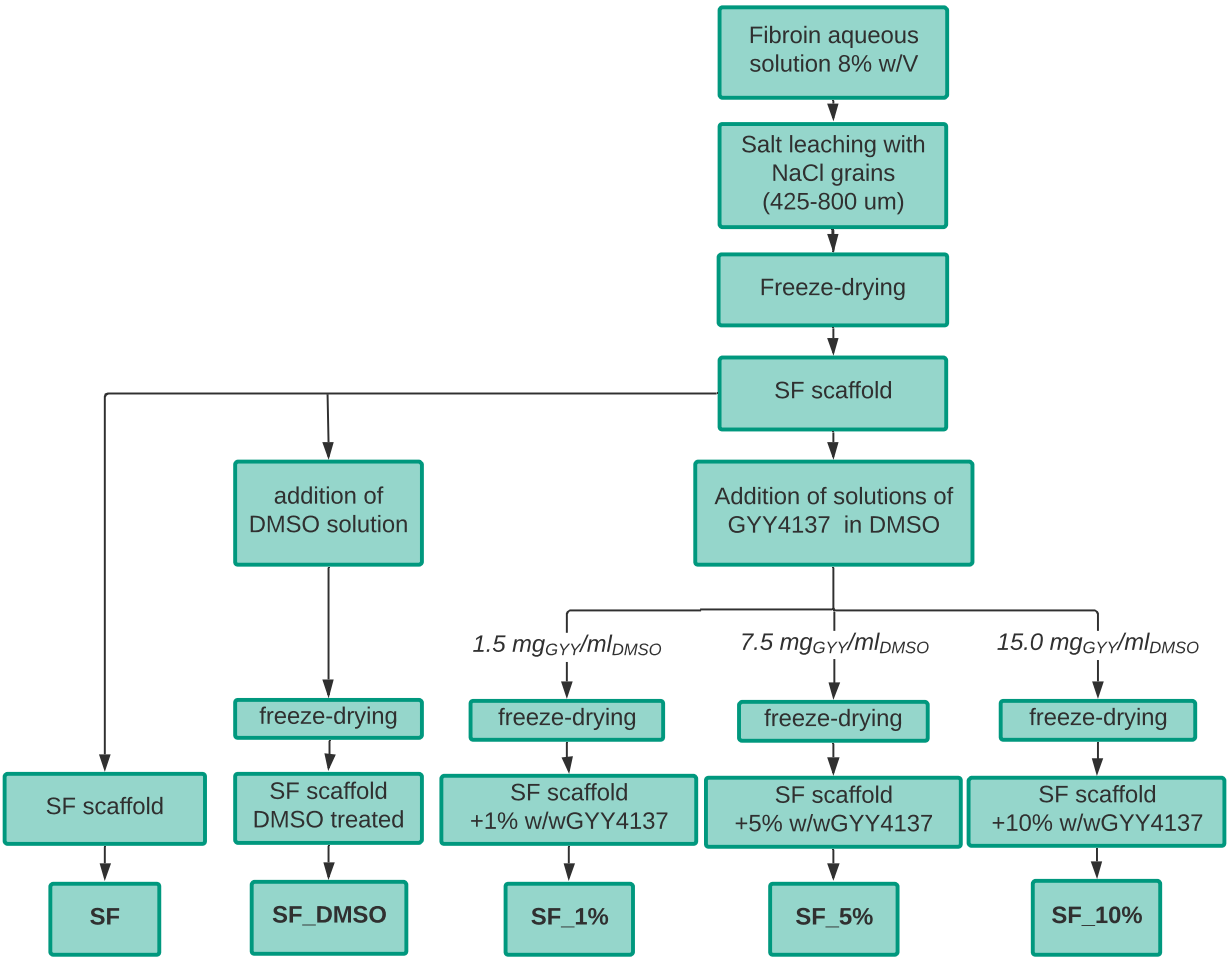

Fig. 13 Scheme of the preparation procedure, composition and codes of the scaffolds fabricated. In parallel with GYY-loaded scaffolds, also scaffolds treated with DMSO and untreated fibroin scaffolds were produced as controls.

3.2.7. Scanning electron microscopy

The analysis of the morphology, the microstructure and in particular the porosity of the SF scaffolds was performed by electron

microscopy. Specimens obtained from scaffolds of different composition were sputter-coated with a thin platinum/palladium layer (by a Q150T Turbo-Pumped Sputter Coater/Carbon Coater, Quorum Technologies, UK), and then observed with a Field Emission Scanning Electron Microscope (FE-SEM, Zeiss Supra 40, Carl Zeiss, Germany), in secondary electron mode. Pore size was measured with Image-J software (NIH, USA), considering around 100 pores for each group of scaffolds. Pore size distribution was evaluated using OriginPro 8 (OriginLab, USA) software, and expressed as mean ± standard error of the mean (SE). Gaussian distribution of pore dimension was assumed.

3.2.8. Fourier transform infrared (FT-IR) spectroscopy

Fourier transform infrared spectroscopy was used to investigate the chemico-physical properties of the materials fabricated, and, in particular: the chemical structure of GYY; the chemical structure of SF scaffolds loaded with GYY; the secondary protein structure of fibroin in the scaffolds. A Spectrum One FT-IR spectrometer (PerkinElmer, Waltham, MA, USA) equipped with selenide crystal working in attenuated total internal reflection (ATR) mode was used to collect the spectra of the different materials. Four scans for each spectrum were registered in the wavenumber range 4000-650 cm^{-1}, with a resolution of 4 cm^{-1}. Samples were analysed in dry state, deposited on FT-IR sampling surface and compressed until a minimum force of 120 N was reached, to have good peak intensity. FT-IR spectra peaks were detected by SEARCH Plus Software for PerkinElmer Spectrum One FT-IR (PerkinElmer, Waltham, MA, USA), and assigned to specific vibrations (Mistry, 2009).

To study the influence of the incorporation process into the scaffolds on GYY chemical properties, commercial GYY was solubilized in DMSO at 15 mg/ml, lyophilised and characterized by FT-IR. The GYY samples objects of the study are listed in Table 2.

Sample code	Details
GYY	commercial GYY
GYY_exDMSO	GYY solubilized in DMSO, freeze-dried

Table 2 The different forms of GYY considered in this work.

GYY absorptions were studied and assigned to investigate differences between the two forms (Alexander et al., 2015b). The presence of different fibroin secondary structures in the scaffolds was determined by analysing the Amide I region (1705-1610 cm^{-1}) of the correspondent FT-IR spectra, by OriginPro 8 (OriginLab, USA) (Barth, 2007). After selection of amide I absorption region, spectra profiles were smoothed with a nine-point Savitzky-Golay smoothing filter. Then, by using the wavenumber ranges of seven fitting peaks assigned to the different secondary structures adapted from literature, Fourier self-deconvolution (FDS tool of OriginPro 8) was applied (Hu et al., 2006; Bucciarelli et al., 2017). The seven peaks were assumed to be Gaussian and were assigned to the four different proteins secondary structures that we decided to consider for SF: β-sheet, random coil, α-helix and turns. Peaks assignment is reported in Table 3.

Band wavenumber range (cm^{-1})	Structure assignment
1616-1621	β-sheet
1622-1637	β-sheet
1638-1655	random coil
1656-1662	α-helix
1663-1670	turns
1671-1696	turns
1697-1703	β-sheet

Table 3 Infrared vibrational band assignments for the Amide I region of fibroin spectra adapted from (Hu et al., 2006).

The content percentage of secondary structures present in the scaffolds was calculated by integrating the area of each deconvoluted peak and then normalizing to the total area of the Amide I spectra region analysed.

3.2.9. Solid-state nuclear magnetic resonance (NMR) spectroscopy

NMR analyses were performed on ^{13}C and ^{31}P nuclei, which were considered interesting for the chemical composition of the samples characterized. In particular, the study of ^{13}C nuclei was used for the characterization of GYY, before and after solubilisation in DMSO, and of GYY-loaded scaffolds. Since ^{13}C chemical shift is an intrinsic and sensitive parameter for the evaluation of protein conformations, it was used to examine the possible conformational behaviour of SF induced by the scaffold preparation processes. Following a profile fitting of SF alanine β-^{13}C peak previously reported, the dominant polymorphic conformation between Silk II (β-sheets crystals in amorphous matrix) and Silk I (random coil, turn and α-helix

structures) assumed by the protein in the scaffolds was calculated (Asakura et al., 2015; Callone et al., 2016). Since GYY molecules contain a phosphorus atom, ^{31}P NMR was used for the selective study of GYY chemical shifts.

NMR analyses were performed with a Bruker 400WB spectrometer (Bruker Corporation, Billerica, MA, USA) operating at a proton frequency of 400.13 MHz. NMR spectra were acquired with cross-polarization (CP) and single pulse (SPu) sequences, under the following conditions: for ^{13}C, frequency 100.23 MHz, π/2 3.4 μs, contact time 2 ms, decoupling length 6.7 μs, recycle delay 5 s and 30 s for CP and SPu respectively, 2k scans; for ^{31}P, frequency 162.49 MHz, π/2 3.65 μs, contact time 5 ms, decoupling length 6.7 μs, recycle delay 5 s and 100 s for for CP and SPu respectively, 8 scans (1k scans for loaded sponges). Samples were packed in 4 mm zirconia rotors, which were spun at 7.5 kHz under air flow. Adamantane CH_2 at 38.5 ppm and ammonium dihydrogen phosphate at 0.81 ppm were used as external secondary references for ^{13}C and ^{31}P, respectively.

3.2.10. Differential Scanning Calorimetry (DSC) and Thermogravimetric Analysis (TGA)

DSC and TGA techniques were used to investigate the thermal behaviour of GYY and the GYY-loaded scaffolds. DSC experiments were performed using a DSC20 calorimeter (Mettler-Toledo, Milan, Italy). For each sample, approximately 15 mg of material were placed in aluminium pans and tested under flushing nitrogen (100 ml/min), in the temperature range 30-330°C, at a heating rate of 10°C/min. TGA was conducted in a TA Instruments Q5000 thermobalance, testing

about 10 mg of material in freshly cleaned platinum pans, under N_2 flow (10 ml/min), in the temperature range 30-700°C, at a heating rate of 10°C/min.

3.2.11. Water uptake measurement

To measure the water uptake of the scaffolds, the samples were immersed in DI water and placed at 37°C. Then, excess of water was removed from the sample surfaces by gently dabbing with paper and the wet weight (W_{wet}) was determined. The same procedure was repeated at various time intervals until W_{wet} was stable. Samples were then dried in oven at 65°C overnight and the dry weight (W_{dry}) was determined. The water uptake was calculated as (W_{wet} - W_{dry}) / W_{dry}. Values were expressed as mean with SE (n=3 samples for each group).

3.2.12. Compressive mechanical test

The mechanical properties of the scaffolds were evaluated by comparison of the scaffolds compressive moduli obtained in a compression test. First, scaffolds were immersed in DI water for 2 h to reach the hydration equilibrium. Five specimens for each experimental group were measured. The compression test was performed at room temperature on wet scaffolds, at a strain rate of 2 mm/min in unconfined uniaxial compression mode on cylindric specimens (6 mm in diameter and 4 mm in height) with a Bose® Electroforce® 3200 test instrument (TA Instruments, DE, USA). Stress and strain data were calculated from load and displacement measurements. The Young's modulus was calculated as the slope of the initial linear section of the stress-strain curves.

3.2.13. Amperometric detection of H_2S release

H_2S release was measured during incubation of the scaffolds in aqueous PBS 0.01 M at pH 7.4, at room temperature, in presence of L-cysteine 4 mM. Three replicates of each sample were studied. The concentration of hydrogen sulfide in the incubation medium was monitored, initially, for 2.5 hours, and then until H_2S-generation by GYY was exhausted (around 12 hours), with a sulfide gas amperometric microsensor H_2S-500 (Unisense, Aarhus N, Denmark), connected to a microsensor multimeter (Unisense, Aarhus N, Denmark) as amplifier for data acquisition. The signal was collected in mV and converted in concentration units. The H_2S microsensor was calibrated with Na_2S*9H_2O 0.01 M dissolved in a N_2-flushed solution buffered at pH 3.6, in accordance to manufacturer instructions (Nielsen et al., 2015).

3.3. Results and discussion

SF scaffolds were characterized for their chemico-physical properties before and after the loading process with GYY, and before and after sterilization by γ-irradiation. H_2S-donor loaded scaffolds were also characterized for their sulfide releasing abilities. In this paragraph, the most significant results obtained during this part of the research activity are reported. Since materials modifications due to the sterilization process were not detected, only results obtained on γ-irradiated samples are reported.

3.3.1. Morphology of the scaffolds

The class of scaffolds produced were designed to provide the tissue site of potential implantation with adequate space for growth, and this

explains the essential need for a structure with many pores, interconnected and of the suitable dimension.

With this perspective, the morphology of the SF scaffolds, composed by pure fibroin or loaded with different amounts of GYY, was investigated by scanning electron microscopy. SEM images of Fig. 14 revealed similar morphology characteristics for all the groups of scaffolds prepared. The scaffolds showed a highly porous sponge-like structure. The round-shaped pores appeared homogeneously distributed and characterized by a high degree of interconnectivity. A bimodal distribution of the pore dimensions could be appreciated. The larger pores had an average size of 350 ± 8 μm, 345 ± 11 μm, 365 ± 8 μm, 369 ± 5 μm, and 378 ± 4 μm, for SF, SF_DMSO, SF_1%, SF_5% and SF_10%, respectively. The smaller pores, distributed on the surfaces of the large pores and creating an interconnected network between them, had an average size of 61 ± 4 μm, 69 ± 8 μm, 73 ± 5 μm, 90 ± 5 μm, and 95 ± 7 μm, for SF, SF_DMSO, SF_1%, SF_5% and SF_10% respectively. Even at high values of magnification, neither crystals nor agglomerates of GYY were visible on GYY-loaded fibroin matrices (Fig. 15, bottom images). Only small agglomerates were visible on the pore surfaces, but they were due to fibroin, as they were present also in pure SF scaffolds (Le et al., 2018).

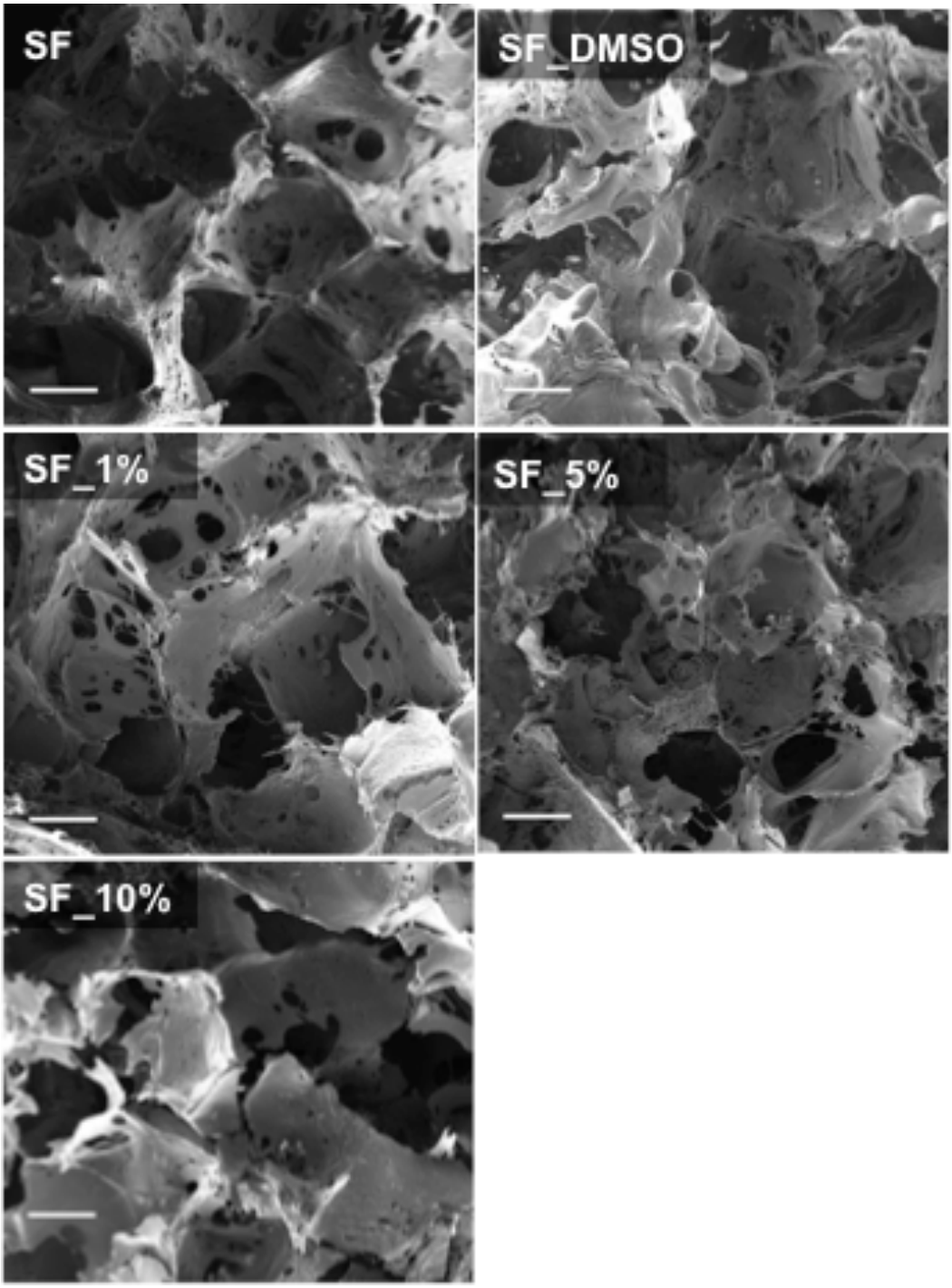

Fig. 14 FE-SEM images of the internal porous structure of dry SF scaffolds: SF, untreated scaffold; SF_DMSO, scaffolds treated with DMSO; SF_1%, scaffold containing 1%GYY; SF_5%, scaffold containing 5%GYY; SF_10%, scaffold containing 10%; scale bar 200 um.

The two top images of Fig. 15, which were representative for SF, and similar for the scaffolds of all the different compositions, also showed

details of a pore, and of the internal microstructure of pores' walls, which were also characterized by a very fine porosity.

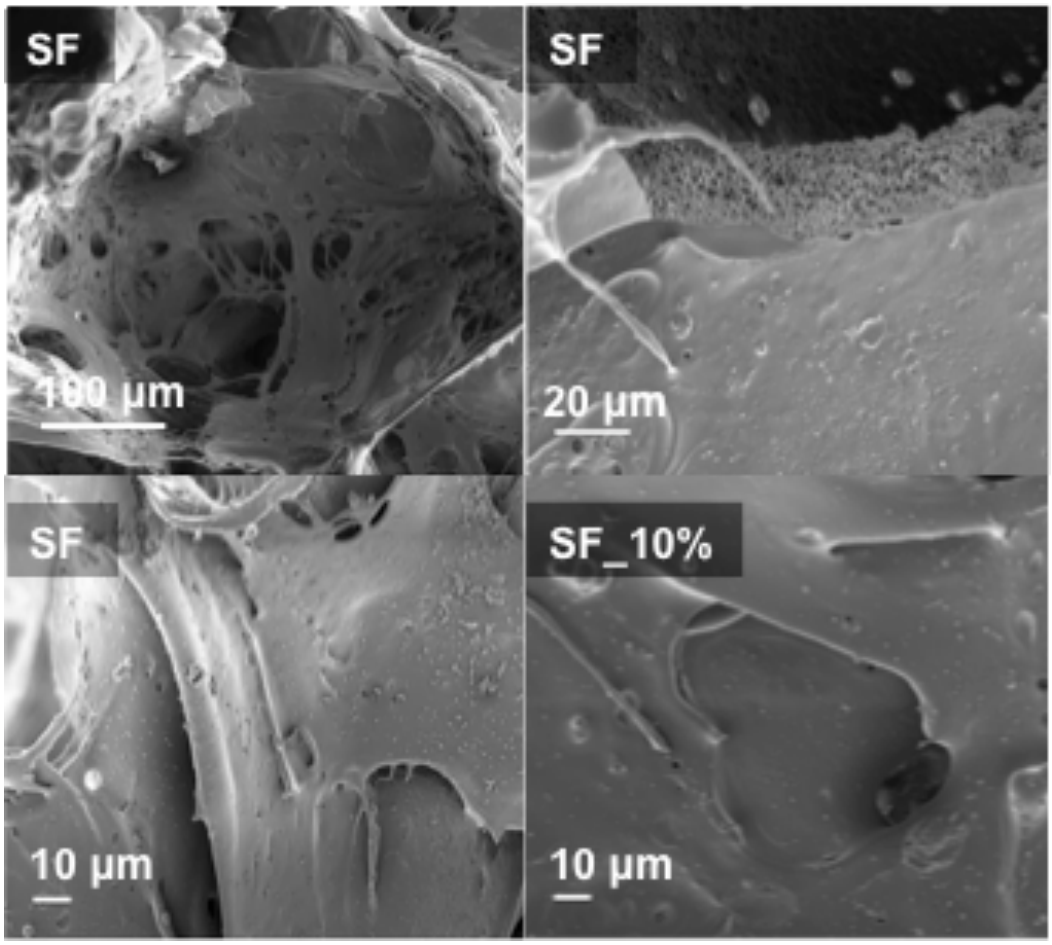

Fig. 15 Representative FE-SEM images at high magnification, to show the fine microstructure of SF scaffolds, of pure fibroin and loaded with the highest concentration of GYY.

The FE-SEM images showed that the loading process with the H_2S donor preserved the original scaffold morphology. The absence of visible GYY4137 agglomerates indicated that a fine dispersion of small GYY4137 crystals was obtained inside the SF scaffolds. Salt leaching process left a porosity with large and small pores, with dimensions (up to 500 µm) indicated as appropriate for the formation of bone tissue within the scaffold (Hutmacher, 2000). Finally, we should notice that pores were smaller than NaCl grains used,

because of the partial dissolution of the salt occurred during the addition of the SF solution.

3.3.2. Scaffolds composition and protein structure

Infrared spectroscopy was used to investigate the chemical structure of GYY and GYY_exDMSO, and the composition of GYY-loaded scaffolds. In addition, FT-IR bands of SF were used to study the protein secondary structure in the scaffolds. In general, the chemical structure of a protein cannot be deduced from the infrared spectrum because of many overlapping bands (Barth, 2007). However, some typical proteins absorption bands are sensitive to the structure of the protein backbone, and are commonly used in protein studies for the analysis of secondary structure (Oberg et al., 2004). Secondary structure analysis of proteins is mainly done using the amide I band, but the amide II, and amide III, bands as well as have also been shown to be useful (Fu et al., 1994). Fig. 16 showed that GYY and GYY_exDMSO had similar spectrum profiles.

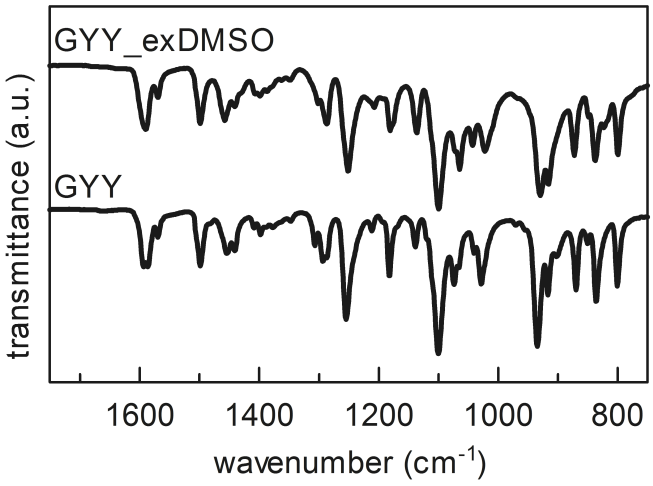

Fig. 16 IR spectra of GYY and GYY_exDMSO.

The assignments of the bands of samples GYY and GYY_exDMSO to specific groups vibrations are proposed in Table 4. Their absorption bands were consistent with the infrared spectrum of GYY previously reported (Alexander et al., 2015b).

GYY v (cm^{-1})	GYY_exDMSO v (cm^{-1})	Band assignment
1593, 1586, 1569, 1498	1589, 1569, 1498	aromatic C=C stretch (1600-1475) and N-H bend above 1550
1453, 1440	1457	Alkanes C-H deformation
1408, 1397	1398	CH_3 bend
1306, 1293	1286	C-N vibrations
1254	1251	Aromatic C-O stretch (pheyl-O-alkyl)
1181, 1138	1180, 1136	C-N vibrations and C-O-C stretch
1099	1099	C-O and/or C-N stretch
1073, 1040	1064, 1042	n.a.
1028	1022	Phenyl-O-alkyl
934, 916, 902	929, 915	n.a.
869	872	Para substituted aromatic ring C-H deformation
836	837	Benzene ring C-H deformation
800	799	=C-H aromatics or N-H (out-of-plane bend)
721, 708	722, 709	Benzene ring C-H deformation

Table 4 Infrared vibrations and assignments of GYY and GYY_exDMSO.

Many bands assigned to GYY bonds stretch were maintained on both spectra (Rose et al., 2015). However, some changes in peaks relative intensities and shape before and after dissolution of GYY in

DMSO and lyophilisation were clearly visible, especially for peaks at 1593 cm^{-1}, 1453 cm^{-1}, 1182 cm^{-1}, around 1028 cm^{-1}, and 935 cm^{-1}, in GYY's compounds spectra. Most of these absorption peaks can be assigned to vibrations of C-N and C-O bonds present in the structure of the two morpholine groups of GYY molecule.

Fig. 17 reported the FT-IR spectra of GYY-loaded scaffolds and, for comparison, the spectra of GYY, SF and SF_DMSO.

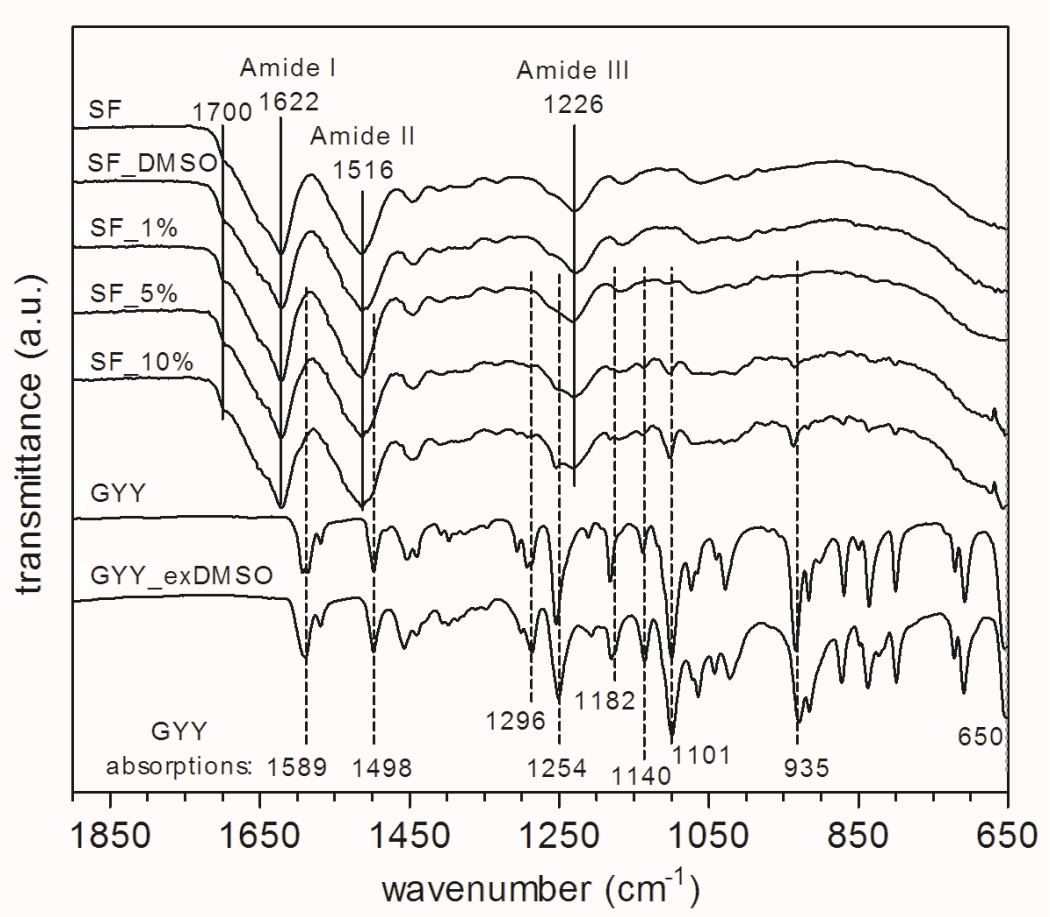

Fig. 17 Comparison between the IR spectra of GYY and GYY_exDMSO (GYY solubilized in DMSO and lyophilised), and IR spectra of fibroin scaffolds: SF, untreated; SF_DMSO, treated with DMSO; SF_1%, containing 1% of GYY; SF_5%, containing 5% of GYY; SF_10%, containing 10% of GYY. Solid lines indicate absorption bands characteristic of SF; dashed lines indicate peaks of GYY discussed in the text. Adapted with permission from (Raggio et al., 2018). Copyright (2019) American Chemical Society.

Spectrum profiles of SF and SF_DMSO were both characterized by the typical protein backbone absorption bands, *i.e.,* Amide I, II and III, which are very useful for conformation studies (Stuart and Ando, 1997; Barth, 2007). In particular, Amide I and Amide II bands appeared broad and centred at wavenumbers correlated with a prevalence of β-sheet secondary structure, respectively at 1622 cm^{-1} and 1516 cm^{-1} (Hu et al., 2006; Callone et al., 2016). Amide I presented a shoulder at 1690 cm^{-1}, suggesting the presence of β-sheet crystallinity of the antiparallel type (Iizukat and Yangt, 1968). Amide III band was centred at 1226 cm^{-1}, with a shoulder at 1265 cm^{-1}, confirming that β-sheet was the main conformation adopted by fibroin in SF scaffold. Curves of GYY-loaded fibroin scaffolds, *i.e.,* SF_1%, SF_5%, and SF_10%, exhibited absorption profiles similar to samples SF and SF_DMSO for Amide I, II and III bands. In fact, the dominant β-sheet secondary structure was induced by the use of NaCl during the salt leaching process that characterized all the scaffolds (Yao et al., 2012; Zhang et al., 2012c). In fact, salt leached SF scaffolds were stable and did not need any further treatment to be insoluble in water. In addition to the amide's bands, peaks derived from the presence of GYY were clearly visible, at least, for samples SF_5% and SF_10% and their intensity increased proportionally with the amount of GYY incorporated in the scaffolds. The curve of SF_5% presented peaks at 1593 cm^{-1} and 1498 cm^{-1}, 1296 cm^{-1}, 1254 cm^{-1}, 1182 cm^{-1}, 1140 cm^{-1}, 1101 cm^{-1}, 935 cm^{-1}, and between 835 and 800 cm^{-1}, related to GYY absorptions. SF_10% spectrum featured similar but more intense absorption frequencies deriving from the presence of GYY. However, it was not possible to appreciate if these absorptions were more like those detected for GYY or for GYY_exDMSO.

The results of the protein Amide I analysis were reported in Fig. 18A and showed similar amounts of secondary structures for all the scaffolds. In particular, the scaffolds displayed similar amounts of β-sheet. Fibroin had 42 %, 44 %, 40 %, 44 % and 41 % of β-sheet secondary structure respectively in SF, SF_DMSO, SF_1%, SF_5% and SF_10%. The differences between these values were considered not significant. The rest of the protein was mainly organized in random coil and turns structures, with a small amount of α-helix. Fig. 18B shows an example of an absorbance spectrum of Amide I, deduced after Fourier self-deconvolution with seven peaks, as described previously in this manuscript. The different secondary structure contributions are highlighted with B for β-sheet, T for turns, A for α-helix and R for random coil.

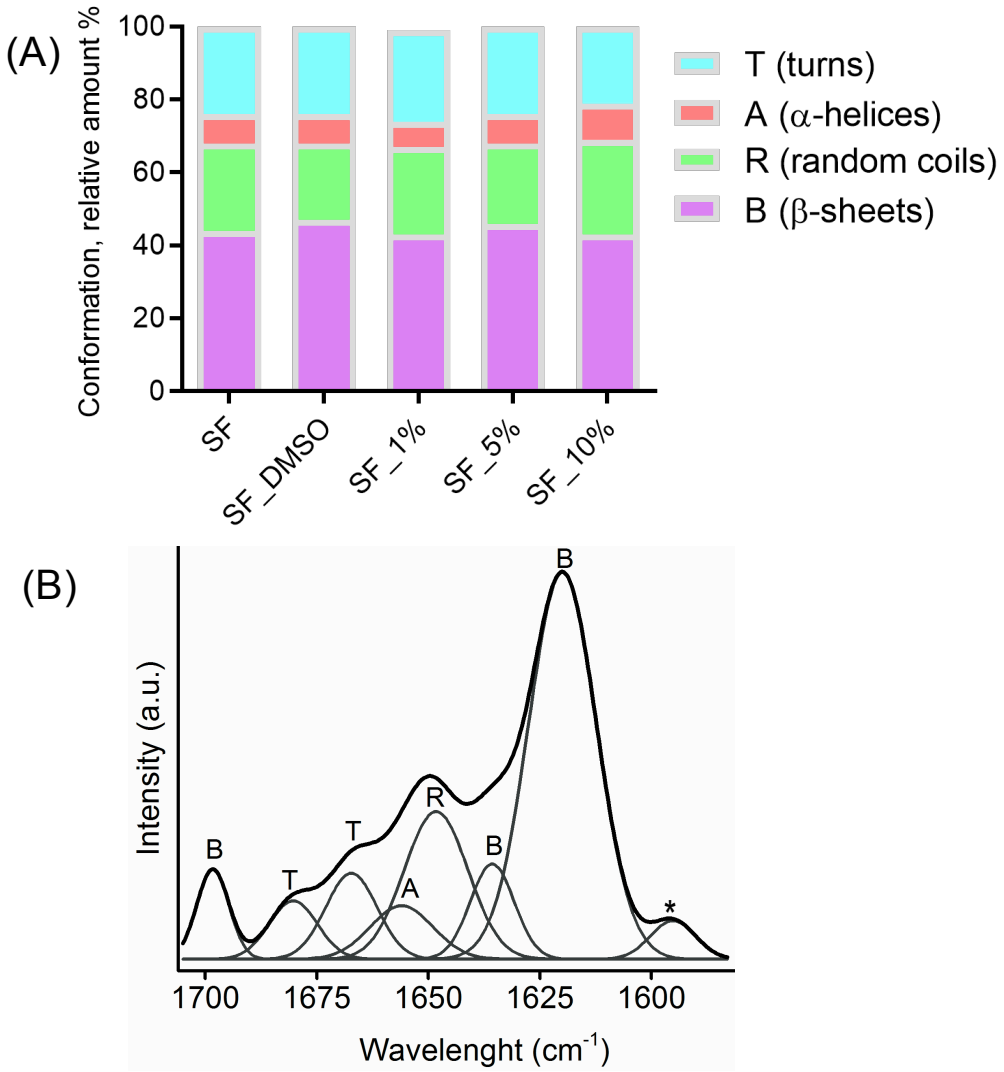

*Fig. 18 (A) Percentages of the four secondary structure (b-sheet, random coil, a-helix, turns) contributing to fibroin Amide I band. Samples are: SF, untreated scaffold; SF_1%, scaffold containing 1% of GYY; SF_5%, scaffold containing 5% of GYY; SF_10%, scaffold containing 10% of GYY. Mean with SD, n = 3. (B) Example of an absorbance spectrum of Amide I, deduced after Fourier self-deconvolution with seven peaks. Peak marked with * is assigned to tyrosine side chains, not considered in the quantification of the secondary structure.*

The ^{13}C CPMAS NMR spectra of relevant samples are shown in Fig. 19.

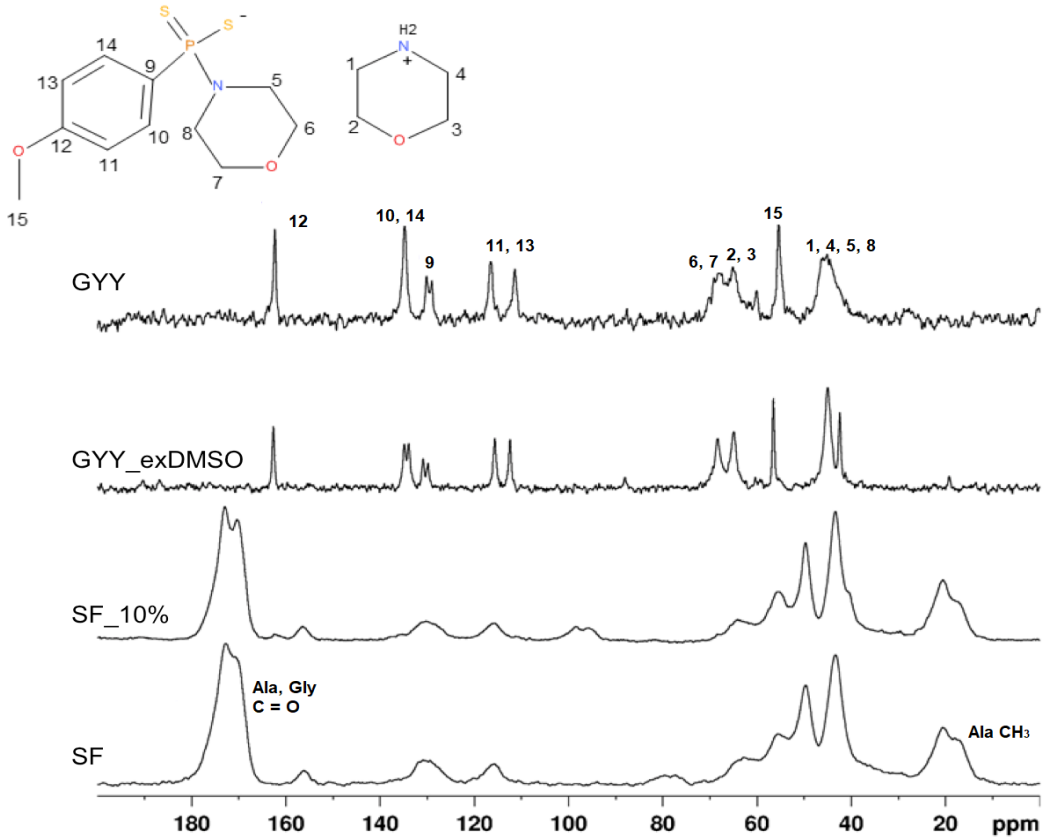

Fig. 19 ^{13}C CPMAS NMR spectra of SF (untreated scaffold), SF_10%, GYY, GYY_exDMSO, and GYY molecular structure with C atoms numbering scheme. Spinning sidebands are visible close to main bands. Adapted with permission from (Raggio et al., 2018). Copyright (2019) American Chemical Society.

Sharp signals and two broad peaks characterized the spectrum profile of GYY (assignments based on GYY labeled structure in the figure and reported in Table 5). After dissolution of GYY in DMSO and lyophilization, in the ^{13}C spectrum the sharpness of the peaks increased, suggesting improved crystallinity. However, the peaks did not show any shift in position, thus confirming that the dissolution in DMSO did not substantially alter the molecular structure.

GYY		
δ (ppm)	**Functional group**	**C labeling**
45.2	$N(CH_2)_2$ morpholinium	1, 4
45.2	$N(CH_2)_2$ morpholinium attached to P	5, 8
55.5	OCH_3	15
65.0	$O(CH_2)_2$ morpholinium	2, 3
68.3	$O(CH_2)_2$ morpholinium attached to P	6, 7
111.4/116.6	arylCH *o*- to OMe	11, 13
129.2/130.2	arylC-P	9
134.9	arylCH *o*- to P	10, 14
162.7	arylC-OMe	12

Table 5 ^{13}C NMR chemical shifts of GYY and assignments (Alexander et al., 2015b)

The ^{13}C CPMAS NMR spectra of samples SF and SF_10%, were both dominated by the signals belonging to the amino acid main sequence AGS(Y)GAG in SF (Zhang et al., 2012a; Callone et al., 2016). Unfortunately, the intense SF resonances hindered the possibility of observing the weak GYY peaks in the spectrum of 10% GYY-loaded scaffold. Only the small peak at 163 ppm, which was attributed to C12, was a proof of the presence of adsorbed GYY. Comparing the fibroin signals in the two samples, small differences could be appreciated in the case of the peak labelled *Ala/Gly C=O* centered at 172 ppm, and *Ala* CH_3 (Cβ) centered at 18 ppm. Moreover, the appearance of a high-field shoulder on the Gly CH_2 resonance (Cα) at 42 ppm could be observed. According to previous reports that pointed out the high sensitivity of SF secondary structure to processing treatments, the profile fitting procedure was applied to the Ala Cβ peak of SF, SF_DMSO and SF_10% spectra, in order to evaluate the percentage of the possible SF conformations (Callone et

al., 2016). The fibroin sponge used in the present work presented 61% of Silk II conformation, which increased up to 65% in SF_DMSO, and reached 74% in the SF_10%.

In order to better characterize the features of GYY in the different samples, the ^{31}P CPMAS NMR spectra were recorded (Fig. 20). Since fibroin does not contain any phosphorus atoms, it was possible to selectively characterize the H_2S donor inside the loaded scaffolds and compare the results with the characterization conducted on GYY.

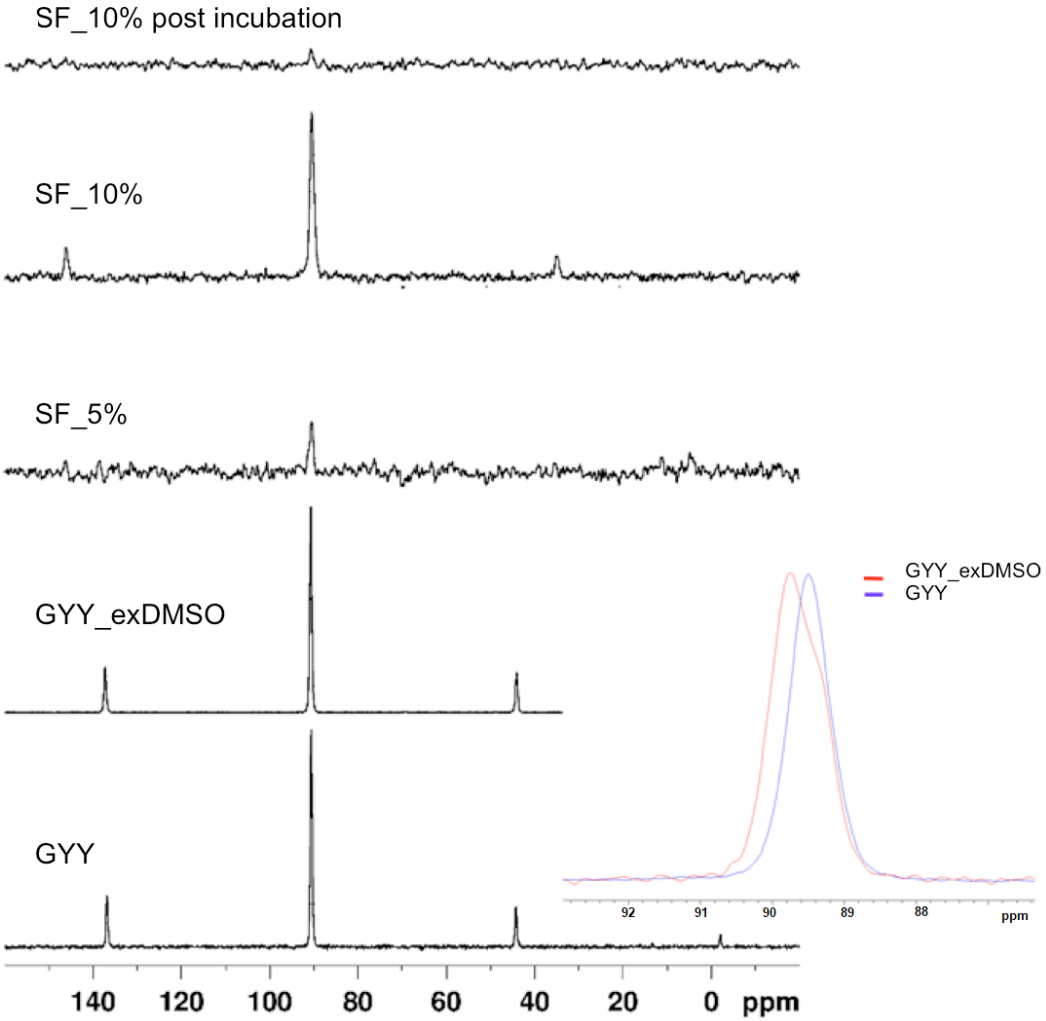

Fig. 20 ^{31}P CPMAS spectra of SF_5%, SF_10%, SF_10% after incubation in liquid medium, GYY and GYY_exDMSO. Spinning sidebands are visible close to main bands. The insert shows the profiles of the ^{31}P peaks at 90.5 ppm of GYY and GYY_exDMSO.

The ^{31}P CPMAS NMR spectrum of GYY was characterized by a single sharp peak at 90.5 ppm. The recrystallization after DMSO (GYY_exDMSO) produced a moderately asymmetric and enlarged resonance at the same position. The spectrum of sample SF_1% was not shown, since the peak was beyond the sensitivity limits. The adsorption of 5 and 10% GYY on SF scaffolds (SF_5% and SF_10%) did not affect the H_2S donor structure and the peak intensity was in agreement with the different nominal GYY loadings.

IR and NMR analyses gave complementary results regarding the chemical composition of GYY and scaffolds loaded with GYY. Dissolution of GYY in DMSO and removal of the solvent to produce GYY_exDMSO were performed to mimic the loading conditions and study their potential effects. This process induced only slight modifications in GYY crystal structure, with no chemical changes. We hypothesized that GYY crystals, after DMSO, re-formed in a new structure containing the morpholinium cation in a different arrangement, which caused a diversification of the signals related to morpholine energetic transitions. In fact, both on IR and NMR spectra, some absorption bands assigned to morpholine appeared sharper and better resolved after recrystallization from DMSO. On the other hand, all peaks were maintained on infrared spectra of GYY_exDMSO, and phosphorus signal was in the same position at 90.5 ppm on ^{31}P NMR spectra. Similarly, the incorporation of GYY into SF scaffolds did not affect the H_2S donor chemical structure: the characteristic bands of GYY, when visible, were maintained in the same positions on scaffolds infrared curves, and phosphorus peak on ^{31}P NMR spectra only changed intensity, in agreement with the GYY % of loading.

As discussed in the introduction of this dissertation, it is fundamental to take in account the influence of all the fabrication processing steps

on the structure of SF-based materials (Callone et al., 2016). Thus, to investigate possible changes related to the GYY-loading process in SF structure and scaffold crystallinity, an analysis of Amide I infrared absorption band was conducted. In particular, the four protein secondary structures considered for fibroin were β-sheet, random coil, α-helix, and turns. The results, shown in Fig. 18A for samples SF, SF_DMSO, SF_1%, SF_5% and SF_10%, indicated that all the scaffolds contained comparable relative amount of secondary structure of the β-sheet type. β-sheet accounted for almost 50% of the scaffold fibroin structure. This resulted in the same levels of crystallinity between the SF matrices, thus proving that the highly ordered secondary conformation, once formed, is stable upon addition of GYY (Wilson et al., 2000; Callone et al., 2016). The profile fitting conducted on the NMR Cβ Ala peak of SF was used to evaluate the % of Silk II conformation, comprising β-sheet crystals and so-called β-sheet-like structures in an amorphous matrix, in the scaffolds. It resulted that manipulation (such as the addition of GYY in SF_10%, see labelled SF Ala peaks of Fig. 19) or ageing (data not shown) of SF induced a slight increase of the Silk II component. A similar effect for SF materials was already monitored before through the study of the NMR Cβ Ala peak (Tian et al., 2017).

3.3.3. Thermal behaviour of the scaffolds

The behaviour of GYY and GYY-loaded scaffolds upon treatments at high temperature was studied by two techniques, DSC and TGA. DSC thermogram of GYY powders were shown in Fig. 21A. It displayed two endothermic peaks, centered, respectively at T^{I} = 123°C (ΔH = 54 J/g), and T^{II} = 169°C (ΔH = 63 J/g). These peaks were assigned to the decomposition of morpholinium and the melting

of (p-methoxyphenyl)morpholino-phosphinodithioate (Li et al., 2008a; Alexander et al., 2015a).

Fig. 21B showed the thermograms of an SF scaffold, compared with GYY-loaded ones. All the materials were characterized by a wide endothermic peak centred around 95°C (T_e), caused by the loss of absorbed water, and a sharp endothermic peak centred at higher temperatures, around 288°C (T_d), generated by thermal degradation of the protein (Motta et al., 2002, 2014; Lu et al., 2011; Callone et al., 2016). In particular, degradation of SF occurred approximately at 293°C (ΔH=168 J/g), with a sharp endothermic peak. GYY-loaded scaffolds showed wider degradation peaks with a shift over lower temperatures, and lower values of the associated enthalpy. These differences became more evident increasing the amount of loaded GYY from sample SF_1% (T_d = 290°C, ΔH = 150 J/g), to SF_5% (T_d = 289°C, ΔH = 127 J/g) and SF_10% (T_d = 283°C, ΔH = 136 J/g). Interestingly, thermal transitions related to GYY were not visible on the thermograms of loaded scaffolds. These effects were presumably related to the presence of GYY decomposing before the temperature of SF degradation. The environment generated locally and diffusely in the SF matrix by the thermal energy exchanges derived from the melting of GYY might induce an anticipated degradation of the scaffolds in their entirety. TGA curves confirmed those evidences. In fact, TGA was performed to investigate the mass losses occurred in GYY powders and in GYY-loaded scaffolds during heating from room temperature up to 700°C. As shown in Fig. 21C, GYY powders lost most of the weight (around 60% of the initial weight of the sample) between 150 and 300°C. In the same temperature range (225-325°C), a visible mass loss could be monitored for scaffolds loaded with GYY, but not for SF: the mass loss % resulted proportional to the amount of GYY loaded into the sponges. All the scaffolds lost

most of the weight above 300°C, *i.e.,* after the beginning of fibroin degradation. A residue of around 30% was left at 700°C.

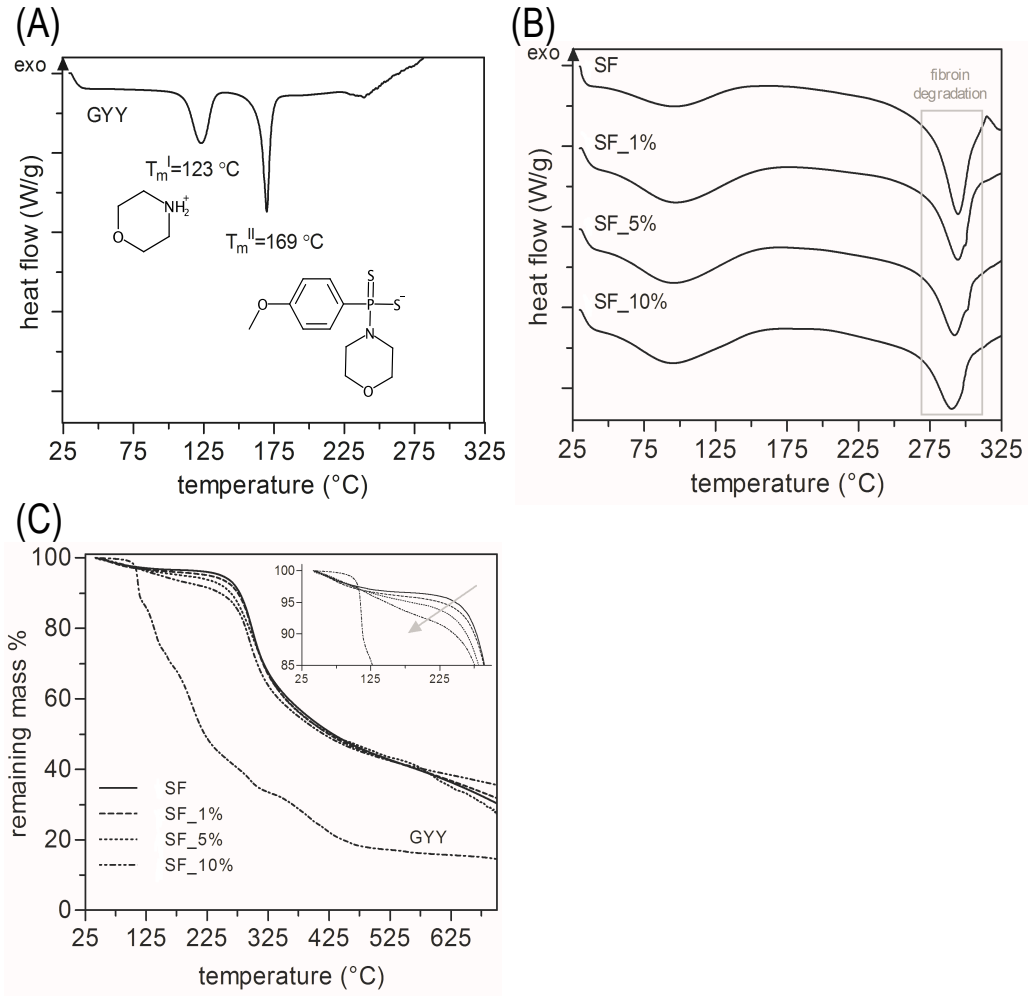

Fig. 21 DSC curve obtained for (A) GYY and for (B) scaffolds. (C) TGA analyses of the different SF scaffolds and of GYY; the insert highlights mass losses in the scaffolds in the temperature range of GYY degradation. GYY content increases in the direction of the arrow. Adapted with permission from (Raggio et al., 2018). Copyright (2019) American Chemical Society.

3.3.4. *In vitro* behaviour of the scaffolds and H_2S release

Fig. 22 showed the curves of the water uptake of the scaffolds, with comparable profiles for the different samples. This evaluation was

performed in order to predict the behaviour of the scaffolds in liquid media. The process of water uptaking was completed after 60 minutes of incubation. After 300 minutes, the weight of wet scaffolds was stable and was used to calculate the water uptake as $(W_{wet} - W_{dry})/W_{dry}$. Water uptake measured 6.0 ± 1.8 for scaffold SF, 7.8 ± 2.0 for SF_1%, 6.1 ± 0.9 for SF_5%, and 6.6 ± 1.0 for SF_10%.

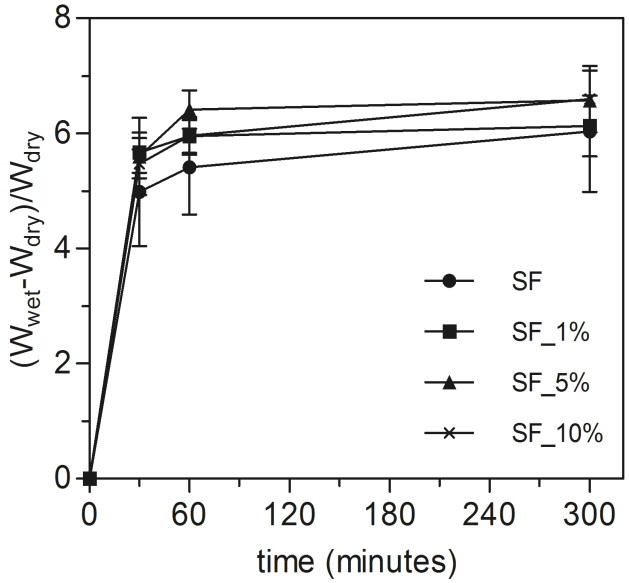

Fig. 22 Water uptake curves of the scaffolds incubated in water at 37°C (mean with SE, n = 3).

Amperometry was used for the continuous record of H_2S in the incubation media of GYY-loaded scaffolds. The H_2S-microsensor measured the concentration of the undissociated species indicated as H_2S in the equilibrium: $H_2S \rightleftarrows HS^- \rightleftarrows S^{2-}$, with $pKa_1 = 6.9$ and $pKa_2 > 11$. It can be calculated that, at pH 7.4, the concentration of H_2S is approximately 30% of the total dissolved sulfide (*i.e.* $H_2S + HS^- + S^{2-}$) (Hughes et al., 2009; Olson, 2012; Kolluru et al., 2013). The incubation media contained L-cysteine, as Martelli *et al.* showed that GYY4137 releases H_2S in a L-cysteine-dependent mechanism, and endogenous organic thiols like this amino acid are always present in biological environments (Martelli et al., 2013). In previous studies, the

kinetic of H_2S generation process was described and it was assessed that solutions of GYY4137 1 mmol/L in PBS at pH 7.4 generated a peak in H_2S concentration in the first 20 minutes, which then decreased (Li et al., 2008a; Martelli et al., 2013). Moreover, the steady state of H_2S release curves was reported to depend on the combination of different processes: not only the concentration of the H_2S source, but also volatilization and oxidation of H_2S dissolved in solution, occurring in parallel at any time (Deleon et al., 2012).

Initially, in our experiments, measurements of the concentration of H_2S were collected in continuum for 2.5 hours in the incubation media of GYY-loaded scaffolds. Results were compared with the curves obtained for SF and SF_DMSO, which did not release H_2S. Fig. 23 showed the curves of H_2S generation in solution during time. All the GYY-loaded fibroin sponges induced a sustained release of H_2S, but the concentration levels reached a plateau that gradually increased with the GYY content of the scaffolds. SF_1% generated a maximum concentration of 6.5 μM of H_2S during the 2.5 hours of the experiment. H_2S concentration profile for SF_5% was similar, but reached higher values at the plateau, settling at 9 μM. Finally, SF_10% generated the highest concentration of H_2S in solution: the H_2S curve increased over the first 100 minutes of incubation and then reached plateau at a concentration of around 31 μM.

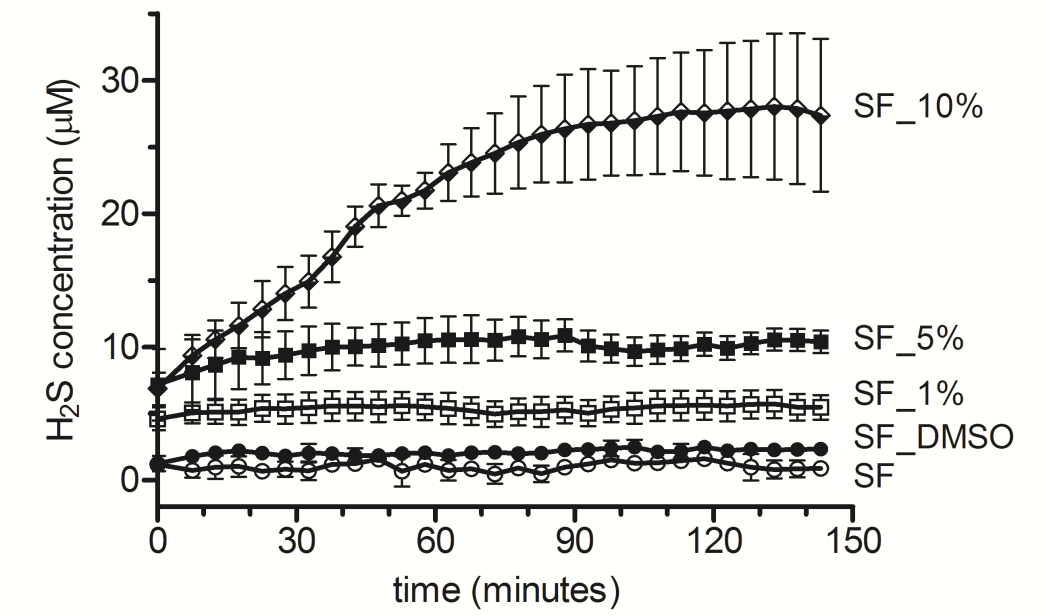

Fig. 23 Release of H_2S monitored by H_2S-selective microelectrode for SF scaffolds incubated in PBS pH 7.4 with L-cysteine 4 mM, at room temperature (mean with SE, n = 4); error bars are not visible when lying within dimensions of symbols. Adapted with permission from (Raggio et al., 2018). Copyright (2019) American Chemical Society.

In a following experiment, scaffolds were placed in aqueous solution and H_2S was monitored, in continuum, for one day. H_2S release could be monitored for at least 12 hours. Furthermore, in agreement with data recorded for the short release, we evidenced a kinetic of H_2S release dependent on the amount of GYY loaded (Fig. 24). In particular, SF_1% generated a steady release of H_2S at concentrations around 5 μM for the entire duration of the experiment. Conversely, SF_5% and SF_10% released increasing concentrations of H_2S for the first 3 hours peaking at around 10 μM and 30 μM, respectively. The time required to reach the concentration of the plateau was approximately the same for all samples, indicating that the release process occurred at similar rates from all the scaffolds. Subsequently, for both samples, H_2S levels slowly decreased to

reach a concentration similar to that of SF_1%. Release profile for sample SF was not repeated, as it did not generate any H_2S release.

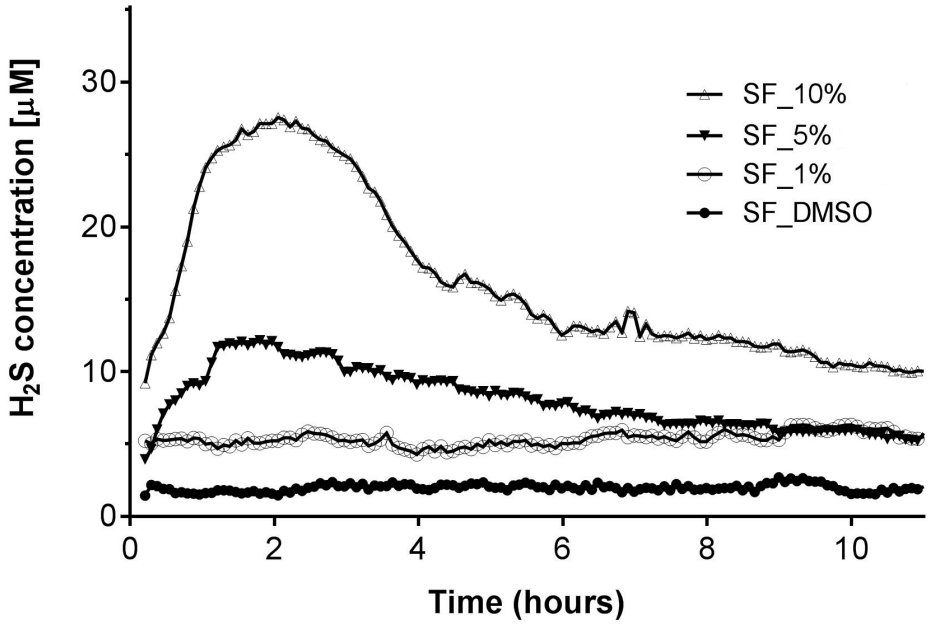

Fig. 24 Graphs of H_2S concentration in buffer as detected by amperometric measurements.

As anticipated, when GYY is put in contact with an aqueous environment, the P=S bonds start to decompose by hydrolysis, and H_2S is generated. Thus, as anticipated, in previous experiments, GYY formulations dissolved in aqueous solution were administered fresh, immediately after the preparation. In this context, the GYY-loaded SF scaffolds described in this work represent a novel approach for the administration of GYY. Anhydrous DMSO was chosen as solvent and vehicle for the loading of GYY into the sponges, since DMSO allowed to prepare solutions where GYY didn't not decompose, thus preventing early release of H_2S from GYY, as proved by spectroscopic analyses. The retention of the H_2S releasing abilities of GYY after the loading into the SF scaffolds was a critical point of this work. Since different amounts of GYY were used, we

expected to detect quantities of H_2S released in solution upon incubation of the scaffolds proportional to the initial concentrations of GYY w/w% in SF. We could assess that the incorporation of GYY in the SF matrix influenced the process of H_2S generation in solution: the curves of real-time H_2S concentration increased gradually, without evident peaks ascribable to burst release phenomena.

3.3.5. Compressive strength of the scaffolds

The mechanical properties of the scaffolds were evaluated under compression test, with the scope of determining the elastic modulus of the materials, and evidence eventual differences between scaffolds of diverse composition.

For the repair and generation of bone, which is a hard and ductile tissue, scaffolds need to have a suitable elastic modulus in order to be retained in the space they were designated for (Fig. 25).

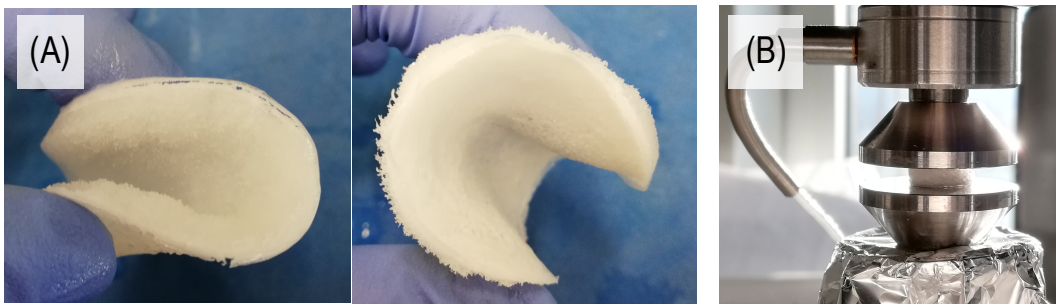

Fig. 25 (A) A typical SF scaffold that can be easily bent on both sides (during scaffold fabrication, one side gels at the air interface and one side gels at the plastic dish interface) in the wet state. (B) The setup of the compressive test, with a representative sample of SF scaffold placed between the plates.

The results obtained from the mechanical compression tests showed that the elastic modulus was: 135.5 ± 7.5 kPa for SF; 128.0 ± 13.3 kPa for SF_1%; 122.2 ± 5.9 kPa for SF_5%.; 81.3 ± 4.7 kPa for SF_10%. The scaffolds of different composition had similar profiles of

stress-strain curves and similar values of Young's modulus, as visible in Fig. 26. The only type of scaffold that showed a statistically significant different mean Young's modulus was SF_10%, indicating that the GYY loading process did not affect the original properties of the fibroin matrix up to 5% w/w of loading. Above this value, the elastic modulus was slightly lower compared to pure SF matrix.

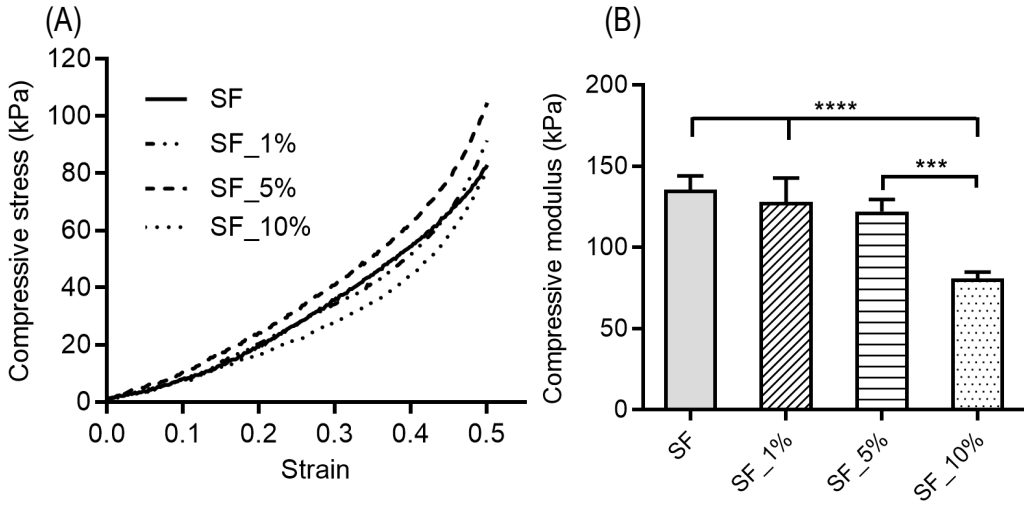

*Fig. 26 (A) Representative stress-strain curves for SF sponge, and SF sponges loaded with 1%, 5% and 10% of GYY. (B) Compressive elastic moduli of the scaffolds presented as mean with standard deviation (n = 5); *** indicates significant differences between values at P ≤ 0.001; **** at P≤ 0.0001.*

The values of scaffolds Young's modulus were lower than the ones of mature human bone (Zysset et al., 1999). However, the scaffolds objectives of the work were designed to serve as temporary devices, especially in case of bone losses and non-healing fractures, *i.e.,* to fill small bone defects, where specific load-bearing abilities are not required. Also, the scaffolds should direct cell behaviour in the early stages of bone development, by acting as temporary supports for the production of collagen and the deposition of ECM inorganic phases. In these stages of bone tissue healing, *i.e.,* when soft callus is

created, semi-rigid engineered matrices with elastic modulus between the kPa and MPa range are appreciated as scaffolds to support hMSCs differentiation towards mature bone cells (Yao et al., 2012).

Chapter IV. Biological evaluation of silk fibroin scaffolds loaded with GYY4137

Part of this chapter has been published in:

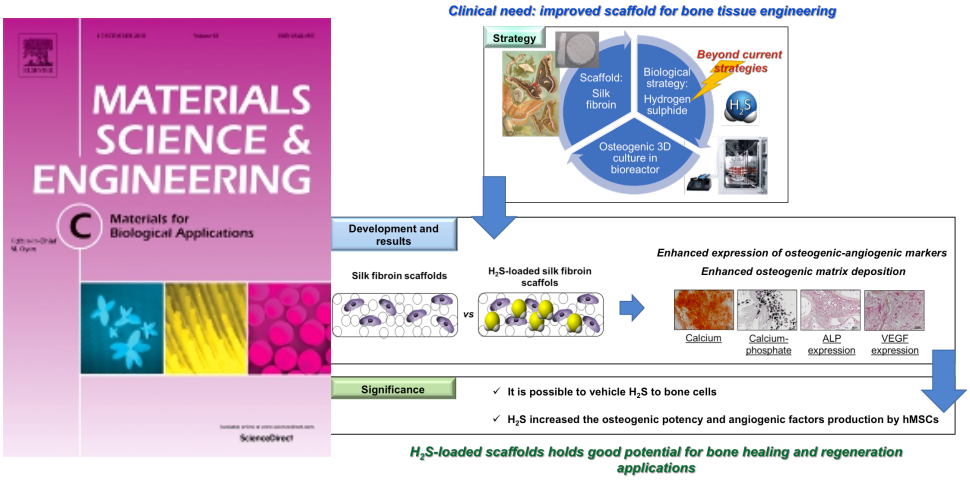

Laura Gambari, Emanuela Amore, Rosasilvia Raggio, Marli Barone, Gina Lisignoli, Brunella Grigolo, Antonella Motta, Francesco Grassi

"Hydrogen Sulfide-Releasing Silk Fibroin Scaffold For Bone Tissue Engineering"

Material Science and Engineering C 102 (2019) 471–482

4.1. Introduction

The biocompatibility and the potential biomedical applications of a scaffold designed for bone tissue engineering are typically tested in *in vitro* and in animal *in vivo* experiments, before translation to experiments in human, and then, if successful, to clinics.

The scaffolds prepared during this PhD research activity (see their description in Chapter III), were tested *in vitro* with different bone related cell lines, and *in vivo* by ectopic implant on mice (ongoing

experiments at Istituto Ortopedico Rizzoli). The goals of the biological evaluations performed, in chronological order, were:

- firstly, the assessment of the cytocompatibility of the scaffolds. In fact, since a new material that was never tested before was fabricated, we were initially interested in evaluating the scaffolds potential cytotoxicity;
- secondly, the evaluation of the ability of the scaffolds to be used for bone regeneration applications (biocompatibility and osteoanabolic activity with human bone marrow mesenchymal stromal cells, osteoblast differentiation, bone mineral metabolism and angiogenesis).

In this chapter, the biological evaluations performed on the scaffolds at BIOtech Research Center are described in detail, together with some mentions regarding the experiments performed at Istituto Ortopedico Rizzoli by our collaborators (Doctor Francesco Grassi and Doctor Laura Gambari).

4.2. Materials and methods

4.2.1. Cell culture

MG63 cells from human osteosarcoma and hMSCs were used for *in vitro* studies conducted on fibroin scaffolds with different contents of GYY. MG63 cells (Istituto Zooprofilattico Sperimentale della Lombardia e dell'Emilia Romagna, Italy) were cultured in Minimum Essential Medium (MEM) (EuroClone, Pero, Italy) supplemented with 10% fetal bovine serum (FBS), 1% of Antibiotic-Antimycotic 100X, 1mM non-essential amino acid, 2 mM L-Glutamine 100X and 1 mM Sodium Pyruvate 100X. hMSCs (Istituto Ortopedico Rizzoli, Bologna, Italy) were obtained as previously described (Manferdini et al., 2011; Grassi et al., 2016). hMSCs were isolated from bone marrow aspirate

during hip-replacement surgery of 2 posttraumatic patients. The cells were washed twice and suspended in α-MEM with 15% FBS (Lonza, Basel, Switzerland), counted, and plated in flask. After 1 week, the non-adherent cells were removed and the adherent hMSCs expanded in vitro. hMSCs were used at passage 3 in culture. Both cell lines were subcultured as monolayers at 37°C, in 5% CO_2 atmosphere, and medium was changed every 2-3 days. Cells were detached when they reached 80% confluence, according to standard protocols (ATCC: The Global Bioresource Center), and used for the experiments.

4.2.2. Measurement of *in vitro* cytotoxicity of GYY-loaded scaffolds

The potential cytotoxic effects of silk fibroin scaffolds loaded with different concentrations of GYY (coded with SF_X, X being GYY concentration), untreated fibroin scaffolds (SF) and scaffolds treated with DMSO (SF_dmso), were measured. Results were compared with positive (ctrl+) and negative (ctrl-) controls corresponding, respectively, to cells seeded on plastic then lysed, and to healthy cells seeded on plastic. The test was based on the detection of lactate dehydrogenase (LDH) enzyme, which is released into the medium from damaged cells, and can be used as a biomarker for the evaluation of cellular toxicity and lysis.

For the experiment, cells were seeded on the top of sterile fibroin scaffolds of all the different compositions, at a density of $5x10^3$ cells/well. Before cell seeding, scaffolds were pre-conditioned for 10 minutes with culture medium that was removed before the deposition of cell suspension.

Cells were cultured for 24 hours, and then positive control for LDH assay was prepared by inducing lysis with Triton X-100 surfactant in cells cultured on tissue culture plate. All media from positive and negative controls, and experimental samples were collected, centrifuged to remove cell debris, and transferred into a new plate to be tested. Lactic Dehydrogenase based assay (TOX7, Sigma-Aldrich) was performed according to manufacturer's instructions. Absorbance was measured using a microplate reader (Spark 10M, Tecan Group, Männedorf, Switzerland) at 490 nm, with background absorbance measured at 690 nm.

4.2.3. Measurement of *in vitro* metabolic activity of cells cultured on GYY-loaded scaffolds

Cells were seeded on the top of the scaffolds for the different experimental groups, and directly on TCPs for the control groups, in 96-well TCPs (5000 cells/well). Before cell seeding, scaffolds were pre-conditioned for 10 minutes with culture medium that was removed before the deposition of cell suspension. Separately, controls for alamarBlue assay (*i.e.*, cells seeded on TCP and cultured with complete medium supplemented with 5% FBS) are also prepared in two other 96-well plates, where scaffolds were placed to perform the metabolic activity evaluation. The cells were cultured in their media for 3 days.

AlamarBlue assay kit (Invitrogen, Oregon, USA) was used to evaluate cell proliferation (proportional to metabolic activity) on 3D scaffolds at the end of each experimental time point. Results were evaluated at two experimental time points: 1 and 3 days. The assay was performed according to the manufacturer's instructions. In brief,

the seeded scaffolds were incubated for 4 hours at 37°C with fresh culture medium (with reduced serum) supplemented with alamarBlue diluted according to manufacturer's data sheet (simply adding the alamarBlue reagent as 10% of the sample volume). A total of five replicates were used for each sample and each replicate was split into four wells for the final reading. The references were taken from wells with unseeded scaffolds incubated with the alamarBlue solution. Absorbance was measured at 570 and 600 nm with a microplate reader.

4.2.4. Confocal Laser Microscopy (CLM) imaging

Evaluation of cell attachment, growth, distribution and migration on the seeded scaffolds was performed by confocal laser microscopy (Nikon Eclipse, Ti-E) after Phalloidin-iFluor 488 Reagent (Abcam) and 4',6-Diamidine-2'-phenylindole dihydrochloride (DAPI, Sigma Aldrich) staining according to the manufacturer's protocol. Fixation with a formaldehyde solution (4% formaldehyde in PBS solution) and permeabilization with Triton-X (0.2% Triton-X in PBS solution) were performed before staining. The study was conducted in parallel with alamarBlue assay, on samples prepared and cultured in the same conditions described before. In the following sections only the representative CLM images are shown for each sample.

4.2.5. Statistical analyses

Results were presented as mean with SEM (n = 5). Statistical analysis was conducted by One-way analysis of variance (ANOVA) using GraphPad Prism version 5.03 (GraphPad software, CA, USA) and Bonferroni's multiple comparison test was used to evaluate

significant differences among the cytotoxicity induced by the different groups of scaffolds. Two sets of samples were considered significantly different when $P < 0.05$.

4.3. Results and discussion

4.3.1. Biological evaluation of scaffolds with MG63 cells

Results of LDH assay performed on culture media after 24 hours from MG63 cell seeding on scaffolds and controls are shown in Fig. 27. Cells cultured in medium on TCP without any scaffold sample were used as negative control (*i.e.*, not cytotoxic), while cells cultured in medium on TCP without any scaffold sample and treated with 0.05% Triton X-100 surfactant were used as positive control (100% cytotoxicity). Results were expressed as LDH signal intensity %, proportional to LDH released in the supernatants, respect to ctrl+ considered equal to 100% of LDH signal intensity.

The results of the LDH assay showed no significant cytotoxicity detected for the scaffolds. In particular, for MG63 cells, the mean relative cytotoxicity value measured for the various samples were: 23% for samples SF, 18% for SF_dmso, 31% for SF_1%, 27% for SF_5% and 26% for SF_10%. All samples showed a significantly lower cytotoxicity compared to ctrl+. Only scaffold SF_1% showed a statistically significant higher cytotoxicity compared to ctrl- (around 6%), and, in general, a dependency between the content of GYY in the scaffolds and their toxic effects could be evidenced. In fact, the scaffold with different contents of GYY (SF_1%, SF_5%, SF_10%) led to a higher cytotoxicity compared to the other samples and the negative control. This could be explained by considering the static conditions used in the experiment. In fact, the culturing parameters

adopted could cause the cells to be in contact with excess of H_2S, at least in the first period of culture, as shown by amperometry measurement of released H_2S (Raggio et al., 2018; Gambari et al., 2019). However, the value of 30% of cytotoxicity was never exceeded, compared to the 100% cytotoxicity detected for cells treated with Triton X-100 surfactant.

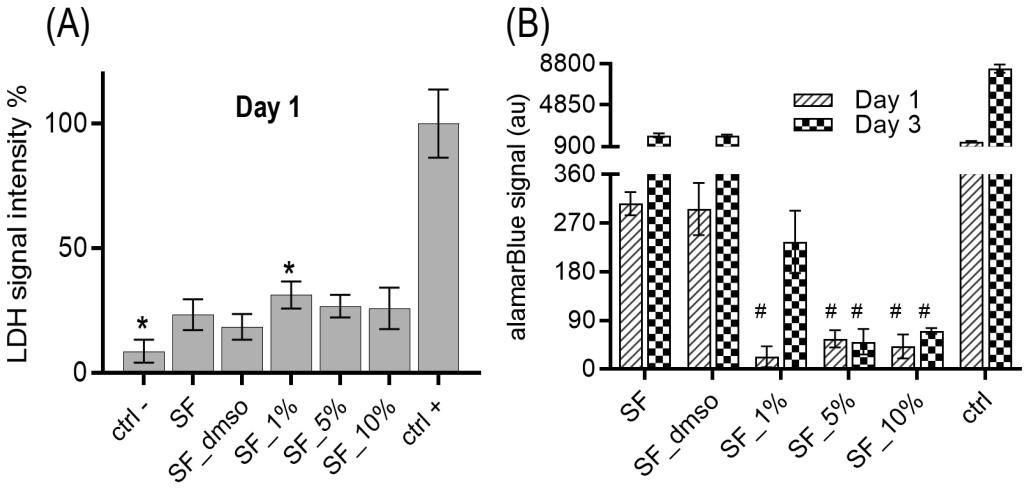

Fig. 27 (A) Cytotoxicity, measured after 1 day from cell seeding, of the different groups of scaffolds (SF, SF_DMSO, treated with DMSO; SF_1%, containing 1% of GYY; SF_5%, containing 5% of GYY; SF_10%, containing 10% of GYY) on MG63 cells. Cells cultured on plastic were used as negative control, while cells treated with 0.05% Triton X-100 surfactant were used as positive control (100% of LDH release). (B) Metabolic activity of cells cultured on the scaffolds of different compositions, measured after 1 and 3 days, expressed as alamarBlue absorption intensity. The values are represented as mean with SEM (n = 5). (*) indicates statistically significant difference at $P<0.01$; (#) indicates that mean values were not statistically different.

Regarding metabolic activity assay, it is well known that higher proliferation causes a larger absorbance value as well as a larger percentage of reduced alamarBlue (Al-Nasiry et al., 2007). For samples SF and SF_dmso, the results obtained for MG63 metabolic activity are in good agreement with the LDH assay data just discussed. Their metabolic activity was high at day 1 and had a relevant increase at day 3. For scaffolds SF_1%, SF_5% and SF_10%, a lower cell metabolic activity reflected the effect of the

presence of GYY in the scaffolds. In particular, results were similar at day 1. Then, at day 3, the metabolic activity of cells on SF_1% clearly increased, while for SF_5% and SF_10% the increase was little. As hypothesized before to explain the scaffolds cytotoxicity, it is possible that the presence of GYY, in the static conditions of the experiment, generated a temporary excessive H_2S level in solution that slowed down the metabolic activity of cells (Raggio et al., 2018). However, the number of viable cells in those scaffolds was not significantly lowered, as their presence could be detected by CLM, in all the scaffolds of different formulations (see Fig. 28). The cell viability and cell distribution on scaffolds after 1 and 3 days from cell seeding were assessed with CLM. Confocal images showed the adhesion of cells on all the scaffolds tested, with significant cell proliferation at day 3. Between different samples, cell adhesion and proliferation appeared comparable. This result might seem in contrast with alamarBlue assay, but it can be explained with a reduction in cell metabolic activity, and not in cell number, induced by H_2S-release from GYY. Image *SF no cells* (Fig. 28 (top), on the top right side) was reported to show fibroin autofluorescence. This effect was useful to visualize the scaffold morphology but, in many cases, it masked the cell nuclei stained with DAPI. Both at day 1 and day 3, cells displayed good adhesion to the scaffolds structure, as shown in the images at higher magnification, where the actin filaments of the cytoskeletons, stained in green, appeared stretched and well distributed on the fibroin matrices. Finally, a representative image of a scaffold cross section was reported, for sample SF_5%: it clearly showed that cells could proliferate in the scaffold, and could migrate inside it, moving from the seeding side towards the interior. This result was relevant, as it indicated that the fabricated GYY-scaffolds could meet, in addition to their proven cytocompatibility, the morphology

requirements of scaffolds for bone TE (Karageorgiou and Kaplan, 2005).

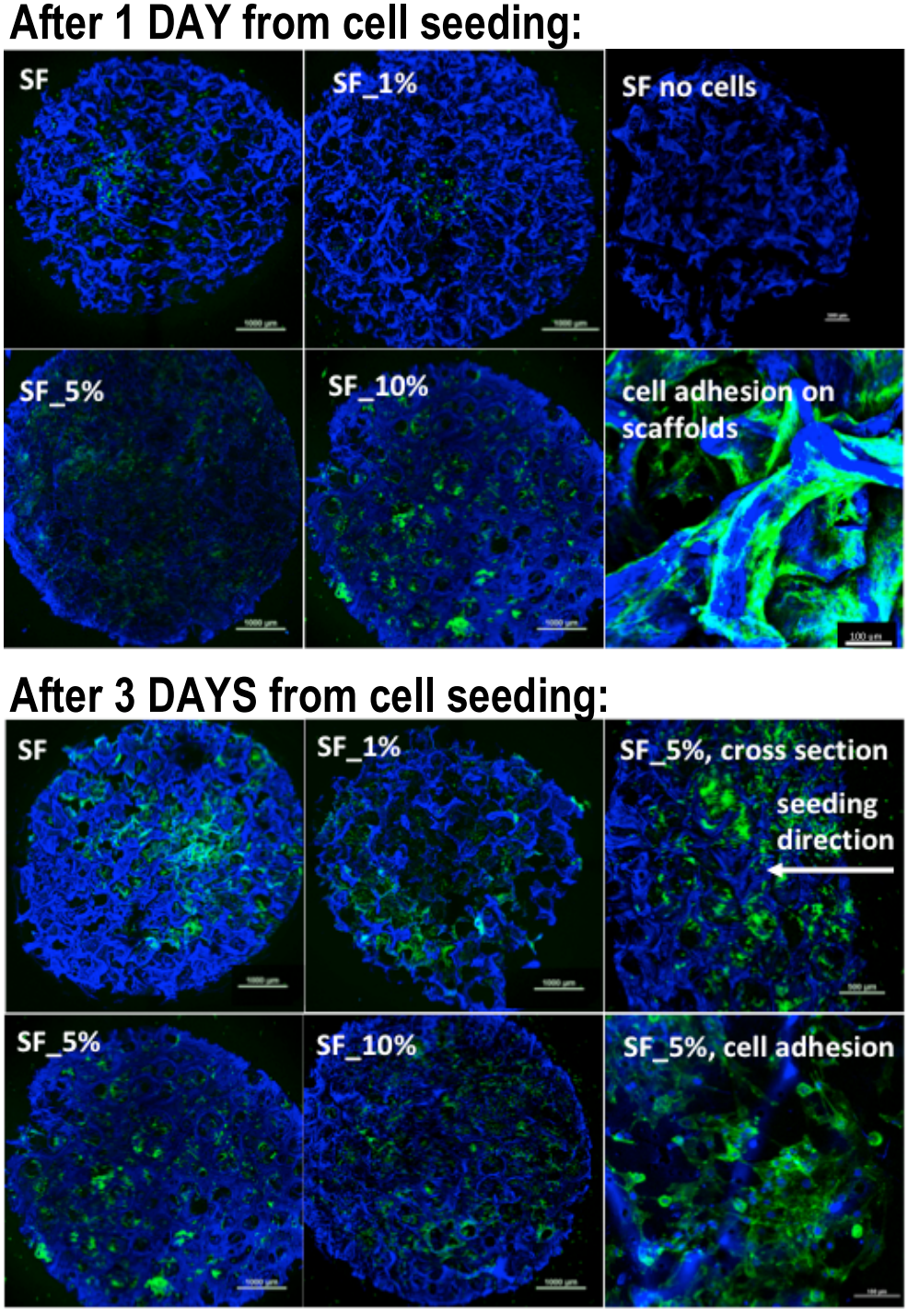

Fig. 28 MG63 cultured on the different scaffolds after 1 day (top) and 3 days (bottom) from seeding. Phalloidin-iFluor 488 stained actin filaments in green, DAPI stained cell nuclei in blue. Scaffolds are blue because of fibroin autofluorescence (see the unstained image SF no cells). Scale bar is 1 cm, except for the bottom right images of both time points, where scale bar is 0.1 cm.

The biological evaluations described in this dissertation (*i.e.*, LDH and alamarBlue assays, and CML imaging with fluorescent stainings) showed that scaffolds containing GYY were cytocompatible and allowed cell adhesion and proliferation. However, these analyses had some limitations, as they were performed in *in vitro* static conditions and for a limited time period. The breakthrough in the characterization of the biological activity of the scaffolds, in particular referring to their potential osteogenic activity, was provided by the deep study performed by our collaborators at Istituto Ortopedico Rizzoli. The scaffolds were cultured in a perfusion bioreactor (Gambari et al., 2019) and characterized for their ability to induce bone formation from hMSCs.

4.3.2. Biological evaluation of scaffolds with hMS cells

Our collaborators at Istituto Ortopedico Rizzoli performed this part of the scaffold's biological evaluation, by testing in a perfusion bioreactor, with hMCS cells, the specific osteogenic biological activity of the scaffolds designed and fabricated by me and my group at the BIOtech Research Center. For this reason, the results obtained are not reported in this dissertation, but the author would like to refer the readers to the articles where results regarding this biological evaluation were published (Raggio et al., 2018; Gambari et al., 2019).

Chapter V. Fibroin/alginate beads containing β-TCP for the treatment of bone defects

Part of this work was performed at the Department of Chemical Engineering of Chulalongkorn University (Bangkok, Thailand), under the supervision of Professor Sorada Kanokpanont, and it was funded by "REMIX" Project, G.A. 778078 H2020-MSCA-RISE-2017.

5.1. Introduction

The objective of this work is the context of a major project ("REMIX" Project, G.A. 778078 H2020-MSCA-RISE-2017) whose main focus regards the design and fabrication of natural based multi-functional biomaterials for therapeutic applications. In particular, with this project, we aimed to realize and characterize a new composite system based on calcium phosphate (CaP) and silk fibroin (SF) that could be potentially exploited in bone tissue engineering applications.
As previously anticipated, around 35% of bone is constituted by inorganic minerals, mainly calcium phosphates with hydroxyapatite-like structure (Bilezikian et al., 2008). The most important feature of CaP compounds used as biomaterials is their capability to be solubilized by the biological fluids and consequently promote osteogenesis processes, which lead to new bone formation (Bose and Tarafder, 2012). The mechanism is based on the partial dissolution of CaP ceramics with release of Ca^{2+} and PO_4^{3-} at the implant/bone interface. Since the concentration of these ions increases locally up to saturation levels, re-precipitation as apatite microcrystals occurs, with contemporary incorporation of other ions

(such as Mg^{2+}) and macromolecules like proteins and growth factors, subtracted from the surrounding biological fluids (Daculsi et al., 1989). The formation of this new osteoconductive material enhances cell attachment, proliferation and differentiation, as well as the secretion of new collagen and the successive bone growth inside the organic-inorganic matrix. Dissolution of implanted CaP, which is performed by cellular activities analogously to bone remodelling, is strongly influenced by multiple factors, such as: chemical formulation of the ceramic (Ca/P ratio, ionic substituents); initial porosity, crystallite size and defects; environment conditions (pH, temperature, fluid motion) (Wang and Nancollas, 2008).

In summary, the properties for which CaPs are used in medical applications, in addition to the already cited bioactivity and resorbability, are (Eliaz and Metoki, 2017):

- osteoinductivity and osteoconductivity, which are the capabilities, respectively, to induce osteogenesis and then bone healing, and to form a functional connecting interphase with the living bone;
- mechanical stability, which allows to prevent mechanical failure, especially for larger implants. In this project, CaPs were used as powders incorporated into a protein matrix, thus were not intended for severe load-bearing conditions;
- biostability, to maintain their biological properties in vivo;
- low hydrophobicity, which ensures that CaP materials attract water and proteins, enhancing the cell adhesion.

In particular, among the different forms of CaP, β-tricalcium phosphate is one of the most appreciated ones for biomedical applications. β-TCP is the rhombohedral β-form of tricalcium phosphate. With the chemical formula of $Ca_3(PO_4)_2$, β-TCP has Ca/P ratio of 1.5, lower than that of hydroxyapatite; this may be the reason

of accelerated degradation and absorption, respect to HA (Wang and Yeung, 2017). After implantation of β-TCP materials *in vivo*, the majority would be resorbed by phagocytosis after 6-24 months. This, together with its excellent osteoconductive and osteointegrative properties, makes the β-TCP effective for filling bone defects caused by trauma and benign tumours (Ogose et al., 2005). In fact, β-TCP was successfully used as an effective inorganic filler to treat small bone defects, and has already been applied in clinics (Gao et al., 2016; Wang and Yeung, 2017; Han et al., 2018). Moreover, recent research started to focus on the enhanced angiogenesis generated by the tricalcium phosphate during bone defects treatment (Chen et al., 2015). In mice implants, CaP ceramics with high content of β-TCP could increase the density of microvessels, probably thanks to the porous structure, and the effects of ions transfer after degradation of CaP.

β-TCP commercially occurs as a fine powder, which can be difficult to manipulate, and needs to be formed into specific structures before implantation. A good strategy to work with β-TCP and to implant it into bone defects is to obtain the dispersion of its powders into polymer solutions. Then, the suspensions prepared can be formed into different shapes, typically micro or millimetric beads (CAM Bioceramics, 2019).

The properties of silk fibroin as biomaterial were described in detail inside the first chapter of this dissertation. In the study reported here, SF was chosen as the main organic material in the composite spheres because of its well known *in vitro* and *in vivo* bioactivity (Altman et al., 2003; Aramwit, 2012).

Sodium alginate, or alginate, is a naturally occurring polysaccharide isolated from brown seaweeds. It was firstly used as a biomaterial in the 1980s, to encapsulate pancreatic islets, and nowadays has many

applications in the medical field (Zimmermann et al., 2007; Cagol et al., 2017). Alginates are linear polymers consisting of 1,4-linked residues of β-D-mannuronic acid (M) and α-L-guluronic acid (G) (Pawar and Edgar, 2012). Alginate has a proven cytocompatibility, rapid ionic gelation kinetic in presence of divalent cations, hydrophilic nature, and tunable properties depending on the processing techniques adopted (Lee and Mooney, 2012). The alginate hydrogel derives from a water-based solution of sodium alginate. The ionic gelation occurs in presence of divalent cations such as Ca^{2+}, or Sr^{2+}. When they are added to a water-based sodium alginate solution, they bind two adjacent residues allowing the formation of interchain bridges that cause a rapid sol-gel transition. Once the gel is formed, it can be dissolved by the exchange of ions with a buffer with low or absent calcium ions, or by treatment with a chelating agent for divalent cations (for example, citric acid or ethylenediamine tetraacetic acid). By combining in solution SF and ALG, which are both water soluble, the ability of ALG to easily gel when contacted with Ca^{2+} ions can be exploited to form SF-based spheres, with an easy, low-cost, organic solvent-free approach (Lee et al., 2013). The addition of β-TCP was simply performed at the solution stage, since we expected that the gelation could allow retaining β-TCP into the spheres.

On the base of these evidences, the aims of this project were:

- the design of a system with a high content of osteoconductive material (β-TCP), embedded in a matrix made bioactive by the presence of fibroin;
- the fabrication of SF/ALG/β-TCP spheres, as selected system to obtain a biocompatible, bioresorbable and effective system with potential application as filler for bone defects.

In particular, with respect to previous studies (Jo et al., 2017), spheres formulation was designed in order to have the maximum amount of inorganic CaP source in the sphere compatible with their formation (*i.e.*, which did not prevent ALG gelation).

5.2. Materials and methods

5.2.1. Materials

White polyhybrid *Bombyx mori* silk cocoons (purchased from Chul Thai Silk Co., Phetchabun, Thailand) were used as source of fibroin. To degum and dissolve fibroin we used the same reagents of the activity of Chapter 3, briefly: sodium carbonate (Na_2CO_3); lithium bromide (LiBr); DI water. Then, the following materials were used in the experiments: PBS buffer (0.05 M sodium hydrogen phosphate, pH 6.5) and alginic acid sodium salt, from brown algae, medium viscosity, in fine powders (Sigma-Aldrich, Saint Louis, MO, USA); β-tri-Calcium phosphate in fine powders (Fluka Analytical, Germany); Calcium chloride ($CaCl_2$), dried (UNILAB, Ajax Finechem, Australia).
For the *in vitro* experiments we used: Saos-2 cell line (from human osteosarcoma, ATCC, Manassas, Virginia, USA); glutaraldehyde and DMSO (Sigma-Aldrich, Saint Louis, MO, USA); MTT assay Kit (Abcam); cell culture medium Dulbecco's Modified Eagle Medium (DMEM) high glucose, foetal bovine serum, and Penicillin/Streptomycin (Thermo Fisher Scientific, Waltham, Massachusetts, USA).

5.2.2. Preparation of silk fibroin solution

Silk cocoons were degummed as described in Chapter 3. The fibres obtained were deeply rinsed with deionized water, and then air-dried. Degummed fibroin was dissolved at a concentration of 10% w/V in

9.3 M aqueous LiBr at 65 °C for 4 h. To eliminate LiBr, the solution was dialyzed in a Slide-A-Lyzer™ Dialysis Cassette (Thermo Fisher Scientific, Waltham, MA, USA) with 3.5 KDa of molecular weight cut-off (MWCO), against DI water for 3 days, with regular water changes. Finally, SF aqueous solution was removed from the cassettes and centrifuged twice at 9000 rpm, 4°C, for 20 minutes, to precipitate any solid residue in suspension and the concentration was measured. SF solutions were used fresh.

5.2.3. Alginate solution preparation

Alginate powders were added to DI water and stirred vigorously until dissolution (around 4 hours), to obtain 2.44% w/W solutions. ALG solutions were used fresh or kept at 4°C before usage.

5.2.4. Preparation of SF/ALG/β-TCP formulations

During the project, different formulations were prepared for the sphere's preparation, and different parameters were tested for the spheres fabrication techniques. In this report, only the most interesting preparations, considered suitable for the final expected applications, are reported.

Starting from solutions of silk fibroin at 7% w/W and alginate 2.44% w/W, and by addition of β-TCP powders, the following formulations were prepared:

Formulation code	SF /ALG (% w/W)	β-TCP (% w/W)	% organic *vs* total solid	% inorganic *vs* total solid
ALG1	0 - 1	-	100	-
ALG1/β-TCP	0 - 1	7.5	40	60
SF4/ALG1	4 - 1	-	100	-
SF4/ALG1/β-TCP	4 - 1	7.5	40	60

Table 6 Description of the formulations prepared starting from ALG and SF solutions, and β-TCP powders, to fabricate spheres of different composition.

β-TCP powders were sieved (100 μm) before addition to alginate solution, in order to break possible aggregates.

The different components were added in glass containers and mixed by magnetic stirring. In particular, the components were mixed in this order: alginate solution; DI water; β-TCP powders; fibroin solution. Silk fibroin solution was always added as the last component and by gently stirring the suspension. The final weight of each suspension was 10 g, and DI water was added when necessary.

The suspensions obtained were always used fresh and were stable (*i.e.,* with no visible precipitation or gelation processes) for at least 6 hours.

5.2.5. Preparation of SF/ALG/β-TCP spheres

Two different techniques were adopted to process the different formulations into beads.

5.2.5.1. Preparation of SF/ALG/β-TCP spheres by gravity dripping

The principle is based on the natural gravity and is the simplest method of drop generation. The solution goes through the tip of a

needle, drops grow and separate from the stream, then fall into a hardening solution. In the experiments, a syringe equipped with a needle of 0.16 mm (30 Gauge) in inner diameter was used to drop the different formulations into $CaCl_2$ 0.1 M aqueous solutions. The flow of the different formulations through the needle was adjusted by applying a constant pressure on the syringe, by using a geared motor (Tsukasa Electric, Japan). The distance between the needle tip and the collection bath was approximately 100 mm.

5.2.5.2. Preparation of SF/ALG/β-TCP spheres by coaxial N_2-flow assisted dripping

The basic principle of the technique is the use of a coaxial gas stream to blow droplets of a polymer-based solution from a needle tip into a gelling bath, before they would fall due to gravity.

A home-made coaxial gas-flow device was used to prepare beads of controlled dimension.

It consisted of an inner needle of 0.41 mm (22 Gauge) in inner diameter, and an outer concentric nozzle, for compressed gas flow, around 1.5 mm in inner diameter. The nitrogen flow was set at 15 L/min by a gas regulator and flowmeter. The flow of the different formulations was adjusted by applying pressure. The same single coaxial nozzle was used to produce beads from all silk fibroin-alginate solutions containing β-TCP powders in suspension, by dripping into $CaCl_2$ 0.1 M. The distance between the nozzle and the collection bath was approximately 100 mm. The schematic representation of the techniques of preparation is shown in the figure.

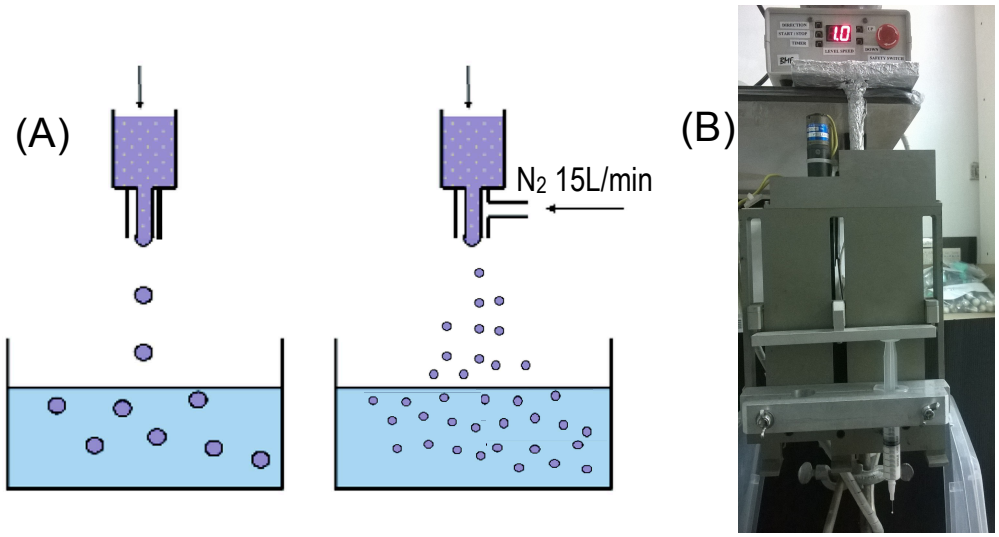

Fig. 29 (A) Schematic representation of the beads preparation techniques: gravity dripping (left) and coaxial N_2-flow assisted dripping (right) (adapted from www.nisco.ch). (B) Picture of the equipment.

5.2.6. Post-fabrication procedures

After dripping, beads were aged in $CaCl_2$ solutions for around 2 hours, to complete alginate gelation. Then, the products were rinsed with DI water and sieved to remove the solution and, in case of beads produced by coaxial N_2-flow assisted dripping, also to separate fractions of beads of different dimensions.

Beads were placed in DI water and frozen in liquid N_2. Then, beads were freeze-dried before starting all the chemico-physical characterizations.

Some beads of the composition SF4/ALG1/β-TCP, were exposed to water vapour for 12 hours to evaluate the effect of this treatment on SF protein structure (coded SF4/ALG1/β-TCP_stab or (W)_stab). In fact, as described previously in this dissertation, various treatments (*e.g.,* exposition to water vapour) are required to obtain structural transitions of regenerated fibroin materials, and make them insoluble in water (Rockwood et al., 2011b).

5.2.7. Characterization techniques

An electron microscope (JEOL, JSM-6610LV, Tokyo, Japan) was used to study the microstructure of the spheres. To investigate functional groups in chemical structure, the lyophilized beads were pressed prior to Fourier Transform Infrared (FT-IR) spectroscopic (Perkin Elmer, Waltham, MA) analysis. All spectra were recorded in the wavenumber range from 2200 to 600 cm^{-1}.

To measure the liquid uptake of the scaffolds, the samples were immersed in DMEM and placed at 37°C. Then, excess of liquid was removed from the sample surfaces by gently dabbing with paper and the wet weight (W_{wet}) was determined. The same procedure was repeated at various time intervals until W_{wet} was stable. Samples were then dried in oven at 65°C overnight and the dry weight (W_{dry}) was determined. The DMEM uptake percentage was calculated as $((W_{wet} - W_{dry}) / W_{dry})*100$. Values were expressed as mean with SEM (n = 3 samples for each group).

The SF release from spheres was evaluated by bicinchoninic acid (BCA) assay (Thermo Scientific Pierce, Waltham, Massachusetts, USA), a colorimetric test for protein quantification that was measured, following the manufacturer's instruction, with a standard plate reader at 562 nm. In the preliminary experiments performed to evaluate the biological response of the new material prepared, MTT colorimetric assay was used to estimate the number of viable cells, at different time points, cultured in presence of the spheres. MTT (3-(4,5-Dimethylthiazol-2-yl)-2,5-diphenyltetrazolium bromide) Assay Kit (Cell Proliferation) was purchased from Abcam. The assay was performed following the manufacturer instructions, and absorbance measurements were recorded at 570 nm using a microplate reader

(Spectrometer FLUOstar Omega, equipped with Reader Control Software Omega, BMG LABTECH, Germany).

5.3. Results and discussion

Spheres of different compositions, fabricated with the two techniques previously described, were characterized for their morphology, chemico-physical properties and biological activity. Since the coaxial N_2-flow assisted dripping method led to beads with largely dispersed dimensions, and poorly reproducible morphology, it was decided to focus the study and the characterization on the spheres obtained by gravity dripping.

In this study, the composition of interest is SF4/ALG1/β-TCP. Spheres of this composition were deeply characterized, while results relative to different compositions are reported for comparison.

5.3.1. Macroscopic aspect of the beads

In the following figure, a schematic representation of the beads structure for the formulation SF4/ALG1/β-TCP is reported.

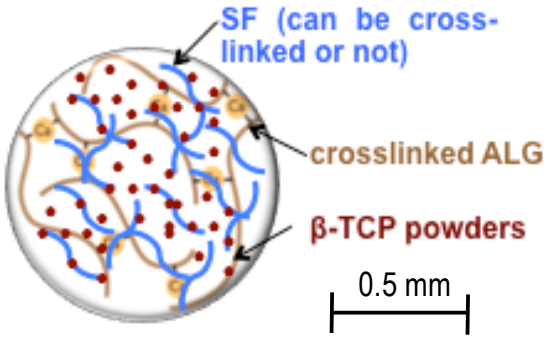

Fig. 30 Schematic representation of SF/ALG/ b-TCP bead composition, with approximate scale dimension.

In Fig. 31, the macroscopic aspect of the beads produced by gravity dripping with 30G needle and just separated from $CaCl_2$ solution is reported.

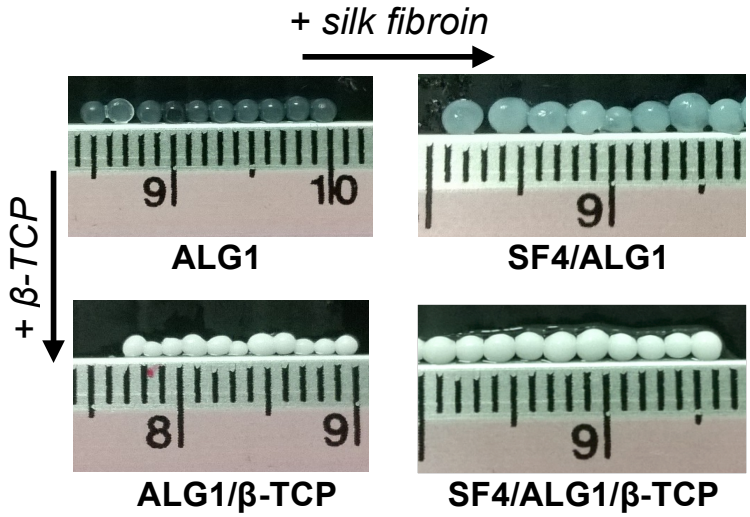

Fig. 31 Pictures of beads of different composition by gravity dripping.

Alginate beads were transparent, while when SF was added beads became opaque. Beads containing β-TCP were white and non-transparent. The differences in the dimensions of the beads, between 0.5 and 1.5 mm in diameter, are probably due to the different surface tension of the solutions, which influences the capability of the bead to detach from the needle tip, and to the density variation in the beads prepared from the different formulations. Beads produced by gravity dripping had uniform dimensions and round shape.

5.3.2. Microstructure of the spheres

The microstructure of spheres of formulation SF4/ALG1 and SF4/ALG1/β-TCP was characterized by scanning electron microscopy (SEM) (Fig. 32). The samples were freeze-dried, coated with gold and characterized (in secondary electron mode, 15 kV).

To obtain images of the cross-sections, freeze-dried beads were immersed in liquid nitrogen and cut with a sharp scalpel.

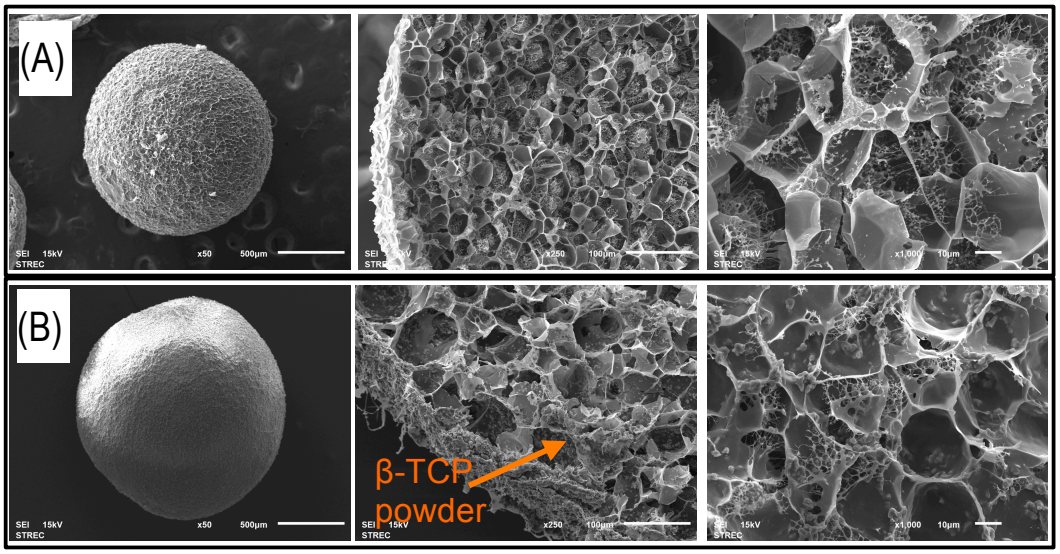

Fig. 32 Images (A) and (B) represent, from left to right, the surface, the cross section and a magnification of the cross section, for sample SF4/ALG1 and SF4/ALG1/β-TCP, respectively.

The presence of dispersed β-TCP powders was clearly visible in the images of the beads of Fig. 32B, both inside and on the surface. The surface of the beads was rough and non-porous. The beads had internal porosity of around 50 μm in dimension.

5.3.3. Infrared spectroscopy analyses of the spheres

Infrared spectroscopy analyses were performed on the beads in order to study the composition and the secondary structure adopted by fibroin in SF4/ALG1/β-TCP beads and in SF4/ALG1/β-TCP_stab, treated by water vapour annealing to obtain fibroin cross-linking.
In Fig. 33, the spheres spectra are reported, together with β-TCP, freeze-dried calcium alginate (Ca ALG) and freeze-dried fibroin (fibroin with mainly random coil secondary structure) spectra. Moreover, also the spectrum of spheres obtained at the end of the

SF release test was recorded, to investigate the composition of the remaining material (sample SF4/ALG1/β-TCP_stab_degr, or (W)_stab_degr).

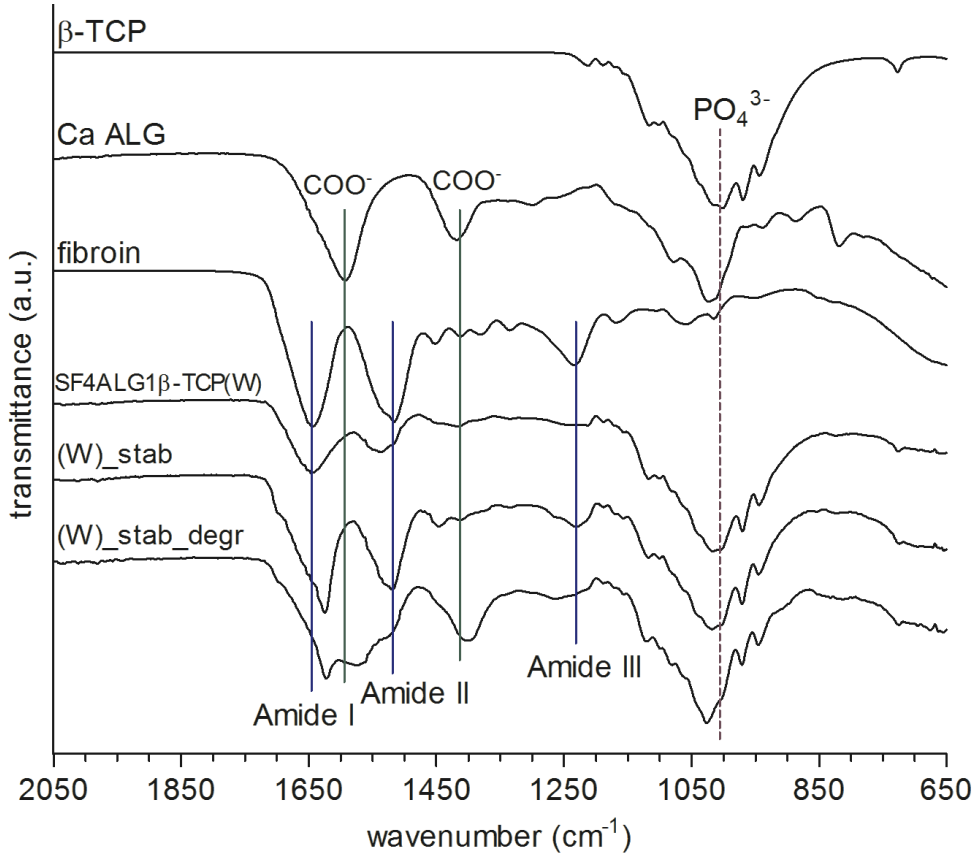

Fig. 33 FT-IR spectra of the starting materials and the different spheres formulations prepared. The spectra of spheres treated with water vapour and at the end of SF release test is also shown.

SF4/ALG1/β-TCP spheres displayed the typical broad absorption band of β-TCP (generated by the composition of the vibrational modes of PO_4^{3-} groups), between 1150 and 850 cm^{-1} (Moreira et al., 2011). Peaks of calcium alginate were also visible at 1600 and 1430 cm^{-1}, corresponding to the carboxylate groups antisymmetric stretching and symmetric stretching respectively (Voo et al., 2015). These bands had a small shift compared to the bands of the pure alginate (1594 and 1460 cm^{-1}) (Lee et al., 2011). The peak shift observed could be due to a chemical interaction between the mineral

phase and the organic matrix, with bond formation between Ca atoms of the β-TCP molecule and the carboxyl groups of alginate samples. The peaks of ALG and β-TCP were visible on the SF4/ALG1/β-TCP and SF4/ALG1/β-TCP_stab beads spectra. On these spectra, also the presence of SF could be detected from:

- shoulder at 1630 cm^{-1} (Amide I band)
- shoulder at 1529 cm^{-1} (Amide II band)
- only for SF4/ALG1/β-TCP_stab, weak absorption at 1245 cm^{-1} (Amide III band) (Callone et al., 2016).

The position of these absorptions suggested that fibroin in the spheres was partially in the β-sheet secondary structure, with some random coil, as discussed also in the third chapter of this dissertation. It could be noticed that the protein absorption bands in the sample SF4/ALG1/β-TCP_stab were sharper and shifted at lower wavenumbers compared to SF4/ALG1/β-TCP. This feature confirmed that a structural transition towards ordered β-sheet dominated conformations occurred in fibroin after exposition to vapour, as expected. Finally, the spectrum of spheres obtained at the end of the SF release test (SF4/ALG1/β-TCP_stab_degr) showed a reduction in SF absorption bands, confirming that a significant amount of SF was released from spheres after 8 days of incubation, as shown and discussed further in Fig. 35.

5.3.4. *In vitro* behaviour of the spheres

5.3.4.1. DMEM uptake

The dry weight of the beads of the two formulations of interest (SF4/ALG1/β-TCP, SF4/ALG1/β-TCP H_2O vapour annealed) was measured (n=3 for each group), then the spheres were placed in 1 ml of DMEM at 37°C, in static conditions. At different time points, the

wet weight of the beads was measured, and the amount of DMEM absorbed was calculated. The profiles of the curves of DMEM uptake % by the two groups of spheres are reported in Fig. 34.

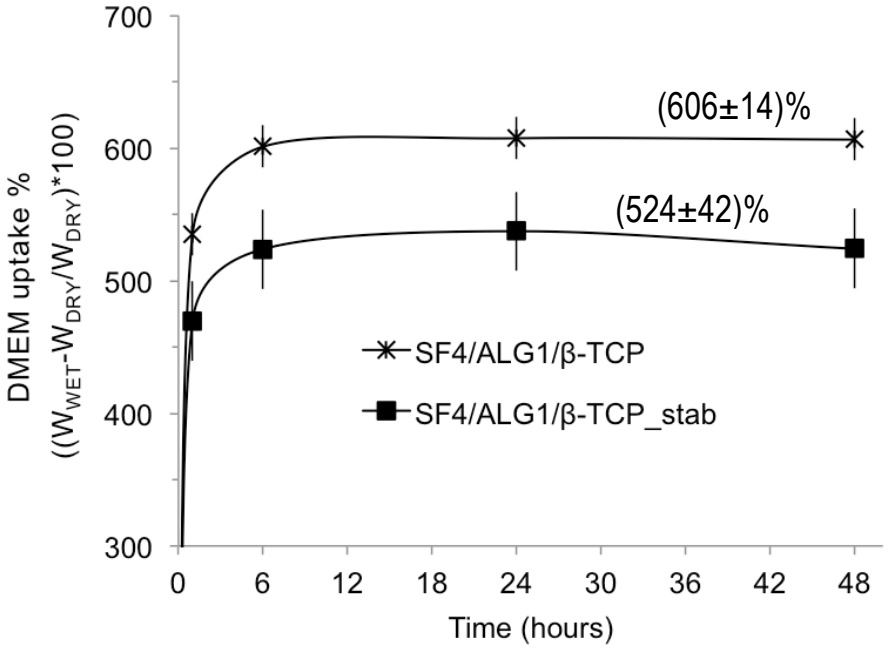

Fig. 34 Profiles of the DMEM uptake % of SF4/ALG1/b-TCP, SF4/ALG1/b-TCP_stab.

The value of the DMEM uptake was stable after 48 hours of incubation, equal to (606±14)% for SF4/ALG1/β-TCP and (524±42)% for SF4/ALG1/β-TCP_stab. The water vapour treatment, which probably induced a higher β -sheet secondary structure content in the SF4/ALG1/β-TCP_stab beads, increased the hydrophobicity of the beads, and altered the beads structure. These two effects might influence the beads DMEM uptake.

5.3.4.2. Evaluation of fibroin release

Spheres of three groups were incubated in 0.5 ml of 4-(2-hydroxyethyl)-1-piperazineethanesulfonic acid buffer (HEPES free acid 25 mM, NaOH, $CaCl_2$ 1 mM) at pH 7.4, 37°C, in 5% CO_2

atmosphere, in static conditions, for 8 days. At different time points, the incubation solutions were collected and frozen, until BCA protein assay for the determination of the protein (fibroin) content was performed (Fig. 35).

The Pierce™ BCA Protein Assay Kit was used for the experiment, with a calibration curve calculated on fresh silk fibroin solutions at different concentrations (calibration not shown).

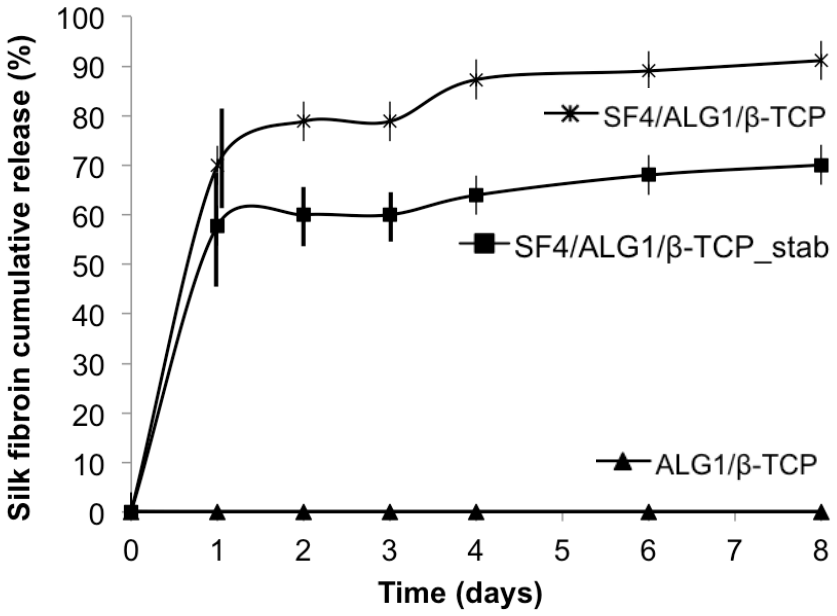

Fig. 35 Profiles of the SF cumulative release % of SF4/ALG1/b-TCP, SF4/ALG1/b-TCP_stab, ALG1/b-TCP.

As expected, no fibroin release was detected for ALG1/β-TCP beads. SF4/ALG1/β-TCP_stab spheres had 65% of the total protein content released after 8 days, while for SF4/ALG1/β-TCP was around 90%. We can assume that the percentage of SF that was retained inside the beads reflects the amount of SF that was arranged in a crystalline structure. This result is in good agreement with FT-IR analyses conducted on the spheres, which featured better resolved and more intense absorptions typical of β-sheet secondary structure for sample SF4/ALG1/β-TCP_stab.

To summarize, the organic part of the spheres started to dissolve in the first 8 days of the test, with most of the inorganic part still forming the sphere. Probably, β-TCP could be confined by the small percentages of SF and ALG remained, as shown by FT-IR that indicated the presence of the two organic components in the composition of sample SF4/ALG1/β-TCP_stab_degr. The aspect of a degraded sphere is shown in SEM images of Fig. 36: the sphere partially retained its structure (left image), and β-TCP particles were still present in the hybrid organic/inorganic matrix (right image).

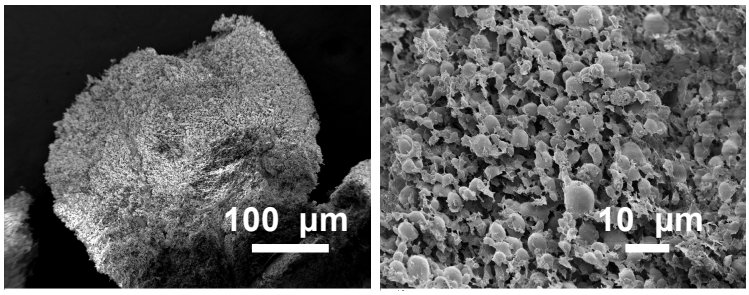

Fig. 36 SEM image of SF4/ALG1/β-TCP_stab_degr sphere on the left, with a magnification of the surface on the right, showing the presence of β-TCP particles embedded in the remaining matrix.

This degradation process could be advantageous for potential application in bone tissue healing. In fact, the inherent bioactivity of SF, both the part released and the part still inside the sphere's matrix, could stimulate cell migration and adhesion in the implant site. In parallel, β-TCP gradually gets in contact with biological fluids and starts to dissolve in turn, inducing mineralization, as previously explained.

5.3.5. Cell culture on SF/ALG/β-TCP spheres

The aim of this preliminary experiment was the evaluation of the *in vitro* cell compatibility of beads made of silk fibroin, alginate and β-

tricalcium phosphate, prepared to function as systems for the easy and efficient implantation of β-TCP into bone defects.

Saos-2 (ATCC® HTB85™) cell line, purchased from American Type Culture Collection, USA, was chosen for the experiments because it is a well-established human cell line of an osteoblast phenotype.

The MTT assay was used to evaluate the viability and the early cell adhesion on the beads after 6 hours, and the number of cells proliferated on the beads after 24 hours, 72 hours and 7 days. MTT is a viability assay, since it is based on the colorimetric detection of formazan, a product with a deep purple colour that forms when viable cells reduce the MTT reagent by NAD(P)H-dependent oxidoreductase enzymes. It was used to measure cellular metabolic activity as a proxy for cell viability (Riss et al., 2004).

Three groups of spheres were tested:

- B: SF4/ALG1/β-TCP
- BS: SF4/ALG1/β-TCP_stab
- BA: ALG1/β-TCP

Before cell seeding, the beads of the 3 groups were sterilized by ethylene oxide (EtO) treatment, in order to remove any possible trace of microbiological agents. The spheres were seeded with Saos-2 cells, and maintained in culture at 37 °C, 5% CO_2 on an orbital shaker at 60 rpm for different periods of time (6 hours, 1 day, 3 days, 7 days) before the assays were carried out.

The number of cells attached to the beads after 6 hours (early cell adhesion), and the number of cells on the beads after 1 day, 3 days and 7 days (cell proliferation), were estimated by MTT assay (Fig. 37).

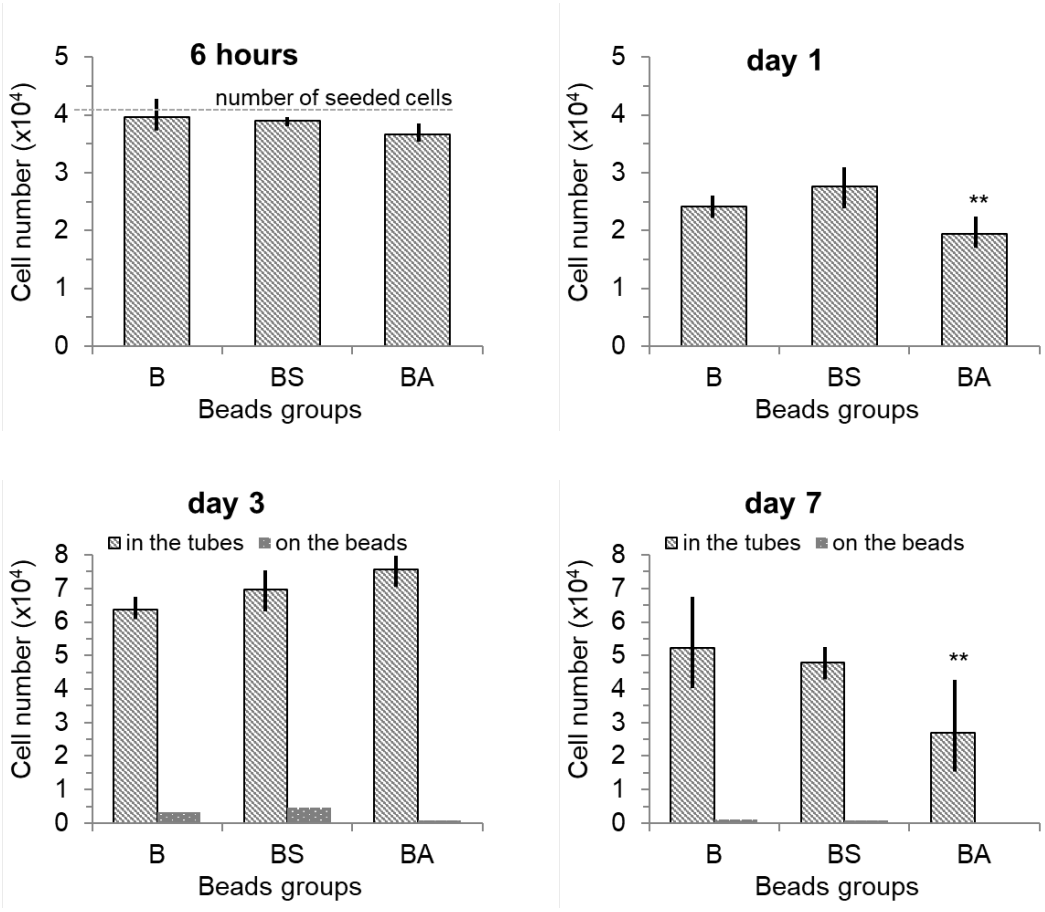

*Fig. 37 Results of MTT assay performed on three different set of samples cultured with Saos-2 cell line. B is SF4/ALG1/b-TCP, BS is SF4/ALG1/b-TCP_stab, BA is ALG1/b-TCP. ** indicates significant differences between values at P ≤ 0.01.*

At time points “6 hours” and “day 1”, MTT assay was performed in the tubes containing the beads. After time point “day 1”, when the cells were supposed to be adherent to the spheres, spheres were moved to a new plate, and the MTT assay was performed separately, in parallel, on the beads and in the tubes used for the incubation. This operation allowed us to discriminate between the total viable cells, and the number of viable cells effectively attached to the spheres. As visible at days 3 and 7, most of the cells did not adhere

to the beads, but to the tubes. However, the beads did not induce any toxic effects on the cells that could proliferate. Even if BA allowed cell viability, formulations containing SF featured the best results in terms of cell proliferation and adhesion to the spheres. These results are preliminary and indicate that spheres of different composition allowed cell viability and proliferation, with better results for materials containing SF. However, in the initial experiments performed until now, cell attachment on the spheres was limited. Therefore, a more complete biological evaluation of the spheres should be performed, and spheres surface features, morphology and composition should be optimized for cell adhesion, proliferation and penetration, for instance by creating surface porosity on the spheres (Karageorgiou and Kaplan, 2005).

Chapter VI. Fibroin films combined with the neuropeptide substance P as models of immunomodulatory systems

Part of this work was performed in collaboration with Doctor Roberta Tasso, Regenerative Medicine Laboratory, Ospedale Policlinico San Martino, Genoa, Italy

6.1. Introduction

This chapter contains the description of the research activity that has been focused on the design of a fibroin biomaterial-based strategy to target macrophage behaviour during inflammation processes. The ability to control macrophage phenotype is of particular interest in the tissue engineering field because macrophages have an active role in all the phases of tissues regeneration, exactly when a biomaterial is expected to fulfil its functions (Panilaitis et al., 2003). These cells remove cellular debris, remodel the ECM, and synthesize cytokines and growth factors. Macrophage classification, which is rather complex, can be simplified and these cells can be denoted as either pro-inflammatory "M1" (*i.e.,* initiating an acute response) or pro-healing "M2" (*i.e.,* promoting the proliferative phase) (Graney et al., 2018). An illustrative scheme of the different macrophages phenotypes, with their inducers and functions, is reported in Fig. 38 (Kou and Babensee, 2011).

Graney et al. provided a detailed review of macrophages and biomaterial design strategies to control them, especially for angiogenesis and wound healing purposes. Macrophages were described for their ability to shift phenotypes between extremes (from

M1 to M2), resulting in pro-inflammatory or anti-inflammatory, pro-fibrotic or matrix-degrading, depending on the situation. The response time of the macrophages to shifting between phenotypes was described as fundamental, since M1 and M2 are required at different stages of tissue repair and regeneration (Boniakowski et al., 2017). As a consequence, from the tissue engineering point of view, biomaterials that can regulate macrophages behaviour in a temporally controlled manner are of great interest (Hotaling et al., 2015).

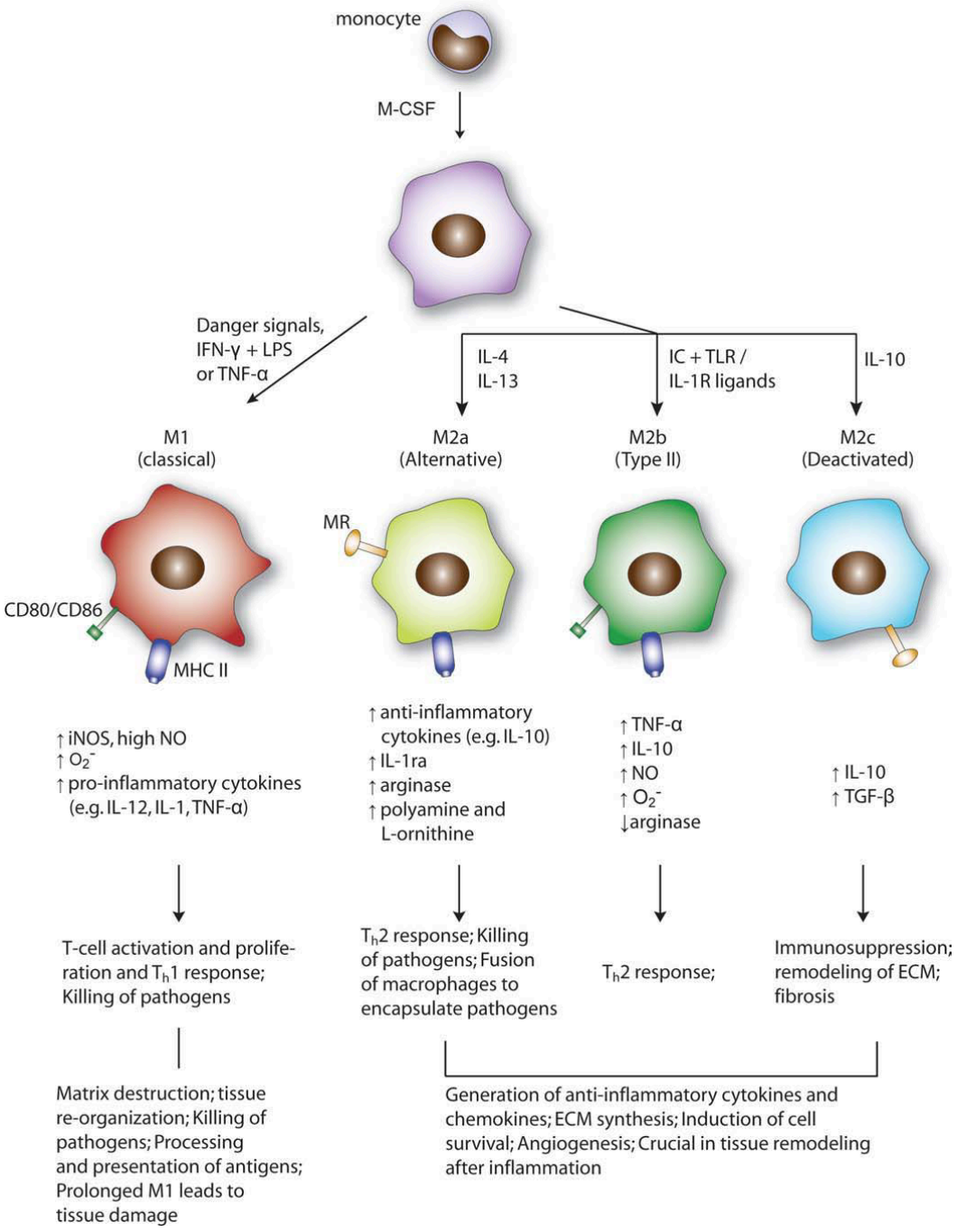

Fig. 38 A scheme of the different phenotypes of macrophages, with their inducers and functions. They are derived from the circulating precursors, monocytes, in response to macrophage colony-stimulating factor (M-CSF). In response to stimuli (cytokines, activated oxygen or nitrogen species, etc.) the plasticity of macrophages allows them to polarize into different populations with specific functions (Kou and Babensee, 2011). With permission of John Wiley and Sons.

Substance P (SP) is an eleven amino acid neuropeptide (sequence: RPKPQQFFGLMNH_2) of the tachykinin neuropeptide family. It is secreted by nerves and inflammatory cells such as macrophages, eosinophils, lymphocytes, and dendritic cells, and acts by binding to the neurokinin-1 receptor (NK-1R) (O'Connor et al., 2004). It was shown that treatment of skin wounds with exogenously administered SP could modulate inflammation, leading to a resolution of the wound (Leal et al., 2015). In particular, during the inflammatory phase of the pathological situation of a diabetic skin wound, Leal *et al.* showed that: the SP neuropeptide expression was reduced; a chronic pro-inflammatory state aroused; a high M1/M2 macrophage ratio was reached. Local treatment with SP modulated that ratio in favour of M2, and reduced the expression of pro-inflammatory cytokines, indicating resolution of inflammation and progression to the proliferative and healing phases (Leal et al., 2015).

Silk fibroin, which features were already described in detail in the introduction chapter, was proven to be a compatible matrix for the encapsulation and sustained delivery of protein therapeutics and growth factors for biomedical applications, and for the stabilization and protection of entrapped enzymes and peptides. In different experiments, silk fibroin matrices of different morphologies could be combined by various strategies with biomolecules, and used to modulate their release and/or preserve their bioactivity for significant periods until the final application (Lu et al., 2009, 2010a). For example, a lyophilized silk fibroin hydrogel matrix was described for the sustained release of monoclonal antibodies (Guziewicz et al., 2011). In other studies, 2D fibroin materials like films or membranes were produced, for the ease of fabrication and characterization (Gil et al., 2013; Ju et al., 2016). Fibroin films, prepared by casting of sulfonated silk fibroin solutions, allowed binding (through ionic and

hydrophobic-hydrophilic interactions) and release of FGF-2 (Wenk et al., 2010). Silk solutions with embedded NGF (nervous growth factors) were used to prepare NGF-loaded films and tubes that could release the growth factor upon incubation (Uebersax et al., 2007).
With these premises, in this part of my research activity, SF films were chosen as models for the preparation of an immunomodulatory biomaterial, which could provide fibroin with the macrophage modulatory abilities of SP. To pursue this goal, silk fibroin films with substance P were prepared by using two different strategies, in parallel:

- direct mixing of fibroin and SP solutions;
- incorporation of SP by covalent coupling to prefabricated fibroin film.

The two strategies allowed us to study the range of properties, with differences and analogies, featured by SP-films of the two types.

6.2. Materials and methods

6.2.1. Materials

White polyhybrid *Bombyx mori* silk cocoons (purchased from Chul Thai Silk Co., Phetchabun, Thailand) were used as source of fibroin. To degum and dissolve fibroin we used the same reagents of the activity of Chapter 3, briefly: sodium carbonate (Na_2CO_3); lithium bromide (LiBr); DI water. PBS buffer (0.1 M sodium phosphate, 0.5 M NaCl, pH 6.5), 1-ethyl-3-(dimethylaminopropyl)carbodiimide hydrochloride (EDC), N-hydroxysuccinimide (NHS), and bovine serum albumine (BSA) were purchased from Sigma-Aldrich (Saint Louis, MO, USA). Substance P acetate salt (SP) (Fig. 39 and Table 7), Substance P ELISA (Enzyme-Linked Immunosorbent Assay) Kit

and Anti-substance P antibody [SP-DE4-21] were purchased from Abcam (Cambridge, United Kingdom). SP solution was prepared and stored following manufacturer instructions. Goat anti-Mouse IgG Secondary Antibody conjugated to Alexa Fluor 488 was purchased from Thermo Fisher Scientific (Waltham, MA, USA).

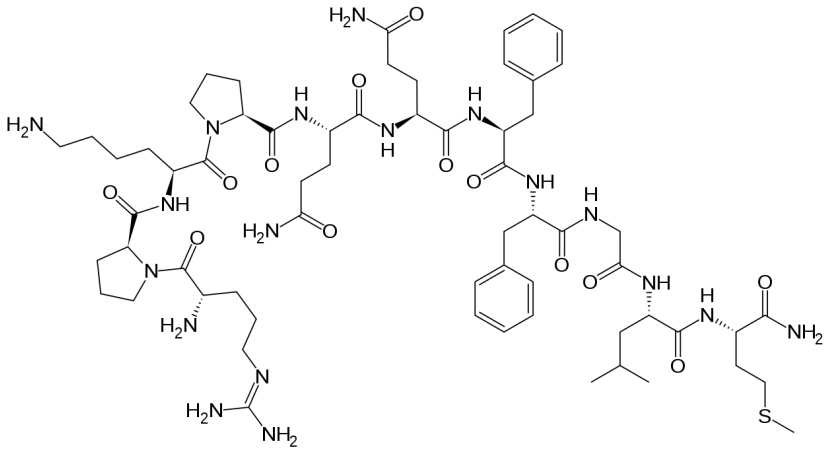

Fig. 39 Structural formula of Substance P neuropetide.

General chemico-physical properties of SP peptide	
amino acids:	Arg- Pro- Lys- Pro- Gln- Gln- Phe- Phe- Gly- Leu- Met
MW:	1347.65 g/mol
solubility:	50 mg/ml in 1M acetic acid
isoelectric point:	~11
charge at pH 7.4:	2

Table 7 General properties of SP peptide (http://isoelectric.ovh.org)

6.2.2. Preparation of silk fibroin aqueous solution

Silk cocoons were degummed as described in Chapter 3. The fibers obtained were deeply rinsed with deionized water, and then air-dried. Degummed fibroin was dissolved at a concentration of 10% w/V in

9.3 M aqueous LiBr at 65 °C for 4 h. To eliminate LiBr, the solution was dialyzed in a Slide-A-Lyzer™ Dialysis Cassette (Thermo Fisher Scientific, Waltham, MA, USA) with 3.5 KDa of molecular weight cut-off (MWCO), against DI water for 3 days, with regular water changes. Finally, SF aqueous solution was filtered using a glass porous septum to eliminate any solid residue in suspension. The concentration was measured and adjusted to 2% w/V (0.2 g of silk per ml of water), by dilution with DI water.

6.2.3. Preparation of silk fibroin films

6.2.3.1. Pure fibroin films

Fibroin films were prepared by casting 10 ml of fibroin aqueous solution at 2% w/V in 55 mm-diameter Petri dishes. The films were dried overnight in a laminar flow hood at room temperature. Dry films were then treated by annealing process to induce structural transition and make them insoluble in water: films were placed in a desiccator under vacuum in presence of water vapour, and maintained for 24 hours, at room temperature.
Finally, films were briefly hydrated and cut in disks of 6 mm in diameter by biopsy punch.

6.2.3.2. Fibroin films with substance P

Silk fibroin films containing substance P were prepared by using, in parallel, the two different strategies described in the following paragraph.
To prepare fibroin films containing SP by direct mixing of their solutions (*strategy (I)*), 100 µl of DI water containing 0.1% BSA (for stabilization of SP) and 2.5 mg of SP (corresponding to 25 mg/ml SP) were added to 10 ml of fibroin solution at 2% w/V (corresponding to

0.2 mg/ml fibroin). The solution was poured in 55 mm-diameter Petri dishes, dried overnight, and the films obtained were treated with water vapour, as described before. Films were hydrated and cut in disks of 6 mm in diameter by biopsy punch.

To prepare fibroin films containing SP by covalent conjugation post-fabrication to their surfaces (*strategy (II)*), fibroin films were produced by casting and treated with water vapour, as described before. Then, films were soaked in PBS buffer (0.1 M sodium phosphate, 0.5 M NaCl, pH 6.5) for 30-45 minutes to hydrate. Subsequently, SF films were transferred into a solution of EDC/NHS (0.5 mg/mL of EDC with 0.7 mg/mL NHS in PBS buffer) for 15 min at room temperature, in order to improve the reactivity of -COOH groups exposed by SF aspartic and glutamic acids (present respectively at around 0.5 mol% and 0.6 mol% of the total amino acids based on the amino acid composition of fibroin) (Murphy et al., 2008; Murphy and Kaplan, 2009). After rinsing with PBS buffer, each film was contacted with a solution containing 2.5 mg of SP in PBS with 0.1% BSA, for 2 h at room temperature. At the completion of peptide coupling, the films were rinsed for 5 minutes in fresh PBS buffer solution, and then rinsed with DI water to remove buffer salts. Films were cut in disks of 6 mm in diameter by biopsy punch, and air-dried. In parallel with this set of films, also SF films, treated with the same processes but in absence of SP, were prepared for the use as controls in some characterization analyses.

The following scheme (Fig. 40) represents the two strategies used, starting from fibroin in solution, to combine SP with SF films, together with the reaction of SP conjugation to -COOH residues of Asp and Glu fibroin amino acids.

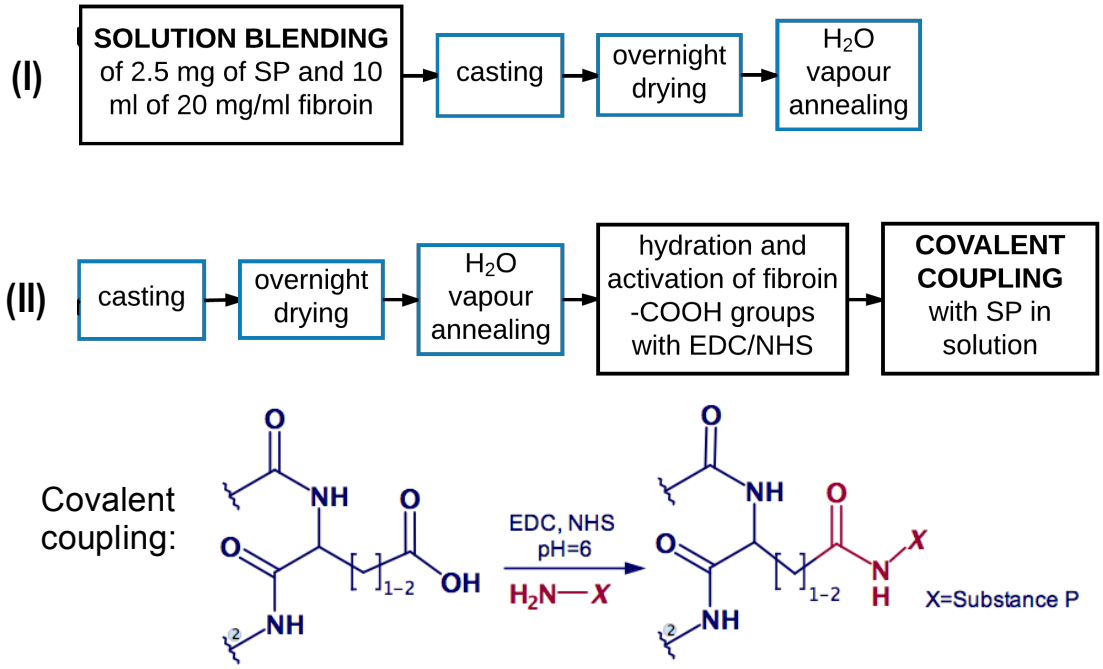

Fig. 40 Schematic representation of SP combination with fibroin films by simple mixing (or solution blending) and by covalent conjugation, with a focus on the chemical reaction occurred. Subscript 1 or 2 indicate the number of C atoms in the chain, 1 is for Asp and 2 is for Glu.

The material quantities used allowed obtaining a final theoretical amount of 32 µg of SP (corresponding to 0.024 µmoles) per each disk of 6 mm. These doses were decided in agreement with a study that showed the optimal diabetic foot ulceration healing promoted by local treatment with SP (Leal et al., 2015). In particular, a dry weight of 2.3 mg for each 6-mm fibroin film disk was considered, corresponding to a content of 0.34 µmoles of Asp and Glu residues (the targeted amino acids residues that were exploited for the covalent coupling of SP onto -COOH groups exposed on fibroin films). Both the strategies were supposed to allow a 100% incorporation of SP: the first one, because SP was incorporated directly into fibroin solution, and should be all retained in the dry films; the second one, because the equivalents of Asp and Glu (-

COOH reactive groups) available were around 14 times the equivalents of SP used (0.34 µmoles of Asp+Glu/0.024 µmoles of SP = 14.2).

The different types of materials prepared are schematically presented in the table, together with the sample codes (Table 8).

Sample Code	Description
FF	pure fibroin film (control)
FF_edc/nhs	fibroin film activated by EDC/NHS (control)
FF_covSP	fibroin film + SP covalently coupled post-fabrication
FF_mixSP	fibroin film + SP incorporated in solution

Table 8 Codes of the different samples of fibroin films prepared.

6.2.4. Characterization techniques

Most of the characterization techniques used to analyse fibroin films were already described in the previous chapters, except for water contact angle, Atomic Force Microscopy, spectrophotometric detection of SP in solution, confocal imaging of films.

6.2.4.1. Water contact angle

The water contact angle of a 10 µl droplet of DI water deposited on films surfaces by a Hamilton glass syringe was used to determine the films hydrophobicity. The films were fixed on a glass substrate and placed on an optical bench equipped with a light and a camera with Cosmicar lens (Pentax, Tokyo, Japan), connected to a computer. Left and right contact angles were measured from the pictures taken on three droplets for each film, by using an ImageJ plugin.

6.2.4.2. Atomic force microscopy

Fibroin films were studied by Atomic Force Microscopy in order to investigate possible changes in surface topography before and after the combination with the Substance P peptide (Hansma, 2013). An SPM (Scanning Probe Microscope) NT-MDT Solver Pro system (NT-MDT, Moscow, Russia) equipped with S7 scanner was used. All samples were imaged in semi-contact mode using silicon tips (NSG-11, NT-MDT, 10 nm nominal tip radius, resonance frequency of 181 kHz), collecting 2x2 μm, 512-points resolution images. Gwyddion (Czech Metrology Institute, 2004), a modular program for SPM data visualization and analysis, was used to elaborate AFM images and calculate surface roughness.

6.2.4.3. Immuno-detection of SP

ELISA assay was used to quantitatively analyse SP release from films in solution. SP release studies were conducted by incubating 6-mm-diameter fibroin films in PBS pH 7.4 at 37°C, for 10 days. Every 12 hours supernatants were harvested and frozen, and fresh PBS (0.1 ml) was placed in contact with the films.

Competitive ELISA assay was performed in duplicates on the supernatants, following the manufacturer instructions. The samples absorbance at 405 nm was measured using a microplate reader Spark 10M (Tecan, Austria).

The presence of SP on the films was also evaluated using a Nikon A1 confocal microscopy (Nikon Instruments, Amsterdam, The Netherlands), upon incubation of the films with anti-substance P antibody and fluorescent secondary antibody to label and visualize SP.

6.3. Results and discussion

The main objectives of the characterizations were:

- the investigation of fibroin films with and without SP, in order to have an indication of the efficacy of loading of SP into the films, and evaluate possible changes in the chemico-physical properties of fibroin or the neuropeptide;
- the determination of the dynamics of release of SP from fibroin films, with preserved SP bioactivity, in order to assess the possibility to use fibroin matrices as platforms for a macrophage modulation system.

FT-IR spectroscopy was used to evaluate the secondary structure adopted by fibroin in the films. In particular, films prepared by incorporating SP directly into fibroin solution (FF_mixSP), i.e. contacted with fibroin still in water before inducing any protein secondary structure, were taken in careful consideration and compared with films prepared by the other methodologies. Moreover, also films prepared by covalent functionalization with SP post-film-fabrication in solution (FF_covSP) could potentially show differences in fibroin secondary structure, deriving from the activation step with EDC/NHS.

All the samples presented the Amide I band centred at 1623 cm^{-1}, indicating prevalent β-sheet secondary structure (Fig. 41). A shoulder at 1648 cm^{-1} was also visible and was more evident for samples FF and FF_mixSP, indicating the presence of some random coil conformation. It is possible that the treatment with EDC/NHS (that act as crosslinkers) used to prepare samples FF_edc/nhs and FF_covSP, induced a further transition of residual random coils to β-sheet conformation, resulting in a slight intensity decrease of the shoulder at 1648 cm^{-1} for these films.

Amide II and Amide III bands were present for all samples respectively at 1516 and 1235 cm^{-1}, typical of fibroin in β-sheet conformation.

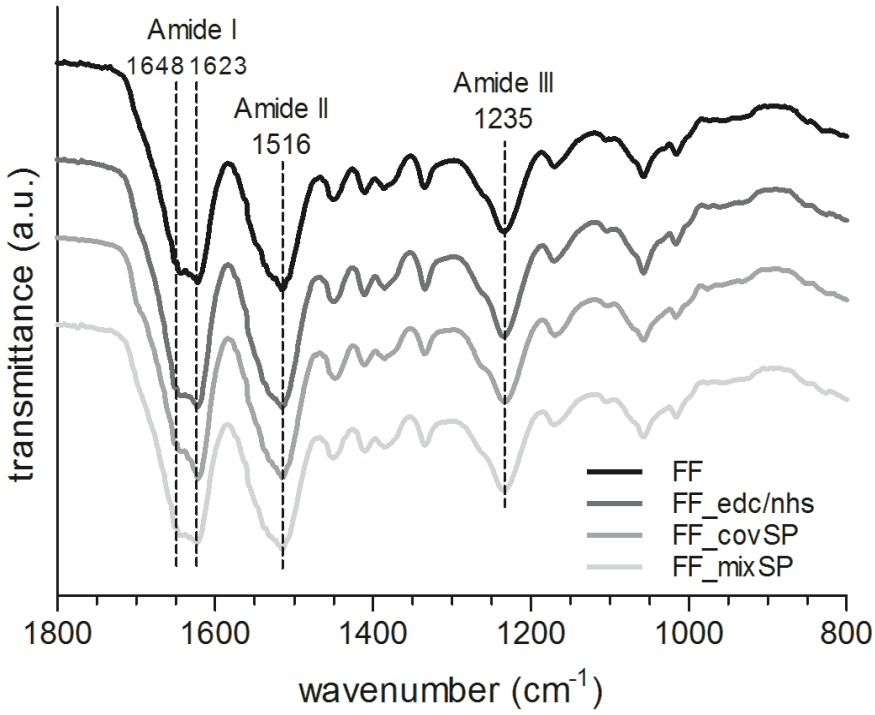

Fig. 41 Infrared spectra of films: FF (fibroin film); FF_edc/nhs (fibroin films treated with EDC and NHS); FF_covSP (fibroin film + SP covalently coupled post-fabrication of film); FF_mixSP (fibroin film + SP incorporated in solution).

The incorporation of SP to fibroin films didn't generate any clear additional absorption band or modifications of the existing ones on the corresponding spectra, in comparison with FF spectrum. This result could be expected, considering that fibroin vibrations dominate the infrared spectrum, and SP, being also a peptide but with only 11 amino acids and no particular features, is not characterized by specific or particularly intense absorptions discernible from fibroin.

Results of the water contact angles measured on the different samples are shown in the following figure and table (Fig. 42 and Table 9).

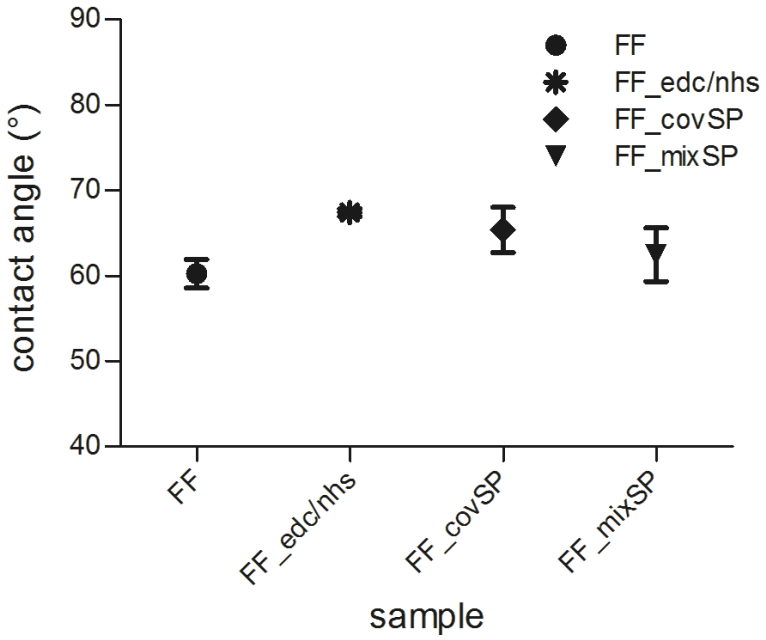

Fig. 42 Water contact angles of the films. Mean with SD, n=6

	FF	FF_edc/nhs	FF_covSP	FF_mixSP
Mean θ (°)	60.2	67.4	65.4	62.4
SD (°)	2.9	0.8	4.6	5.4

Table 9 Water contact angles values of the films.

The mean values of contact angle measured for the different films were very similar, indicating that no significant changes in the hydrophobicity of the films occurred after incorporation of SP with the two different strategies. These results could be correlated with the FT-IR analyses. In fact, the protein structure determines the nature of the fibroin material (in this specific case, films) interaction with water. In this study, values of contact angle indicating a moderately hydrophilic surface were in agreement with the FT-IR analyses, which revealed prevalence of β-sheet secondary structure (insoluble in water). Moreover, both contact angles and FT-IR spectra profiles were basically constant between different samples. A representative

image of FF obtained by electron microscopy is here reported, to show the typical thickness and cross-section morphology of the samples prepared (Fig. 43).

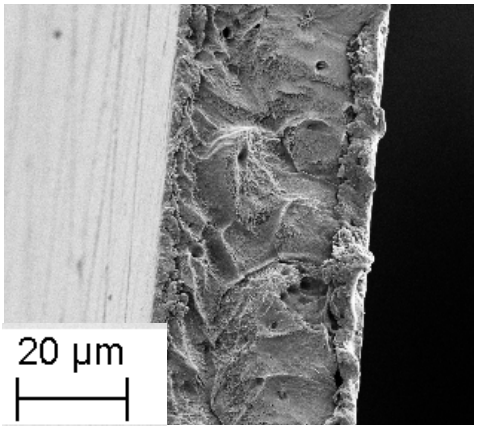

Fig. 43 A representative FE-SEM image of FF film, showing the average thickness of the samples prepared.

Then, fibroin films were studied by Atomic Force Microscopy in order to investigate possible changes in surface topography after the combination with the Substance P peptide (Hansma, 2013).
The AFM images collected on SP peptide cast on mica substrate and on the fibroin-based films were used to estimate the roughness and to identify the presence of specific surface features that could indicate the presence of SP peptide exposed on fibroin films. For the images, which were collected in semi-contact mode and by scanning 2x2 µm areas, the colour scale reflected the Z scale, *i.e.* the surface roughness. The most relevant images collected are shown and discussed (Fig. 44). The surface roughness was calculated on the images in terms of R_{ms} (*i.e.* the root mean square (RMS) average of height deviations from the mean image data plane) (Table 10).

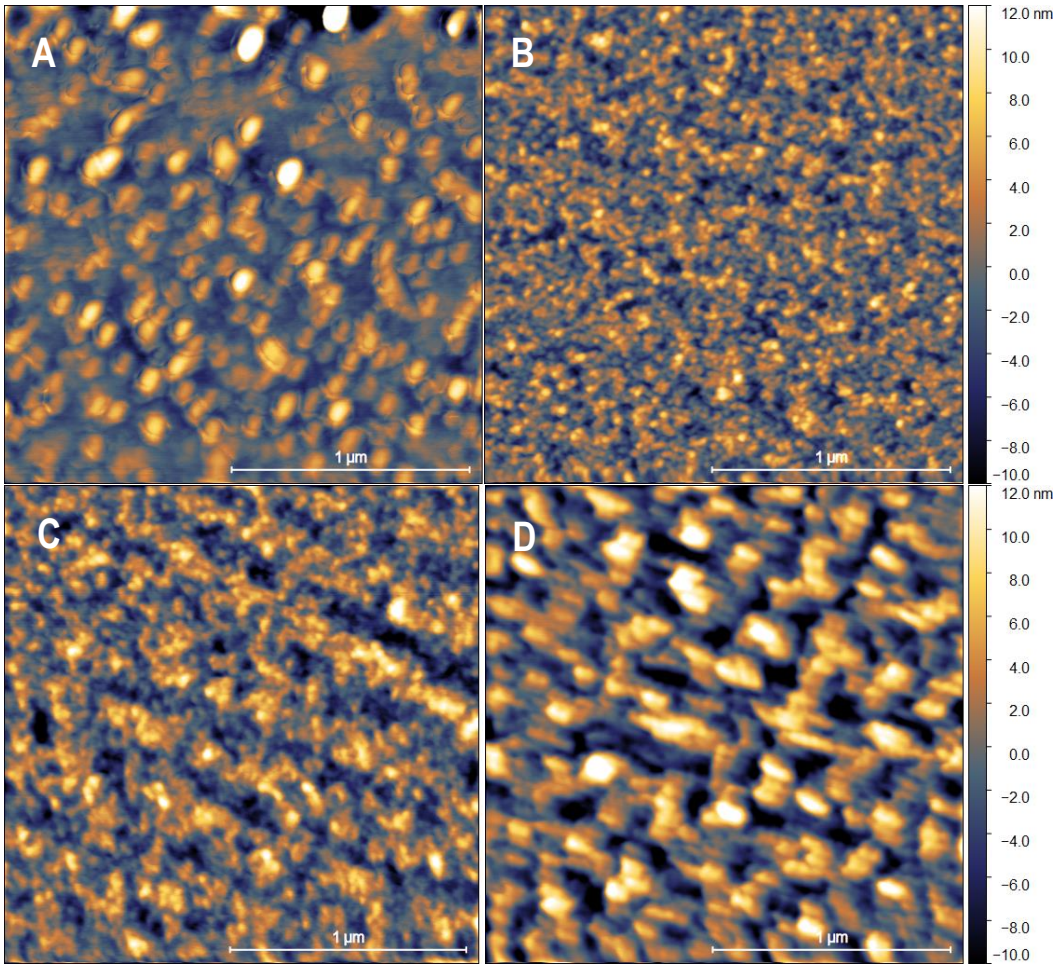

Fig. 44 AFM images of SP layer on mica substrate and fibroin films of different compositions. Images codes are illustrated in the following table.

Image	Sample code	Description	Rms (Sq), nm
A	SP peptide	solution 0.05 mg/ml, on mica	3.9
B	FF	pure fibroin film (control)	2.7
C	FF_covSP	fibroin film + SP covalently coupled	3.8
D	FF_mixSP	fibroin film + SP incorporated in solution	5.1

Table 10 Roughness values of SP peptide and films from AFM images.

Image (A) was collected on SP peptide deposited on an ultra-flat mica substrate from an SP diluted solution (0.05 mg/ml in water). This image could be used as references to study fibroin films samples containing SP. The roughness values obtained and the dimensions of the round shaped features visible in the image are compatible with SP peptide in the globular arrangement typical of proteins deposited on a flat substrate from solution.

Untreated fibroin film (FF film, (B)) had a mean roughness value (Rms) around 2.7 nm. Fibroin film combined with SP by covalent conjugation in solution featured a higher mean roughness value, calculated around 3.8 nm. The increased roughness detected for FF_covSP film could be an indicator of the occurred conjugation of SP to fibroin film surface, since the difference between the Rms values of the two different types of films (FF and FF_covSP) was compatible with the height of the SP peptide. The sample FF_mixSP (D) showed the higher roughness between the different samples studied (Rms was 5.1 nm). This could suggest the presence of the SP peptide that was mixed with fibroin solution before film casting and could have diffused partially to the film surface during solvent evaporation or fibroin crosslinking.

Experiments of SP immuno-detection were firstly performed by the use of fluorescent-labelled antibodies and confocal microscopy, to assess the possibility of visualizing SP attached to fibroin films in samples FF_covSP and FF_mixSP.

The fluorescent secondary antibody (AbII) was only visible, after film incubation with the primary antibody (AbI) antiSP, on samples FF_covSP and FF_mixSP (images B and C), confirming that SP could be recognized and visualized on fibroin films surface, and that fibroin didn't give any signal due to adsorption or nonspecific binding of AbI or AbII to pure fibroin (image A).

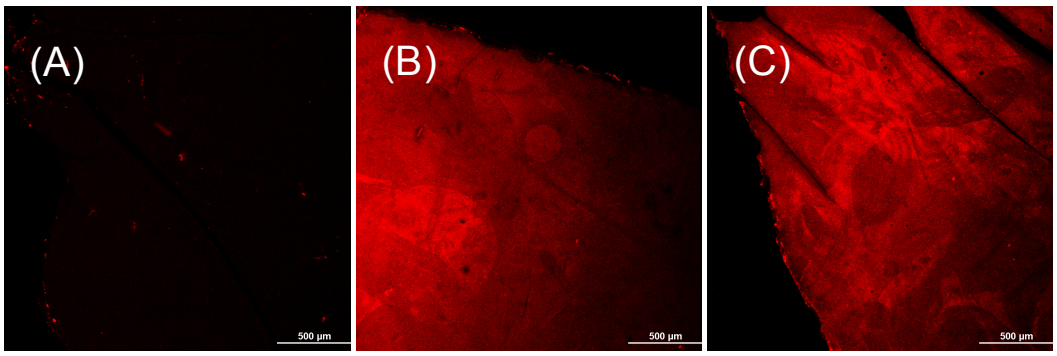

Fig. 45 FF (A), FF_covSP (B) and FF_mixSP (C) images, obtained by confocal microscopy after incubation with anti-SP primary antibody and fluorescent scondary antibody. Scale bar 500 µm.

The quantitative immuno-detection of SP release from the films was performed by ELISA assay (Fig. 46 and Fig. 47). Here are reported the curves of the cumulative release of SP for the different sets of films, and the curves for the cumulative release of SP %, considering the initial SP amount of 30 µg and 9 µg calculated for FF_mixSP and FF_covSP 6 mm-diameter disk, respectively. No SP release was detected for pure SF films (FF and FF_edc/nhs, data not shown).

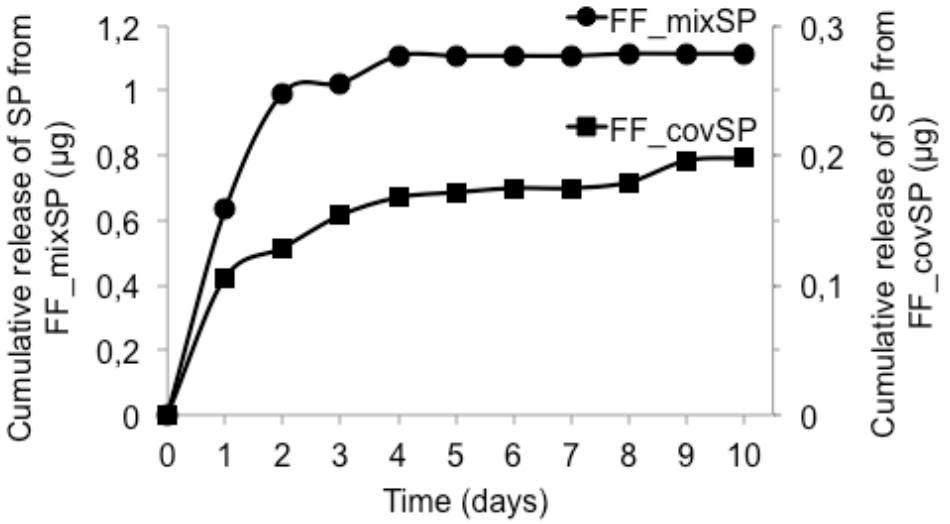

Fig. 46 Cumulative SP release obtained by ELISA assay on incubation media of films FF_mixSP and FF_covSP.

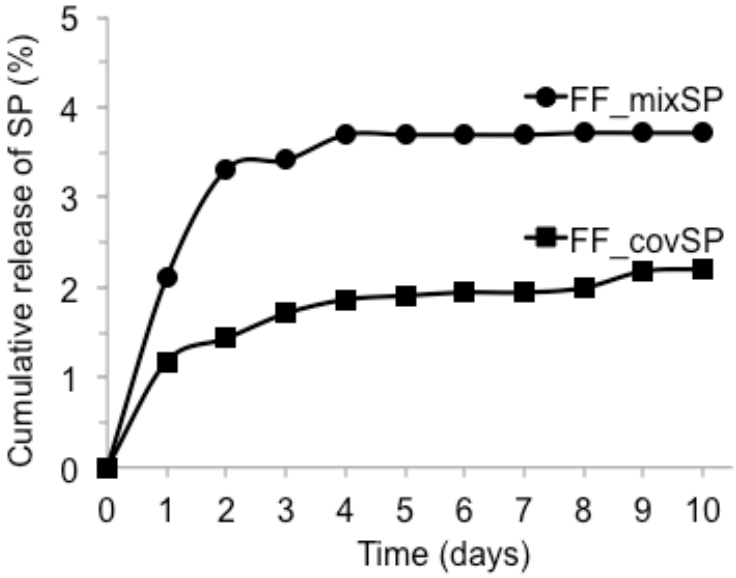

Fig. 47 Cumulative SP release % obtained by ELISA assay on incubation media of films FF_mixSP and FF_covSP.

The curve of release of SP from FF_mixSP films appeared to be characterized by an initial burst release, during the first three days of incubation, and remained then stable from day 4 until day 10. Around 4% of the initially loaded SP was released from films at the end of the incubation. The curve of release of SP from FF_covSP films showed a slow and continuous release of SP over the 10 days of incubation, reaching 2% of initially loaded SP released at the end of the experiment. The results of the immuno-detection studies showed that SP was present on the films and could conjugate the specific primary antibody both in the immuno-labelling for confocal analyses and in the ELISA assay. These are preliminary results that suggested a preserved activity and bioavailability of substance P, in two different situations: after the release in films incubation media, or conjugated to fibroin films, prepared with both strategies.

Moreover, SP release experiments showed that only a minor percentage of SP was found in films incubation media after 10 days, indicating that the rest (95% and 98% for FF_mixSP and FF_covSP,

respectively) was permanently entrapped or conjugated to fibroin. These results could be promising for potential biomedical applications, in which SP should fulfil its activity of macrophages modulator directly on the site of implantation of the biomaterial.

In summary, the set of results obtained during this research could be a starting point for the development of biomaterials with improved functionalities, especially regarding the active control of macrophages behaviour during tissue healing phases, in case of chronic wounds, injuries, inflammatory states, or many other pathological conditions.

The chemico-physical characterization should be necessarily followed by a biological evaluation of the materials, which is under evaluation in *in vitro* on-going experiments, briefly presented in the following paragraph.

6.4. Design of the in vitro biological evaluation of the materials

Fibroin-SP specimens were sterilized by gamma (γ) irradiation with a dose of 25.0 kGy, at the irradiation facility of the Physics Department of the University of Genova.

Mouse bone marrow-derived macrophages were grown in their standard medium, then cultured in presence of Transwell® permeable supports with fibroin films placed above. Cytofluorimetry analyses and molecular analyses (RNA extraction, reverse transcription PCR and real-time quantitative PCR) were conducted on macrophages at specific experimental time points. Experiments are ongoing and the results are not shown in this dissertation.

Chapter VII. Conclusions

"Tissue engineering is the creation of new tissue for the therapeutic reconstruction of the human body, by the deliberate and controlled stimulation of selected target cells, through a systematic combination of molecular and mechanical signals" (Williams, 2006).

In this work, innovative materials derived from silk fibroin processed and combined with selected bioactive compounds were designed and investigated, with the final aim of developing new therapeutic systems for bone tissue engineering applications.

To address the goals of this work, the experimental activity was divided in three main research lines that explored different strategies to engineer silk fibroin at different levels of intervention in the treatment of bone injuries:

- support to the formation of new healthy and functional tissue;
- enhancement of the mineralization processes;
- modulation of the immune response at the injured site.

In fact, with the increasing knowledge of the functions that different bioactive molecules and inorganic materials play in specific bone pathologies and/or injuries, the design of biomaterials that could actively control the metabolism of cells of different phenotypes and promote healing outcomes has obtained a central role in the tissue engineering field. In the context of this dissertation, which focuses on bone tissue engineering, compounds with a specific bioactivity versus bone derived cells and cells of the immune system were considered.

In the three studies conducted, silk fibroin was respectively combined with: the hydrogen sulfide donor GYY; β-tricalcium phosphate; the potential immunomodulatory neuropeptide substance P.

The first research activity conducted focused on the preparation and characterization of fibroin porous scaffolds loaded with the hydrogen sulfide donor GYY. The rationale behind this activity consisted in two main points: the necessity to find new systems to administer and deliver an H_2S-donor in the human body, preserving, in parallel, its H_2S-releasing ability; the investigation of strategies to enhance the bioactivity of the SF scaffolds towards hMSC differentiation into bone cells.

Highly porous matrices were fabricated and a strategy to combine them with GYY was designed. We could assess that the final products featured the chemico-physical and mechanical properties required to soft bone scaffolds, in terms of porous morphology, chemical stability and behaviour under compression stresses. Moreover, the H_2S-releasing abilities of GYY were retained after incorporation into SF scaffolds. Cytocompatibility and cell proliferation and penetration into the scaffolds was successfully confirmed by culture with a bone-derived cell line. The enhanced osteogenic potential of fibroin scaffolds loaded with GYY *in vitro* was evaluated by our collaborators as Istituto Ortopedico Rizzoli, with hMSCs cultured in dynamic conditions on the same scaffolds described in this dissertation.

The second research activity performed focused on the design and fabrication of a new composite system based on calcium phosphate and silk fibroin that could be potentially exploited to enhance mineralization processes in bone formation. In fact, thanks to its excellent osteoconductive and osteointegrative properties, β-tricalcium phosphate (β-TCP) is an effective inorganic filler to treat small bone defects. In this work β-TCP was encapsulated into sphere-shaped matrices of SF and ALG, which resulted to be a tunable matrix for the manipulation of calcium phosphate. This

system, proved to be cytocompatible, might provide a strategy for the easy dosage of β-TCP, with no need for scaling before application in the bone implant site.

Finally, preliminary studies were conducted on strategies for the treatment of inflammation induced by the implantation of a scaffold. For this research, silk fibroin films combined with the neuropeptide substance P were used as models to study the conjugation mechanism of SP with SF, and the processes of release. The results obtained from the characterization performed, in particular the immuno-detection analyses, indicated that both SP chemically conjugated and SP physically blended to fibroin retained their bioactivity. An investigation of the biological activity of the SF-SP system is necessary to demonstrate its ability to modulate macrophages phenotypes in *in vitro* conditions simulating inflammation or *in vivo* experiments.

The results obtained from the three research activities conducted indicate that fibroin can function as a flexible platform to produce various systems for bone tissue regeneration application. Moreover, as conclusion and possible future perspective for this work, the three strategies could be integrated and combined in a unique multifunctional system, based on a fibroin engineered platform with therapeutic potential at different stages of intervention in the treatment of bone injuries.

List of Abbreviations and Acronyms

AbI: Primary antibody
AbII: Secondary antibody
ADSC: Adipose derived stem cell
AFM: Atomic force microscopy
ALG: Alginate
ANOVA: Analysis of variance
APTC: 2-aminopyridine-5-thiocarboxamide
ATR: Attenuated total internal reflection
BCA: Bicinchoninic acid
BMSC: Bone marrow stromal cells
BSA: Bovine serum albumine
β-TCP: β-tricalcium phosphate
CaP: Calcium phosphate
CBS: Cystathionine-beta-synthase
CFDA: China Food and Drug Administration
CLM: Confocal laser microscopy(e)
CSE: Cystathionine-gamma-lyase
DAPI: 4'6-diamidino-2-phenylindole
DI: Deionized
DMEM: Dulbecco's Modified Eagle Medium
DMSO: Dimethyl sulfoxide
DSC: Differential scanning calorimetry
ECM: Extracellular Matrix
EDC: 1-ethyl-3-(dimethylaminopropyl)carbodiimide hydrochloride
ELISA: Enzyme-linked immunosorbent assay
EtO: Ethylene oxide
FBS: Foetal bovine serum
FE-SEM: Field emission scanning electron microscopy

FGF-2: Fibroblast growth factor 2
FSD: Fourier self-deconvolution
FT-IR: Fourier transform infrared
GAG: Glycosaminoglycan
GMP: Good manufacturing practices
GYY or GYY4137: (p-methoxyphenyl) morpholino-phosphinodithioic acid
HA: Hydroxyapatite
hBMSC: Human Bone Marrow Stromal Cells
HEPES: 4-(2-hydroxyethyl)-1-piperazineethanesulfonic acid
HHS: Department of Health and Human Services
hMSC: Human mesenchymal stem cell
HRP: Horseradish peroxidase
H_2S: Hydrogen sulfide
IgG: Immunoglobulin G
LDH: Lactate dehydrogenase
M1: Pro-inflammatory macrophage
M2: Pro-healing macrophage
M-CSF: Macrophage colony-stimulating factor
MEM: Minimum Essential Medium
MFFs: Mass of fibroin fibers
MSC: Mesenchymal stem cell
MW: Molecular Weight
MWCO: Molecular weight cut-off
NADH: Nicotinamide adenine dinucleotide
NADPH: Dihydronicotinamide adenine dinucleotide phosphate
NaHS: Sodium hydrogen sulfide
NGF: Nervous growth factor
NHS: N-hydroxysuccinimide
NIH: National Institutes of Health

NK-1R: Neurokinin-1 receptor

NMR: Nuclear magnetic resonance

OVX: Ovariectomized

PBS: Phosphate-buffered saline

PEG: Polyethylene glycol

RGD: Arginine-glycine-aspartate

RMS: Root mean square

SD: Standard deviation

SE: Standard error

SF: Silk fibroin

SP: Substance P

SPM: Scanning probe microscopy(e)

TERM: Tissue engineering and regenerative medicine

TGA: Thermogravimetric analysis

TNF: Tumour necrosis factor

References

Akai, H.; Imai, T.; Tsubouchi, K. Fine-Structural Changes of Liquid Silk in the Silk Gland during Spinning Stage of Bombyx Larvae. *J. Seric. Sci. Japan* **1987**, *56* (2), 131–137.

Al-Nasiry, S.; Hanssens, M.; Luyten, C.; Pijnenborg, R. The Use of Alamar Blue Assay for Quantitative Analysis of Viability, Migration and Invasion of Choriocarcinoma Cells. *Hum. Reprod.* **2007**, *22* (5), 1304–1309.

Alexander, B. E.; Coles, S. J.; Fox, B. C.; Khan, T. F.; Maliszewski, J.; Perry, A.; Pitak, M. B.; Whiteman, M.; Wood, M. E. Investigating the Generation of Hydrogen Sulfide from the Phosphonamidodithioate Slow-Release Donor GYY4137. *Medchemcomm* **2015a**, *6* (9), 1649–1655.

Alexander, B. E.; Coles, S. J.; Khan, T. F.; Maliszewsi, J.; Perry, A.; Pitak, M. P.; Whiteman, M.; Wood, M. E. Investigating the Generation of Hydrogen Sulphide from the Phosphinodithioate Slow-Release Donor GYY4137: Novel Products and Experimental Tools. *Nitric Oxide* **2015b**, *47*, S52–S53.

Altman, G. H.; Diaz, F.; Jakuba, C.; Calabro, T.; Horan, R. L.; Chen, J.; Lu, H.; Richmond, J.; Kaplan, D. L. Silk-Based Biomaterials. *Biomaterials* **2003**, *24* (3), 401–416.

Applegate, M. B.; Partlow, B. P.; Coburn, J.; Marelli, B.; Pirie, C.; Pineda, R.; Kaplan, D. L.; Omenetto, F. G. Silk Fibroin: Photocrosslinking of Silk Fibroin Using Riboflavin for Ocular Prostheses. *Adv. Mater.* **2016**, *28* (12), 2464–2464.

Aramwit, P. *Silk: Properties, Production and Uses*, 1st ed.; Aramwit, P., Ed.; Nova Science Publishers: New York, **2012**.

Asakura, T.; Miller, T. *Biotechnology of Silk*, 1st ed.; Asakura, T., Miller, T., Eds.; Biologically-inspired systems: 5; Springer Netherlands: Dordrecht, **2014**; Vol. 5.

Asakura, T.; Suzuki, Y.; Nakazawa, Y.; Holland, G. P.; Yarger, J. L. Elucidating Silk Structure Using Solid-State NMR. *Soft Matter*. **2013**, pp 11440–11450.

Asakura, T.; Okushita, K.; Williamson, M. P. Analysis of the Structure of Bombyx Mori Silk Fibroin by NMR. *Macromolecules* **2015**, *48* (8), 2345–2357.

Aznar-Cervantes, S. D.; Vicente-Cervantes, D.; Meseguer-Olmo, L.; Cenis, J. L.; Lozano-Pérez, A. A. Influence of the Protocol Used for Fibroin Extraction on the Mechanical Properties and Fiber Sizes of Electrospun Silk Mats. *Mater. Sci. Eng. C* **2013**, *33* (4), 1945–1950.

Barth, A. Infrared Spectroscopy of Proteins. *Biochim. Biophys. Acta - Bioenerg.* **2007**, *1767* (9), 1073–1101.

Benavides, G. A.; Squadrito, G. L.; Mills, R. W.; Patel, H. D.; Isbell, T. S.; Patel, R. P.; Darley-Usmar, V. M.; Doeller, J. E.; Kraus, D. W. Hydrogen Sulfide Mediates the Vasoactivity of Garlic. *Proc. Natl. Acad. Sci.* **2007**, *104* (46), 17977–17982.

Bilezikian, J.; Raisz, L.; Martin, T. J. *Principles of Bone Biology, Two-Volume Set*; Elsevier, **2008**; Vol. 1–2.

Blitterswijk, C. A. van; Boer, J. de. *Tissue Engineering*, second edi.; Blitterswijk, C. A. Van, Boer, J. De, Eds.; Elsevier/Academic Press, **2015**.

Boniakowski, A. E.; Kimball, A. S.; Jacobs, B. N.; Kunkel, S. L.; Gallagher, K. A. Macrophage-Mediated Inflammation in Normal and Diabetic Wound Healing. *J. Immunol.* **2017**, *199* (1), 17–24.

Bose, S.; Tarafder, S. Calcium Phosphate Ceramic Systems in Growth Factor and Drug Delivery for Bone Tissue Engineering: A Review. *Acta Biomaterialia*. April **2012**, pp 1401–1421.

Bray, L.; Suzuki, S.; Harkin, D.; Chirila, T. Incorporation of Exogenous RGD Peptide and Inter-Species Blending as Strategies for Enhancing Human Corneal Limbal Epithelial Cell Growth on Bombyx Mori Silk Fibroin Membranes. *J. Funct. Biomater.* **2013**, *4* (2), 74–88.

Bucciarelli, A.; Pal, R. K.; Maniglio, D.; Quaranta, A.; Mulloni, V.; Motta, A.; Yadavalli, V. K. Fabrication of Nanoscale Patternable Films of Silk Fibroin Using Benign Solvents. *Macromol. Mater. Eng.* **2017**, *302* (7), 1700110.

Cacciotti, I.; Ciocci, M.; Di Giovanni, E.; Nanni, F.; Melino, S.

Hydrogen Sulfide-Releasing Fibrous Membranes: Potential Patches for Stimulating Human Stem Cells Proliferation and Viability under Oxidative Stress. *Int. J. Mol. Sci.* **2018**, *19* (8), 2368.

Cagol, N.; Bonani, W.; Maniglio, D.; Migliaresi, C.; Motta, A. Effect of Cryopreservation on Cell-Laden Hydrogels: Comparison of Different Cryoprotectants. *Tissue Eng. Part C Methods* **2017**, *24* (1), 20–31.

Cai, Y.; Guo, J.; Chen, C.; Yao, C.; Chung, S. M.; Yao, J.; Lee, I. S.; Kong, X. Silk Fibroin Membrane Used for Guided Bone Tissue Regeneration. *Mater. Sci. Eng. C* **2017**, *70*, 148–154.

Callone, E.; Dirè, S.; Hu, X.; Motta, A. Processing Influence on Molecular Assembling and Structural Conformations in Silk Fibroin: Elucidation by Solid-State NMR. *ACS Biomater. Sci. Eng.* **2016**, *2* (5), 758–767.

Cao, Y.; Wang, B. Biodegradation of Silk Biomaterials. *International Journal of Molecular Sciences*. Multidisciplinary Digital Publishing Institute (MDPI) March 31, **2009**, pp 1514–1524.

Carlomagno, C.; Motta, A.; Sorarù, G. D.; Aswath, P. B.; Migliaresi, C.; Maniglio, D. Breath Figures Decorated Silicon Oxinitride Ceramic Surfaces with Controlled Si Ions Release for Enhanced Osteoinduction. *J. Biomed. Mater. Res. Part B Appl. Biomater.* **2018**, 1–11.

Chan, B. P.; Leong, K. W. Scaffolding in Tissue Engineering: General Approaches and Tissue-Specific Considerations. *Eur. Spine J.* **2008**, *17* (SUPPL. 4), 467–479.

Chao, P.-H. G.; Yodmuang, S.; Wang, X.; Sun, L.; Kaplan, D. L.; Vunjak-Novakovic, G. Silk Hydrogel for Cartilage Tissue Engineering. *J. Biomed. Mater. Res. - Part B Appl. Biomater.* **2010**, *95* (1), 84–90.

Chen, Y.; Wang, J.; Zhu, X. D.; Tang, Z. R.; Yang, X.; Tan, Y. F.; Fan, Y. J.; Zhang, X. D. Enhanced Effect of β-Tricalcium Phosphate Phase on Neovascularization of Porous Calcium Phosphate Ceramics: In Vitro and in Vivo Evidence. *Acta Biomater.* **2015**, *11* (1), 435–448.

Cho, H. J.; Ki, C. S.; Oh, H.; Lee, K. H.; Um, I. C. Molecular Weight Distribution and Solution Properties of Silk Fibroins with

Different Dissolution Conditions. *Int. J. Biol. Macromol.* **2012**, *51* (3), 336–341.

Coburn, J. M.; Na, E.; Kaplan, D. L. Modulation of Vincristine and Doxorubicin Binding and Release from Silk Films. *J. Control. Release* **2015**, *220*, 229–238.

Cooper, D. M. L.; Matyas, J. R.; Katzenberg, M. A.; Hallgrimsson, B. Comparison of Microcomputed Tomographic and Microradiographic Measurements of Cortical Bone Porosity. *Calcif. Tissue Int.* **2004**, *74* (5), 437–447.

Correia, C.; Bhumiratana, S.; Yan, L. P.; Oliveira, A. L.; Gimble, J. M.; Rockwood, D.; Kaplan, D. L.; Sousa, R. A.; Reis, R. L.; Vunjak-Novakovic, G. Development of Silk-Based Scaffolds for Tissue Engineering of Bone from Human Adipose-Derived Stem Cells. *Acta Biomater.* **2012**, *8* (7), 2483–2492.

Cypher, T. J.; Grossman, J. P. Biological Principles of Bone Graft Healing. *J. Foot Ankle Surg.* **1996**, *35* (5), 413–417.

Daculsi, G.; Legeros, R. Z.; Nery, E.; Lynch, K.; Kerebel, B. Transformation of Biphasic Calcium Phosphate Ceramics in Vivo: Ultrastructural and Physicochemical Characterization. *J. Biomed. Mater. Res.* **1989**, *23* (8), 883–894.

DeBari, M. K.; Abbott, R. D. Microscopic Considerations for Optimizing Silk Biomaterials. *Wiley Interdiscip. Rev. Nanomedicine Nanobiotechnology* **2019**, *11* (2), e1534.

Deleon, E. R.; Stoy, G. F.; Olson, K. R. Passive Loss of Hydrogen Sulfide in Biological Experiments. *Anal. Biochem.* **2012**, *421* (1), 203–207.

Eghbal, M. A.; Pennefather, P. S.; O'Brien, P. J. H2S Cytotoxicity Mechanism Involves Reactive Oxygen Species Formation and Mitochondrial Depolarisation. *Toxicology* **2004**, *203* (1–3), 69–76.

Einhorn, T. A.; Gerstenfeld, L. C. Fracture Healing: Mechanisms and Interventions. *Nat. Rev. Rheumatol.* **2015**, *11* (1), 45–54.

Eliaz, N.; Metoki, N. Calcium Phosphate Bioceramics: A Review of Their History, Structure, Properties, Coating Technologies and Biomedical Applications. *Materials (Basel).* **2017**, *10* (4), 334.

Fini, M.; Motta, A.; Torricelli, P.; Giavaresi, G.; Nicoli Aldini, N.; Tschon, M.; Giardino, R.; Migliaresi, C. The Healing of Confined Critical Size Cancellous Defects in the Presence of Silk Fibroin Hydrogel. *Biomaterials* **2005**, *26* (17), 3527–3536.

Font Tellado, S.; Bonani, W.; Balmayor, E. R.; Foehr, P.; Motta, A.; Migliaresi, C.; van Griensven, M. Fabrication and Characterization of Biphasic Silk Fibroin Scaffolds for Tendon/Ligament-to-Bone Tissue Engineering. *Tissue Eng. Part A* **2017**, ten.tea.2016.0460.

Fu, F. N.; DeOliveira, D. B.; Trumble, W. R.; Sarkar, H. K.; Singh, B. R. Secondary Structure Estimation of Proteins Using the Amide III Region of Fourier Transform Infrared Spectroscopy: Application to Analyze Calcium-Binding-Induced Structural Changes in Calsequestrin. *Appl. Spectrosc.* **1994**, *48* (11), 1432–1441.

Fuchs, S.; Jiang, X.; Schmidt, H.; Dohle, E.; Ghanaati, S.; Orth, C.; Hofmann, A.; Motta, A.; Migliaresi, C.; Kirkpatrick, C. J. Dynamic Processes Involved in the Pre-Vascularization of Silk Fibroin Constructs for Bone Regeneration Using Outgrowth Endothelial Cells. *Biomaterials* **2009**, *30* (7), 1329–1338.

Gambari, L.; Amore, E.; Raggio, R.; Bonani, W.; Barone, M.; Lisignoli, G.; Grigolo, B.; Motta, A.; Grassi, F. Hydrogen Sulfide-Releasing Silk Fibroin Scaffold for Bone Tissue Engineering. *Mater. Sci. Eng. C* **2019**, *102*, 471–482.

Gao, P.; Zhang, H.; Liu, Y.; Fan, B.; Li, X.; Xiao, X.; Lan, P.; Li, M.; Geng, L.; Liu, D.; et al. Beta-Tricalcium Phosphate Granules Improve Osteogenesis in Vitro and Establish Innovative Osteo-Regenerators for Bone Tissue Engineering in Vivo. *Sci. Rep.* **2016**, *6*.

Geddes, A. J.; Graham, G. N.; Morris, H. R.; Lucas, F.; Barber, M.; Wolstenholme, W. A. Mass-Spectrometric Determination of the Amino Acid Sequences in Peptides Isolated from Protein Silk Fibroin of Bombyx Mori . *Biochem. J.* **1969**, *114* (4), 695–702.

Ghalia, M. A.; Dahman, Y. Advanced Nanobiomaterials in Tissue Engineering: Synthesis, Properties, and Applications. In *Nanobiomaterials in Soft Tissue Engineering: Applications of Nanobiomaterials*; William Andrew Publishing, **2016**; pp 141–172.

Ghanaati, S.; Unger, R. E.; Webber, M. J.; Barbeck, M.; Orth, C.; Kirkpatrick, J. A.; Booms, P.; Motta, A.; Migliaresi, C.; Sader, R. A.; et

al. Scaffold Vascularization in Vivo Driven by Primary Human Osteoblasts in Concert with Host Inflammatory Cells. *Biomaterials* **2011**, *32* (32), 8150–8160.

Gil, E. S.; Panilaitis, B.; Bellas, E.; Kaplan, D. L. Functionalized Silk Biomaterials for Wound Healing. *Adv. Healthc. Mater.* **2013**, *2* (1), 206–217.

Gil, E. S.; Park, S. H.; Hu, X.; Cebe, P.; Kaplan, D. L. Impact of Sterilization on the Enzymatic Degradation and Mechanical Properties of Silk Biomaterials. *Macromol. Biosci.* **2014**, *14* (2), 257–269.

Good, I. The Archaeology of Early Silk. *Text. Soc. Am. Symp. Proc.* **2002**, 388.

Graney, P. L.; Lurier, E. B.; Spiller, K. L. Biomaterials and Bioactive Factor Delivery Systems for the Control of Macrophage Activation in Regenerative Medicine. *ACS Biomater. Sci. Eng.* **2018**, *4* (4), 1137–1148.

Grassi, F.; Tyagi, A. M.; Calvert, J. W.; Gambari, L.; Walker, L. D.; Yu, M.; Robinson, J.; Li, J. Y.; Lisignoli, G.; Vaccaro, C.; et al. Hydrogen Sulfide Is a Novel Regulator of Bone Formation Implicated in the Bone Loss Induced by Estrogen Deficiency. *J. Bone Miner. Res.* **2016**, *31* (5), 949–963.

Gupta, M. K.; Khokhar, S. K.; Phillips, D. M.; Sowards, L. A.; Drummy, L. F.; Kadakia, M. P.; Naik, R. R. Patterned Silk Films Cast from Ionic Liquid Solubilized Fibroin as Scaffolds for Cell Growth. *Langmuir* **2007**, *23* (3), 1315–1319.

Guziewicz, N.; Best, A.; Perez-Ramirez, B.; Kaplan, D. L. Lyophilized Silk Fibroin Hydrogels for the Sustained Local Delivery of Therapeutic Monoclonal Antibodies. *Biomaterials* **2011**, *32* (10), 2642–2650.

Han, F.; Shi, C.; Yang, H.; Li, B. *Developments and Applications of Calcium Phosphate Bone Cements*; **2018**; Vol. 9.

Hansma, H. G. Atomic Force Microscopy and Spectroscopy of Silk from Spider Draglines, Capture-Web Spirals, and Silkworms; **2013**; pp 123–136.

Hildebrandt, B.; Gillis, C. *Silk: Trade and Exchange along the Silk*

Roads between Rome and China in Antiquity, reprinted.; Oxford & Philadephia: Oxbow Books, Ed.; **2017**.

Holland, C.; Numata, K.; Rnjak-Kovacina, J.; Seib, F. P. The Biomedical Use of Silk: Past, Present, Future. *Advanced Healthcare Materials*. John Wiley & Sons, Ltd January 1, **2019**, p 1800465.

Hotaling, N. A.; Tang, L.; Irvine, D. J.; Babensee, J. E. Biomaterial Strategies for Immunomodulation. *Annu. Rev. Biomed. Eng.* **2015**, *17* (1), 317–349.

Hu, X.; Kaplan, D.; Cebe, P. Determining Beta-Sheet Crystallinity in Fibrous Proteins by Thermal Analysis and Infrared Spectroscopy. *Macromolecules* **2006**, *39* (18), 6161–6170.

Hughes, M. N.; Centelles, M. N.; Moore, K. P. Making and Working with Hydrogen Sulfide. *Free Radic. Biol. Med.* **2009**, *47* (10), 1346–1353.

Hutmacher, D. W. Scaffolds in Tissue Engineering Bone and Cartilage. *Biomaterials*. **2000**, pp 2529–2543.

Iizukat, E.; Yangt, J. T. The Disordered and β-Conformations of Silk Fibroin in Solution. *Biochemistry* **1968**, *7* (6), 2218–2228.

Inoue, S.; Tanaka, K.; Arisaka, F.; Kimura, S.; Ohtomo, K.; Mizuno, S. Silk Fibroin of Bombyx Mori Is Secreted, Assembling a High Molecular Mass Elementary Unit Consisting of H-Chain, L-Chain, and P25, with a 6:6:1 Molar Ratio. *J. Biol. Chem.* **2000**, *275* (51), 40517–40528.

Jin, H. J.; Kaplan, D. L. Mechanism of Silk Processing in Insects and Spiders. *Nature* **2003**, *424* (6952), 1057–1061.

Jin, H. J.; Chen, J.; Karageorgiou, V.; Altman, G. H.; Kaplan, D. L. Human Bone Marrow Stromal Cell Responses on Electrospun Silk Fibroin Mats. *Biomaterials* **2004**, *25* (6), 1039–1047.

Jin, H. J.; Park, J.; Karageorgiou, V.; Kim, U. J.; Valluzzi, R.; Cebe, P.; Kaplan, D. L. Water-Stable Silk Films with Reduced β-Sheet Content. *Adv. Funct. Mater.* **2005**, *15* (8), 1241–1247.

Jo, Y. Y.; Kim, S. G.; Kwon, K. J.; Kweon, H. Y.; Chae, W. S.; Yang, W. G.; Lee, E. Y.; Seok, H. Silk Fibroin-Alginate-Hydroxyapatite Composite Particles in Bone Tissue Engineering

Applications in Vivo. *Int. J. Mol. Sci.* **2017**, *18* (4).

Ju, H. W.; Lee, O. J.; Lee, J. M.; Moon, B. M.; Park, H. J.; Park, Y. R.; Lee, M. C.; Kim, S. H.; Chao, J. R.; Ki, C. S.; et al. Wound Healing Effect of Electrospun Silk Fibroin Nanomatrix in Burn-Model. *Int. J. Biol. Macromol.* **2016**, *85*, 29–39.

Jugdaohsingh, R. SILICON AND BONE HEALTH. *J Nutr Heal. Aging* **2007**, *11* (2), 99–110.

Karageorgiou, V.; Kaplan, D. Porosity of 3D Biomaterial Scaffolds and Osteogenesis. *Biomaterials*. **2005**, pp 5474–5491.

Kim, H. H.; Kim, J. W.; Choi, J.; Park, Y. H.; Ki, C. S. Characterization of Silk Hydrogel Formed with Hydrolyzed Silk Fibroin-Methacrylate via Photopolymerization. *Polymer (Guildf).* **2018**, *153*, 232–240.

Kim, U.-J.; Park, J.; Kim, J.; Wada, M.; Kaplan, D. L. Three-Dimensional Aqueous-Derived Biomaterial Scaffolds from Silk Fibroin. *Biomaterials* **2005**, *26* (15), 2775–2785.

Kiyosawa, M.; Ito, E.; Shirai, K.; Kanekatsu, R.; Miura, M.; Kiguchi, K. Cocoon Spinning Behavior in the Silkworm, Bombyx Mori : Comparison of Three Strains Constructing Different Cocoons in Shape. *Zoolog. Sci.* **2004**, *16* (2), 215–223.

Kolluru, G. K.; Shen, X.; Bir, S. C.; Kevil, C. G. Hydrogen Sulfide Chemical Biology: Pathophysiological Roles and Detection. *Nitric Oxide* **2013**, *35*, 5–20.

Kou, P. M.; Babensee, J. E. Macrophage and Dendritic Cell Phenotypic Diversity in the Context of Biomaterials. *J. Biomed. Mater. Res. - Part A* **2011**, *96 A* (1), 239–260.

Kuboyama, N.; Kiba, H.; Arai, K.; Uchida, R.; Tanimoto, Y.; Bhawal, U. K.; Abiko, Y.; Miyamoto, S.; Knight, D.; Asakura, T.; et al. Silk Fibroin-Based Scaffolds for Bone Regeneration. *J. Biomed. Mater. Res. - Part B Appl. Biomater.* **2013**, *101 B* (2), 295–302.

Kuzmina, E. E. *The Prehistory of the Silk Road*; Mair, V. H., Ed.; University of Pennsylvania Press, **2008**.

Lawrence, B. D.; Omenetto, F.; Chui, K.; Kaplan, D. L. Processing Methods to Control Silk Fibroin Film Biomaterial Features. *J. Mater.*

Sci. **2008**, *43* (21), 6967–6985.

Le, T. D. H.; Liaudanskaya, V.; Bonani, W.; Migliaresi, C.; Motta, A. Enhancing Bioactive Properties of Silk Fibroin with Diatom Particles for Bone Tissue Engineering Applications. *J. Tissue Eng. Regen. Med.* **2018**, *12* (1), 89–97.

Leal-Egaña, A.; Scheibel, T. Silk-Based Materials for Biomedical Applications. *Biotechnol. Appl. Biochem.* **2010**, *55* (3), 155–167.

Leal, E. C.; Carvalho, E.; Tellechea, A.; Kafanas, A.; Tecilazich, F.; Kearney, C.; Kuchibhotla, S.; Auster, M. E.; Kokkotou, E.; Mooney, D. J.; et al. Substance P Promotes Wound Healing in Diabetes by Modulating Inflammation and Macrophage Phenotype. *Am. J. Pathol.* **2015**, *185* (6), 1638–1648.

Lee, B. B.; Ravindra, P.; Chan, E. S. Size and Shape of Calcium Alginate Beads Produced by Extrusion Dripping. *Chem. Eng. Technol.* **2013**, *36* (10), 1627–1642.

Lee, B. R.; Lee, K. H.; Kang, E.; Kim, D. S.; Lee, S. H. Microfluidic Wet Spinning of Chitosan-Alginate Microfibers and Encapsulation of HepG2 Cells in Fibers. *Biomicrofluidics* **2011**, *5* (2).

Lee, K. Y.; Mooney, D. J. Alginate: Properties and Biomedical Applications. *Prog. Polym. Sci.* **2012**, *37* (1), 106–126.

Li, C.; Jiang, C.; Deng, Y.; Li, T.; Li, N.; Peng, M.; Wang, J. RhBMP-2 Loaded 3D-Printed Mesoporous Silica/Calcium Phosphate Cement Porous Scaffolds with Enhanced Vascularization and Osteogenesis Properties. *Sci. Rep.* **2017**, *7* (1), 41331.

Li, J. J.; Kaplan, D. L.; Zreiqat, H. Scaffold-Based Regeneration of Skeletal Tissues to Meet Clinical Challenges. *J. Mater. Chem. B* **2014**, *2* (42), 7272–7306.

Li, L.; Whiteman, M.; Guan, Y. Y.; Neo, K. L.; Cheng, Y.; Lee, S. W.; Zhao, Y.; Baskar, R.; Tan, C.-H.; Moore, P. K. Characterization of a Novel, Water-Soluble Hydrogen Sulfide-Releasing Molecule (GYY4137): New Insights Into the Biology of Hydrogen Sulfide. *Circulation* **2008a**, *117* (18), 2351–2360.

Li, L.; Whiteman, M.; Guan, Y. Y.; Neo, K. L.; Cheng, Y.; Lee, S. W.; Zhao, Y.; Baskar, R.; Tan, C.-H.; Moore, P. K. Characterization of a Novel, Water-Soluble Hydrogen Sulfide–Releasing Molecule

(GYY4137). *Circulation* **2008b**, *117* (18), 2351–2360.

Liang, W.; Chen, J.; Li, L.; Li, M.; Wei, X.; Tan, B.; Shang, Y.; Fan, G.; Wang, W.; Liu, W. Conductive Hydrogen Sulfide-Releasing Hydrogel Encapsulating ADSCs for Myocardial Infarction Treatment. *ACS Appl. Mater. Interfaces* **2019**, *11* (16), 14619–14629.

Lin, Y.; Xia, X.; Shang, K.; Elia, R.; Huang, W.; Cebe, P.; Leisk, G.; Omenetto, F.; Kaplan, D. L. Tuning Chemical and Physical Cross-Links in Silk Electrogels for Morphological Analysis and Mechanical Reinforcement. *Biomacromolecules* **2013**, *14* (8), 2629–2635.

Liu, B.; Song, Y. wei; Jin, L.; Wang, Z. jian; Pu, D. yong; Lin, S. qiang; Zhou, C.; You, H. jian; Ma, Y.; Li, J. min; et al. Silk Structure and Degradation. *Colloids Surfaces B Biointerfaces* **2015**, *131*, 122–128.

Liu, Y.; Yang, R.; Liu, X.; Zhou, Y.; Qu, C.; Kikuiri, T.; Wang, S.; Zandi, E.; Du, J.; Ambudkar, I. S.; et al. Hydrogen Sulfide Maintains Mesenchymal Stem Cell Function and Bone Homeostasis via Regulation of Ca 2+ Channel Sulfhydration. *Cell Stem Cell* **2014**, *15* (1), 66–78.

Lu, Q.; Wang, X.; Hu, X.; Cebe, P.; Omenetto, F.; Kaplan, D. L. Stabilization and Release of Enzymes from Silk Films. *Macromol. Biosci.* **2010a**, *10* (4), 359–368.

Lu, Q.; Hu, X.; Wang, X.; Kluge, J. A.; Lu, S.; Cebe, P.; Kaplan, D. L. Water-Insoluble Silk Films with Silk I Structure. *Acta Biomater.* **2010b**, *6* (4), 1380–1387.

Lu, Q.; Zhang, B.; Li, M.; Zuo, B.; Kaplan, D. L.; Huang, Y.; Zhu, H. Degradation Mechanism and Control of Silk Fibroin. *Biomacromolecules* **2011**, *12* (4), 1080–1086.

Lu, S.; Wang, X.; Lv, Q.; Hu, X.; Uppal, N.; Kaplan, D. L. Stabilization of Enzymes in Silk Films. *Biomacromolecules* **2009**, *10* (5), 1032–1042.

Mackenzie, D. The History of Sutures. *Med. Hist.* **1973**, *17* (2), 158–168.

Manferdini, C.; Gabusi, E.; Grassi, F.; Piacentini, A.; Cattini, L.; Zini, N.; Filardo, G.; Facchini, A.; Lisignoli, G. Evidence of Specific Characteristics and Osteogenic Potentiality in Bone Cells from Tibia.

J Cell Physiol **2011**, *226* (10), 2675–2682.

Maniglio, D.; Bonani, W.; Migliaresi, C.; Motta, A. Silk Fibroin Porous Scaffolds by N2O Foaming. *J. Biomater. Sci. Polym. Ed.* **2018**, *29* (5), 491–506.

Maraldi, T.; Riccio, M.; Resca, E.; Pisciotta, A.; La Sala, G. B.; Ferrari, A.; Bruzzesi, G.; Motta, A.; Migliaresi, C.; Marzona, L.; et al. Human Amniotic Fluid Stem Cells Seeded in Fibroin Scaffold Produce In Vivo Mineralized Matrix. *Tissue Eng. Part A* **2011**, *17* (21–22), 2833–2843.

Marks, S. C.; Popoff, S. N. Bone Cell Biology: The Regulation of Development, Structure, and Function in the Skeleton. *Am. J. Anat.* **1988**, *183* (1), 1–44.

Martelli, A.; Testai, L.; Breschi, M. C.; Blandizzi, C.; Virdis, A.; Taddei, S.; Calderone, V. Hydrogen Sulphide: Novel Opportunity for Drug Discovery. *Med. Res. Rev.* **2012**, *32* (6), 1093–1130.

Martelli, A.; Testai, L.; Citi, V.; Marino, A.; Pugliesi, I.; Barresi, E.; Nesi, G.; Rapposelli, S.; Taliani, S.; Da Settimo, F.; et al. Arylthioamides as H2S Donors: L-Cysteine-Activated Releasing Properties and Vascular Effects in Vitro and in Vivo. *ACS Med. Chem. Lett.* **2013**, *4* (10), 904–908.

Matsumoto, A.; Chen, J.; Collette, A. L.; Kim, U. J.; Altman, G. H.; Cebe, P.; Kaplan, D. L. Mechanisms of Silk Fibroin Sol-Gel Transitions. *J. Phys. Chem. B* **2006**, *110* (43), 21630–21638.

Meinel, L.; Karageorgiou, V.; Hofmann, S.; Fajardo, R.; Snyder, B.; Li, C.; Zichner, L.; Langer, R.; Vunjak-Novakovic, G.; Kaplan, D. L. Engineering Bone-like Tissue in Vitro Using Human Bone Marrow Stem Cells and Silk Scaffolds. *J. Biomed. Mater. Res. - Part A* **2004**, *71* (1), 25–34.

Meinel, L.; Hofmann, S.; Karageorgiou, V.; Kirker-Head, C.; McCool, J.; Gronowicz, G.; Zichner, L.; Langer, R.; Vunjak-Novakovic, G.; Kaplan, D. L. The Inflammatory Responses to Silk Films in Vitro and in Vivo. *Biomaterials* **2005**, *26* (2), 147–155.

Melke, J.; Midha, S.; Ghosh, S.; Ito, K.; Hofmann, S. Silk Fibroin as Biomaterial for Bone Tissue Engineering. *Acta Biomater.* **2016**, *31*, 1–16.

Minoura, N.; Tsukada, M.; Nagura, M. Physico-Chemical Properties of Silk Fibroin Membrane as a Biomaterial. *Biomaterials* **1990**, *11* (6), 430–434.

Minoura, N.; Aiba, S. -I; Gotoh, Y.; Tsukada, M.; Imai, Y. Attachment and Growth of Cultured Fibroblast Cells on Silk Protein Matrices. *J. Biomed. Mater. Res.* **1995**, *29* (10), 1215–1221.

Mistry, B. D. *A Handbook of Spectroscopic Data Chemistry*, Edition 20.; Oxford Book Company, Ed.; Jaipur, India, 2009.

Mondal, M.; Trivedy, K.; Nirmal Kumar, S. The Silk Proteins, Sericin and Fibroin in Silkworm. *Casp. J. Environ. Sci.* **2007**, *5* (2), 63–76.

Moreira, A. P. D.; Sader, M. S.; Soares, G. D. de A.; Leão, M. H. M. R. Microfluidic Wet Spinning of Chitosan-Alginate Microfibers and Encapsulation of HepG2 Cells in Fibers. *Biomicrofluidics* **2011**, *5* (2), 967–973.

Morgan, E. F.; Barnes, G. L.; Einhorn, T. A. The Bone Organ System. Form and Function. In *Osteoporosis: Fourth Edition*; Academic Press, **2013**; pp 3–20.

Morris, A. A. M.; Kožich, V.; Santra, S.; Andria, G.; Ben-Omran, T. I. M.; Chakrapani, A. B.; Crushell, E.; Henderson, M. J.; Hochuli, M.; Huemer, M.; et al. Guidelines for the Diagnosis and Management of Cystathionine Beta-Synthase Deficiency. *Journal of Inherited Metabolic Disease*. Springer Netherlands January 24, **2017**, pp 49–74.

Motta, A.; Fambri, L.; Migliaresi, C. Regenerated Silk Fibroin Films: Thermal and Dynamic Mechanical Analysis. *Macromol. Chem. Phys.* **2002**, *203* (10–11), 1658–1665.

Motta, A.; Migliaresi, C.; Faccioni, F.; Torricelli, P.; Fini, M.; Giardino, R. Fibroin Hydrogels for Biomedical Applications: Preparation, Characterization and in Vitro Cell Culture Studies. *J. Biomater. Sci. Polym. Ed.* **2004**, *15* (7), 851–864.

Motta, A.; Maniglio, D.; Migliaresi, C.; Kim, H. J.; Wan, X.; Hu, X.; Kaplan, D. L. Silk Fibroin Processing and Thrombogenic Responses. *J. Biomater. Sci. Polym. Ed.* **2009**, *20* (13), 1875–1897.

Motta, A.; Foss, C.; Migliaresi, C. Tailoring Silk-Based Matrices

for Tissue Regeneration. In *ACS Symposium Series*; **2013**; Vol. 1135, pp 281–299.

Motta, A.; Segnana, P.; Verin, L.; La Monica, S.; Fumarola, C.; Bucci, G.; Gussago, F.; Cantoni, A. M.; Ampollini, L.; Migliaresi, C. Physico-Chemical Characterization and Biological Evaluation of Two Fibroin Materials. *J. Tissue Eng. Regen. Med.* **2014**, *8* (11), 874–885.

Mouriño, V.; Boccaccini, A. R. Bone Tissue Engineering Therapeutics: Controlled Drug Delivery in Three-Dimensional Scaffolds. *Journal of the Royal Society Interface*. February **2010**, pp 209–227.

Muffly, T. M.; Tizzano, A. P.; Walters, M. D. The History and Evolution of Sutures in Pelvic Surgery. *J. R. Soc. Med.* **2011**, *104* (3), 107–112.

Murphy, A. R.; Kaplan, D. L. Biomedical Applications of Chemically-Modified Silk Fibroin. *J. Mater. Chem.* **2009**, *19* (36), 6443–6450.

Murphy, A. R.; John, P. St.; Kaplan, D. L. Modification of Silk Fibroin Using Diazonium Coupling Chemistry and the Effects on HMSC Proliferation and Differentiation. *Biomaterials* **2008**, *29* (19), 2829–2838.

Nelson, D. L.; Lehninger, A. L.; Cox, M. M. *Lehninger Principles of Biochemistry*; W. H. Freeman, 2008, Ed.; Lehninger Principles of Biochemistry; W. H. Freeman, **2008**.

Ng, A. M. H.; Tan, K. K.; Phang, M. Y.; Aziyati, O.; Tan, G. H.; Isa, M. R.; Aminuddin, B. S.; Naseem, M.; Fauziah, O.; Ruszymah, B. H. I. Differential Osteogenic Activity of Osteoprogenitor Cells on HA and TCP/HA Scaffold of Tissue Engineered Bone. *J. Biomed. Mater. Res. - Part A* **2008**, *85* (2), 301–312.

Nielsen, M.; Larsen, L. H.; Ottosen, L. D. M.; Revsbech, N. P. Hydrogen Microsensors with Hydrogen Sulfide Traps. *Sensors Actuators, B Chem.* **2015**, *215*, 1–8.

O'Brien, F. J. Biomaterials & Scaffolds for Tissue Engineering. *Mater. Today* **2011**, *14* (3), 88–95.

O'Connor, T. M.; O'Connell, J.; O'Brien, D. I.; Goode, T.; Bredin, C. P.; Shanahan, F. The Role of Substance P in Inflammatory

Disease. *J. Cell. Physiol.* **2004**, *201* (2), 167–180.

Oberg, K. A.; Ruysschaert, J. M.; Goormaghtigh, E. The Optimization of Protein Secondary Structure Determination with Infrared and Circular Dichroism Spectra. *Eur. J. Biochem.* **2004**, *271* (14), 2937–2948.

Ogose, A.; Hotta, T.; Kawashima, H.; Kondo, N.; Gu, W.; Kamura, T.; Endo, N. Comparison of Hydroxyapatite and Beta Tricalcium Phosphate as Bone Substitutes after Excision of Bone Tumors. *J. Biomed. Mater. Res. - Part B Appl. Biomater.* **2005**, *72* (1), 94–101.

Olson, K. R. A Practical Look at the Chemistry and Biology of Hydrogen Sulfide. *Antioxid. Redox Signal.* **2012**, *17* (1), 32–44.

Panilaitis, B.; Altman, G. H.; Chen, J.; Jin, H. J.; Karageorgiou, V.; Kaplan, D. L. Macrophage Responses to Silk. *Biomaterials* **2003**, *24* (18), 3079–3085.

Partlow, B. P.; Hanna, C. W.; Rnjak-Kovacina, J.; Moreau, J. E.; Applegate, M. B.; Burke, K. A.; Marelli, B.; Mitropoulos, A. N.; Omenetto, F. G.; Kaplan, D. L. Highly Tunable Elastomeric Silk Biomaterials. *Adv. Funct. Mater.* **2014**, *24* (29), 4615–4624.

Pawar, S. N.; Edgar, K. J. Alginate Derivatization: A Review of Chemistry, Properties and Applications. *Biomaterials* **2012**, *33* (11), 3279–3305.

Phillips, D. M.; Drummy, L. F.; Conrady, D. G.; Fox, D. M.; Naik, R. R.; Stone, M. O.; Trulove, P. C.; De Long, H. C.; Mantz, R. A. Dissolution and Regeneration of Bombyx Mori Silk Fibroin Using Ionic Liquids. *J. Am. Chem. Soc.* **2004**, *126* (44), 14350–14351.

Phillips, D. M.; Drummy, L. F.; Naik, R. R.; De Long, H. C.; Fox, D. M.; Trulove, P. C.; Mantz, R. A. Regenerated Silk Fiber Wet Spinning from an Ionic Liquid Solution. *J. Mater. Chem.* **2005**, *15* (39), 4206–4208.

Pignatelli, C.; Perotto, G.; Nardini, M.; Cancedda, R.; Mastrogiacomo, M.; Athanassiou, A. Electrospun Silk Fibroin Fibers for Storage and Controlled Release of Human Platelet Lysate. *Acta Biomater.* **2018**, *73*, 365–376.

Qi, Y.; Wang, H.; Wei, K.; Yang, Y.; Zheng, R. Y.; Kim, I. S.; Zhang, K. Q. A Review of Structure Construction of Silk Fibroin

Biomaterials from Single Structures to Multi-Level Structures. *Int. J. Mol. Sci.* **2017**, *18* (3).

Raggio, R.; Bonani, W.; Callone, E.; Dire, S.; Gambari, L.; Grassi, F.; Motta, A. Silk Fibroin Porous Scaffolds Loaded with a Slow-Releasing Hydrogen Sulfide Agent (GYY4137) for Applications of Tissue Engineering. *ACS Biomater. Sci. Eng.* **2018**, acsbiomaterials.8b00212.

Rajkhowa, R.; Gil, E. S.; Kluge, J.; Numata, K.; Wang, L.; Wang, X.; Kaplan, D. L. Reinforcing Silk Scaffolds with Silk Particles. *Macromol. Biosci.* **2010**, *10* (6), 599–611.

Ratner, B. D. The Biocompatibility of Implant Materials. In *Host Response to Biomaterials: The Impact of Host Response on Biomaterial Selection*; Academic Press, **2015**; pp 37–51.

Raynal, L.; Allardyce, B. J.; Wang, X.; Dilley, R. J.; Rajkhowa, R.; Henderson, L. C. Facile and Versatile Solid State Surface Modification of Silk Fibroin Membranes Using Click Chemistry. *J. Mater. Chem. B* **2018**, *6* (48), 8037–8042.

Riccio, M.; Maraldi, T.; Pisciotta, A.; La Sala, G. B.; Ferrari, A.; Bruzzesi, G.; Motta, A.; Migliaresi, C.; De Pol, A. Fibroin Scaffold Repairs Critical-Size Bone Defects In Vivo Supported by Human Amniotic Fluid and Dental Pulp Stem Cells. *Tissue Eng. Part A* **2011**, *18* (9–10), 1006–1013.

Riss, T. L.; Moravec, R. A.; Niles, A. L.; Duellman, S.; Benink, H. A.; Worzella, T. J.; Minor, L. *Cell Viability Assays*; Eli Lilly & Company and the National Center for Advancing Translational Sciences, **2004**.

Rockwood, D. N.; Gil, E. S.; Park, S. H.; Kluge, J. A.; Grayson, W.; Bhumiratana, S.; Rajkhowa, R.; Wang, X.; Kim, S. J.; Vunjak-Novakovic, G.; et al. Ingrowth of Human Mesenchymal Stem Cells into Porous Silk Particle Reinforced Silk Composite Scaffolds: An in Vitro Study. *Acta Biomater.* **2011a**, *7* (1), 144–151.

Rockwood, D. N.; Preda, R. C.; Yücel, T.; Wang, X.; Lovett, M. L.; Kaplan, D. L. Materials Fabrication from Bombyx Mori Silk Fibroin. *Nat. Protoc.* **2011b**, *6* (10), 1612–1631.

Rose, P.; Dymock, B. W.; Moore, P. K. *GYY4137, a Novel Water-Soluble, H2S-Releasing Molecule*, 1st ed.; Elsevier Inc., **2015**; Vol.

554.

Salgado, A. J.; Coutinho, O. P.; Reis, R. L. Bone Tissue Engineering: State of the Art and Future Trends. *Macromolecular Bioscience*. John Wiley & Sons, Ltd August 9, **2004**, pp 743–765.

Sestito, S.; Nesi, G.; Pi, R.; Macchia, M.; Rapposelli, S. Hydrogen Sulfide: A Worthwhile Tool in the Design of New Multitarget Drugs. *Front. Chem.* **2017**, *5*, 72.

Shao, Z.; Vollrath, F. Surprising Strength of Silkworm Silk. *Nature* **2002**, *418* (6899), 741.

Simmons, L.; Tsuchiya, K.; Numata, K. Chemoenzymatic Modification of Silk Fibroin with Poly(2,6-Dimethyl-1,5-Phenylene Ether) Using Horseradish Peroxidase. *RSC Adv.* **2016**, *6* (34), 28737–28744.

Stevens, M. M. Biomaterials for Bone Tissue Engineering. *Materials Today*. **2008**, pp 18–25.

Stoppato, M.; Stevens, H. Y.; Carletti, E.; Migliaresi, C.; Motta, A.; Guldberg, R. E. Effects of Silk Fibroin Fiber Incorporation on Mechanical Properties, Endothelial Cell Colonization and Vascularization of PDLLA Scaffolds. *Biomaterials* **2013**, *34* (19), 4573–4581.

Stuart, B.; Ando, D. *Biological Applications of Infrared Spectroscopy*; Published on behalf of ACOL (University of Greenwich) by John Wiley, **1997**.

Tian, D.; Li, T.; Zhang, R.; Wu, Q.; Chen, T.; Sun, P.; Ramamoorthy, A. Conformations and Intermolecular Interactions in Cellulose/Silk Fibroin Blend Films: A Solid-State NMR Perspective. *J. Phys. Chem. B* **2017**, *121* (25), 6108–6116.

Uebersax, L.; Mattotti, M.; Papaloïzos, M.; Merkle, H. P.; Gander, B.; Meinel, L. Silk Fibroin Matrices for the Controlled Release of Nerve Growth Factor (NGF). *Biomaterials* **2007**, *28* (30), 4449–4460.

Unger, R. E.; Wolf, M.; Peters, K.; Motta, A.; Migliaresi, C.; Kirkpatrick, C. J. Growth of Human Cells on a Non-Woven Silk Fibroin Net: A Potential for Use in Tissue Engineering. *Biomaterials* **2004**, *25* (6), 1069–1075.

Unger, R. E.; Ghanaati, S.; Orth, C.; Sartoris, A.; Barbeck, M.; Halstenberg, S.; Motta, A.; Migliaresi, C.; Kirkpatrick, C. J. The Rapid Anastomosis between Prevascularized Networks on Silk Fibroin Scaffolds Generated in Vitro with Cocultures of Human Microvascular Endothelial and Osteoblast Cells and the Host Vasculature. *Biomaterials* **2010**, *31* (27), 6959–6967.

Valluzzi, R.; Gido, S. P.; Muller, W.; Kaplan, D. L. Orientation of Silk III at the Air-Water Interface. *Int. J. Biol. Macromol.* **1999**, *24* (2–3), 237–242.

Vandiver, M. S.; Snyder, S. H. Hydrogen Sulfide: A Gasotransmitter of Clinical Relevance. *J. Mol. Med.* **2012**, *90* (3), 255–263.

Vepari, C.; Kaplan, D. L. Silk as a Biomaterial. *Progress in Polymer Science (Oxford)*. August **2007**, pp 991–1007.

Voo, W. P.; Lee, B. B.; Idris, A.; Islam, A.; Tey, B. T.; Chan, E. S. Production of Ultra-High Concentration Calcium Alginate Beads with Prolonged Dissolution Profile. *RSC Adv.* **2015**, *5* (46), 36687–36695.

Wallace, J. L. Hydrogen Sulfide-Releasing Anti-Inflammatory Drugs. *Trends Pharmacol. Sci.* **2007**, *28* (10), 501–505.

Wang, L.; Nancollas, G. H. Calcium Orthophosphates: Crystallization and Dissolution. *Chem. Rev.* **2008**, *108* (11), 4628–4669.

Wang, P. On the Etymology of English Silk: A Case Study of IE and Altaic Contact. *Cent. Asiat. J.* **1993**, *37* (3/4), 225–248.

Wang, W.; Yeung, K. W. K. Bone Grafts and Biomaterials Substitutes for Bone Defect Repair: A Review. *Bioact. Mater.* **2017**, *2* (4), 224–247.

Wang, Y.; Rudym, D. D.; Walsh, A.; Abrahamsen, L.; Kim, H. J.; Kim, H. S.; Kirker-Head, C.; Kaplan, D. L. In Vivo Degradation of Three-Dimensional Silk Fibroin Scaffolds. *Biomaterials* **2008**, *29* (24–25), 3415–3428.

Wenk, E.; Wandrey, A. J.; Merkle, H. P.; Meinel, L. Silk Fibroin Spheres as a Platform for Controlled Drug Delivery. *J. Control. Release* **2008**, *132* (1), 26–34.

Wenk, E.; Murphy, A. R.; Kaplan, D. L.; Meinel, L.; Merkle, H. P.; Uebersax, L. The Use of Sulfonated Silk Fibroin Derivatives to Control Binding, Delivery and Potency of FGF-2 in Tissue Regeneration. *Biomaterials* **2010**, *31* (6), 1403–1413.

Wenk, E.; Merkle, H. P.; Meinel, L. Silk Fibroin as a Vehicle for Drug Delivery Applications. *Journal of Controlled Release*. March **2011**, pp 128–141.

Wilding, M. A.; Hearle, J. W. S. No Title. *Polymeric Materials Encyclopaedia*; CRC, Boca Raton, Florida, **1996**; pp 8307–8322.

Williams, D. F. *Definitions in Biomaterials*, Progress i.; Elsevier, Amsterdam, **1987**.

Williams, D. F. To Engineer Is to Create: The Link between Engineering and Regeneration. *Trends Biotechnol.* **2006**, *24* (1), 4–8.

Wilson, D.; Valluzzi, R.; Kaplan, D. L. Conformational Transitions in Model Silk Peptides. *Biophys. J.* **2000**, *78* (5), 2690–2701.

Witte, F.; Ulrich, H.; Palm, C.; Willbold, E. Biodegradable Magnesium Scaffolds: Part II: Peri-Implant Bone Remodeling. *J. Biomed. Mater. Res. - Part A* **2007**, *81* (3), 757–765.

Wu, S.; Liu, X.; Yeung, K. W. K.; Liu, C.; Yang, X. Biomimetic Porous Scaffolds for Bone Tissue Engineering. *Mater. Sci. Eng. R Reports* **2014**, *80* (1), 1–36.

Yamada, H.; Nakao, H.; Takasu, Y.; Tsubouchi, K. Preparation of Undegraded Native Molecular Fibroin Solution from Silkworm Cocoons. *Mater. Sci. Eng. C* **2001**, *14* (1–2), 41–46.

Yamada, H.; Igarashi, Y.; Takasu, Y.; Saito, H.; Tsubouchi, K. Identification of Fibroin-Derived Peptides Enhancing the Proliferation of Cultured Human Skin Fibroblasts. *Biomaterials* **2004**, *25* (3), 467–472.

Yan, L. P.; Oliveira, J. M.; Oliveira, A. L.; Caridade, S. G.; Mano, J. F.; Reis, R. L. Macro/Microporous Silk Fibroin Scaffolds with Potential for Articular Cartilage and Meniscus Tissue Engineering Applications. *Acta Biomater.* **2012**, *8* (1), 289–301.

Yao, D.; Dong, S.; Lu, Q.; Hu, X.; Kaplan, D. L.; Zhang, B.; Zhu, H. Salt-Leached Silk Scaffolds with Tunable Mechanical Properties.

Biomacromolecules **2012**, *13* (11), 3723–3729.

Yi, S.; Ding, F.; Gong, L.; Gu, X. Extracellular Matrix Scaffolds for Tissue Engineering and Regenerative Medicine. *Curr. Stem Cell Res. Ther.* **2017**, *12* (3), 233–246.

Zhang, H.; Li, L. ling; Dai, F. yin; Zhang, H. hao; Ni, B.; Zhou, W.; Yang, X.; Wu, Y. zhang. Preparation and Characterization of Silk Fibroin as a Biomaterial with Potential for Drug Delivery. *J. Transl. Med.* **2012a**, *10* (1), 1.

Zhang, X.; Reagan, M. R.; Kaplan, D. L. Electrospun Silk Biomaterial Scaffolds for Regenerative Medicine. *Adv. Drug Deliv. Rev.* **2009**, *61* (12), 988–1006.

Zhang, X.; Bogdanowicz, D.; Erisken, C.; Lee, N. M.; Lu, H. H. Biomimetic Scaffold Design for Functional and Integrative Tendon Repair. *J. Shoulder Elb. Surg.* **2012b**, *21* (2), 266–277.

Zhang, X.; Cao, C.; Ma, X.; Li, Y. Optimization of Macroporous 3-D Silk Fibroin Scaffolds by Salt-Leaching Procedure in Organic Solvent-Free Conditions. *J. Mater. Sci. Mater. Med.* **2012c**, *23* (2), 315–324.

Zhang, Y. Q. Applications of Natural Silk Protein Sericin in Biomaterials. *Biotechnol. Adv.* **2002**, *20* (2), 91–100.

Zhang, Y. Q.; Shen, W. De; Xiang, R. L.; Zhuge, L. J.; Gao, W. J.; Wang, W. B. Formation of Silk Fibroin Nanoparticles in Water-Miscible Organic Solvent and Their Characterization. *J. Nanoparticle Res.* **2007**, *9* (5), 885–900.

Zhao, Y.; Bhushan, S.; Yang, C.; Otsuka, H.; Stein, J. D.; Pacheco, A.; Peng, B.; Devarie-Baez, N. O.; Aguilar, H. C.; Lefer, D. J.; et al. Controllable Hydrogen Sulfide Donors and Their Activity against Myocardial Ischemia-Reperfusion Injury. *ACS Chem. Biol.* **2013**, *8* (6), 1283–1290.

Zhao, Y.; Biggs, T. D.; Xian, M. Hydrogen Sulfide (H2S) Releasing Agents: Chemistry and Biological Applications. *Chem. Commun.* **2014**, *50* (80), 11788–11805.

Zhou, C. Z.; Confalonieri, F.; Medina, N.; Zivanovic, Y.; Esnault, C.; Yang, T.; Jacquet, M.; Janin, J.; Duguet, M.; Perasso, R.; et al. Fine Organization of Bombyx Mori Fibroin Heavy Chain Gene.

Nucleic Acids Res. **2000**, *28* (12), 2413–2419.

Zhou, C. Z.; Confalonieri, F.; Jacquet, M.; Perasso, R.; Li, Z. G.; Janin, J. Silk Fibroin: Structural Implications of a Remarkable Amino Acid Sequence. *Proteins Struct. Funct. Genet.* **2001**, *44* (2), 119–122.

Zimmermann, H.; Shirley, S. G.; Zimmermann, U. Alginate-Based Encapsulation of Cells: Past, Present, and Future. *Curr. Diab. Rep.* **2007**, *7* (4), 314–320.

Zysset, P. K.; Edward Guo, X.; Edward Hoffler, C.; Moore, K. E.; Goldstein, S. A. Elastic Modulus and Hardness of Cortical and Trabecular Bone Lamellae Measured by Nanoindentation in the Human Femur. *J. Biomech.* **1999**, *32* (10), 1005–1012.

ATCC: The Global Bioresource Center http://www.lgcstandards-atcc.org/en.aspx (accessed Aug 7, 2019).

CAM Bioceramics https://www.cambioceramics.com/ (accessed Aug 5, 2019).

International Sericultural Commission http://inserco.org/en/evolution_of_silk.

U.S. Pharmacopeia https://www.usp.org/ (accessed Jun 27, 2019).

Scientific production

Manuscripts in International journals

L. Gambari, E. Amore, R. Raggio, M. Barone, G. Lisignoli, B. Grigolo, A. Motta, F. Grassi *Hydrogen Sulfide-Releasing Silk Fibroin Scaffold for Bone Tissue Engineering*, Material Science and Engineering Type C **2019** 102, 471-482

R. Raggio, W. Bonani, L. Gambari, F. Grassi, C. Migliaresi, A. Motta *Silk Fibroin Porous Scaffolds Loaded with a Slow-Releasing Hydrogen Sulfide Agent (GYY4137) for Applications of Tissue Engineering*, ACS Biomaterials Science & Engineering **2018** 4 (8), 2956-2966

Participation to congresses and schools

R. Raggio, W. Bonani, L. Gambari, F. Grassi, A. Motta *Silk fibroin scaffolds loaded with a sulphur (H_2S) donor agent as a novel therapeutic approach for bone regeneration*, 3rd TICME CONFERENCE **2019**, 12-15 July 2019, Trento, Italy (POSTER)

R. Raggio *Techniques for the characterization of silk fibroin scaffolds for bone regeneration applications* Workshop "Advanced Characterization of Silk Protein Materials". Chulalongkorn University, Bangkok, March 20-22, **2018** (ORAL COMMUNICATION)

R. Raggio, W. Bonani, L. Gambari, F. Grassi, C. Migliaresi, A. Motta *Silk fibroin scaffolds loaded with a sulphur (H_2S) donor agent as a*

novel therapeutic approach for bone regeneration, FIRM 2017, 25-28 September **2017**, Spain (ORAL COMMUNICATION)

R. Raggio, W. Bonani, F. Grassi, C. Migliaresi, A. Motta *Silk fibroin scaffolds loaded with a sulphur donor agent as a novel therapeutic approach for bone regeneration*, YSC 2016, 16-17 September **2016**, Brown University, Providence, USA (POSTER)

R. Raggio, W. Bonani, F. Grassi, C. Migliaresi, A. Motta *Silk fibroin scaffolds loaded with H_2S donors for bone tissue engineering*, FBPS 2015, 8-11 July **2015**, Riva del Garda, Italy (POSTER)

Internships

March-May 2018. Internship as visiting PhD student and Early Stage Researcher of "REMIX" Project, G.A. 778078 H2020-MSCA-RISE-2017; supervisor Prof. Sorada Kanokpanont; Department of Chemical Engineering, Chulalongkorn University, Bangkok, Thailand. Research activities focused on silk fibroin/alginate-based systems for the delivery of calcium phosphates.

April-September 2016. Internship as visiting PhD student; supervisor Prof. David Kaplan; Department of Biomedical Engineering, Tufts University, Medford, MA, USA. Research activities focused on therapeutically functionalized silk proteins for drug delivery and bone tissue engineering applications; attendance of seminars and workshops; safety training courses.

Acknowledgements

I am sincerely grateful to my supervisor, Professor Antonella Motta, for her mentoring and her support, and for giving me the opportunity to conduct part of my PhD research in collaboration with several national and international research centers. I am grateful to Professor Claudio Migliaresi, Professor Devid Maniglio and Doctor Walter Bonani for sharing their valuable scientific knowledge and for helping me in conducting my research activities.

I want to thank Professor David Kaplan (Tufts University, Medford, USA), and Professor Sorada Kanokpanont (Chulalongkorn University, Bangkok, Thailand) for hosting me in their research groups. These were immensely enriching and stimulating opportunities.

I also want to thank Doctor Francesco Grassi and Doctor Laura Gambari (Istituto Ortopedico Rizzoli, Bologna, Italy), Professor Sandra Dirè and Doctor Emanuela Callone (University of Trento), and Doctor Roberta Tasso (Ospedale Policlinico San Martino, Genoa, Italy), for their productive and extensive collaboration in developing innovative projects and disseminating results.

The years of my PhD have been so important for my personal growth and for my education. The people that have been by my side during this journey will always be very dear to me.

The most affectionate thanks go to my long-time friends, to the people who I had the great fortune to meet during the years of my PhD who shared with me incredible experiences of science, work, fun and friendship in Trento, Boston and Bangkok, to my family who was always there with me throughout these years, and to those who have just arrived but I hope will stay longer.